UNIVERSITAT
POLITÈCNICA
DE VALÈNCIA

Departamento de Máquinas y Motores Térmicos

Doctoral Thesis

“Recuperation of the exhaust gases energy using a Brayton cycle machine”

Presented by: Petar Kleut
Supervised by: Dr. Vicente Dolz Ruiz

in fulfilment of the requirements for the degree of

Doctor of Philosophy

Valencia, December 2016

Doctoral Thesis

“Recuperation of the exhaust gases energy using a Brayton cycle machine”

Presented by: Petar Kleut

Supervised by: Dr. Vicente Dolz Ruiz

THESIS EXAMINERS

Dr. Nenad Miljić

Dr. Luis Le Moyne

Dr. Francisco Vera García

DEFENSE COMMITTEE

Chairman: Dr. Antonio José Torregrosa Huguet

Secretary: Dr. Pedro Acisclo Rodriguez Aumente

Member: Dr. Nenad Miljić

Valencia, December 2016

Abstract

Lately, car manufacturers have been put to a big challenge to reduce the CO_2 emission of their entire fleets. Norms of pollutant emissions limit the ways to achieve the desired CO_2 emission goals, as some of the solutions that would lead to lower CO_2 emission also lead to higher pollutant emission. Waste Heat Recovery (WHR) could be a good solution to lower the CO_2 emission of the Internal Combustion Engine (ICE) without increasing the pollutant emission. In the present thesis different WHR strategies are analysed and the results suggested it would be interesting to further study the Brayton cycle machine.

Air Brayton Cycle (ABC) represents a way to recover a part of the heat energy of the ICE exhaust gases and transform it into mechanical energy. Recovered mechanical energy would then be returned to the crankshaft of the ICE, thereby reducing the amount of energy that has to be liberated by combustion of fuel which lowers the fuel consumption and CO_2 emission.

The study of ABC started with an analysis of the ideal cycle in order to obtain the theoretical maximum of the system. The study continued with an analysis of the semi ideal cycle where all losses are taken into account only by two efficiency coefficients. This analysis showed that for the diesel engine efficiency of the ABC is very low because of the low exhaust gas temperature. For the gasoline engine the cycle could be viable when the ICE is working under steady condition and higher load. These conditions could be fulfilled when the vehicle is driven on the highway.

Detailed analysis was aimed at determining the cycle main losses. They were determined to be: pumping losses, losses caused by heat transfer and mechanical losses. Taking into account these main losses along with other direct and indirect losses it was concluded that the cycle is not viable for the types of the WHR machines that were considered in this study.

In order for the cycle to be viable some other either existing or new machine type should be tested, that would lower the main losses and offer good isentropic and mechanical efficiency for desired conditions.

Resumen

Últimamente los fabricantes de automóviles se han puesto el gran reto de reducir la emisión de CO_2 en la totalidad de sus flotas. Las nuevas normativas para la reducción de las emisiones contaminantes limitan los medios para lograr los objetivos deseados en la emisión de CO_2 porque algunas de las soluciones que llevan a la reducción en la emisión de CO_2 también dan lugar a un incremento en la emisión de otros contaminantes. La recuperación de calor residual (WHR) podría ser una buena solución para reducir las emisiones de CO_2 del motor de combustión interna (ICE) sin poner en peligro la emisión de contaminantes. En la presente Tesis se analizaron diferentes estrategias de WHR y se concluyó que sería interesante estudiar más a fondo la máquina de ciclo Brayton.

El Ciclo Brayton de Aire (ABC) permite recuperar una parte del calor de los gases de escape del ICE y transformar este calor en energía mecánica. La energía mecánica recuperada se devuelve al cigüeñal del ICE, reduciendo de ese modo la cantidad de energía que tiene que ser liberada por la combustión del combustible, lo cual permite reducir el consumo de combustible y las emisiones de CO_2.

En esta Tesis se estudia el ABC mediante un análisis del ciclo ideal con el fin de obtener el máximo teórico del sistema. El modelo se mejora con un análisis del ciclo semi-ideal donde se tienen en cuenta todas las pérdidas mediante el uso de dos coeficientes generales. Este análisis muestra que para el motor diesel la eficiencia del ciclo ABC es muy baja debido a la baja temperatura del gas de escape. Para el motor de gasolina el ciclo podría ser viable cuando el ICE está trabajando bajo condiciones estacionarias y una carga mayor. Estas condiciones se podrían cumplir cuando el vehículo está circulando en autopista.

El análisis detallado de este ciclo tiene como objetivo determinar las pérdidas principales de ciclo. Las pérdidas principales se identificaron como: las pérdidas de bombeo, las pérdidas causadas por la transferencia de calor y las pérdidas mecánicas. Teniendo en cuenta estas pérdidas principales junto con otras pérdidas directas e indirectas, se concluyó que el ciclo no es viable para los tipos de máquinas WHR que fueron considerados en este estudio.

Para que el ciclo sea viable se tiene que buscar alguna otra máquina existente o un nuevo tipo de máquina que reduzca las principales pérdidas y ofrezca un buen rendimiento isentrópico y mecánico para las condiciones deseadas.

Resum

Últimament els fabricants d'automòbils s'han posat el gran repte de reduir l'emissió de CO_2 de la totalitat de les seues flotes. Les noves normatives de reducció de les emissions contaminants limiten els mitjans per assolir els objectius desitjats d'emissió de CO_2 perquè algunes de les solucions que porten a la reducció en l'emissió de CO_2 també donen lloc a un increment a l'emissió de altres contaminants. La recuperació de calor residual (WHR) podria ser una bona solució per reduir les emissions de CO_2 del motor de combustió interna (ICE) sense posar en perill l'emissió de contaminants. En la present Tesi s'han analitzat diferents estratègies WHR i es va concloure que seria interessant estudiar més a fons el cicle Brayton.

El Cicle Brayton d'Aire (ABC) representa una manera de recuperar una part de la calor dels gasos d'escapament de l'ICE i transformar calor a l'energia mecànica. L'energia mecànica recuperada es retorna al cigonyal de l'ICE reduint d'aquesta manera la quantitat d'energia que ha de ser alliberada per la combustió del combustible permitint la reducció del consum de combustible i les emissions de CO_2.

En aquesta Tesi s'ha començat estudiant un ABC amb una anàlisi del cicle ideal per tal d'obtenir el màxim teòric del sistema. Este model es millora amb una anàlisi del cicle semi-ideal on es tenen en compte totes les pèrdues amb tan sols dos coeficients d'eficiència. Aquesta anàlisi va mostrar que per al motor dièsel l'eficiència del cicle ABC és molt baixa a causa de la baixa temperatura del gas d'escapament. Per al motor de gasolina el cicle podria ser viable quan l'ICE està treballant sota condicions estacionàries i una càrrega més gran. Aquestes condicions es podrien complir quan el vehicle està circulant en autopista.

L'anàlisi detallada del cicle va tenir com a objectiu determinar les pèrdues principals de cicle. Les pèrdues principals es van identificar com: les pèrdues de bombament, les pèrdues causades per la transferència de calor i les pèrdues mecàniques. Tenint en compte aquestes pèrdues principals juntament amb altres pèrdues directes i indirectes, es va concloure que el cicle no és viable per als tipus de màquines WHR que van ser considerats en aquest estudi.

Perquè el cicle puga ser viable s'ha de buscar alguna altra màquina existent o un nou tipus de màquina que puga reduir les principals pèrdues i puga oferir un bon rendiment isentròpic i mecànic per a les condicions desitjades.

Acknowledgments

One does not go alone through creating a Doctoral Thesis. There are many people that I owe my gratitude for this accomplishment. I would like to start chronologically and thank, at first place, Dr. Raul Payri for selecting me as a PhD candidate at CMT-Motores Termicos. Also, I must thank Dr. Jose Galindo and Dr. Vicente Dolz for giving me the opportunity to work on this particular project. To Vicente I owe much more gratitude for being a wonderful thesis mentor. I feel privileged to be mentored by such a knowledgeable, kind and patient person. I am very thankful to all the CMT personnel that helped me along the way, especially to my closest colleagues that I had a pleasure to share the office with. I am also very grateful to Mr. Stephane Tondelli from Valeo for a very productive and enjoyable collaboration.

I would like to thank my sister Dr. Duška Kleut for helping me with the English corrections, but even more for her constant support and for always being able to count on her. I would like to thank my girlfriend Dr. Sabina Hodžić also for helping me with the English corrections, but much more for her love, support and for sharing with me the good and the bad through this period.

Doctoral Thesis represents the peak of my academic education, however I cannot stop thinking that I received the most important education even before enrolling in the elementary school. For this I have to thank my parents. I would like to dedicate this thesis to my family as a small compensation for the time we missed while I was away.

Contents

1 Introduction 1
  1.1 Background 1
  1.2 General motivation 4
  1.3 Objectives 7
  1.4 Methodology 8
2 Literature review 11
  2.1 Introduction 13
  2.2 Thermoelectric Generator 14
  2.3 Rankine Cycle 18
  2.4 Stirling cycle 22
  2.5 Brayton cycle 25
  2.6 Summary 30
3 Thermodynamic analysis 33
  3.1 Introduction 35
  3.2 Engine energy levels 35
    3.2.1 Gasoline engine 38
    3.2.2 Diesel engine 39
  3.3 Cycle description 40
    3.3.1 Ideal cycle 43
    3.3.2 Machine selection 50
    3.3.3 Non-ideal cycle 53
4 Heat exchanger 61
  4.1 Introduction 63
  4.2 Heat exchanger efficiency 64
  4.3 Pressure drop 67
  4.4 Pressure wave transmissivity 75

5 Heat recovery system model 85
  5.1 Introduction 87
  5.2 Simple machine model 90
    5.2.1 Poppet valve 93
    5.2.2 Reed valve 110
    5.2.3 Camless poppet valve 117
  5.3 Heat exchanger tube length 119
  5.4 Heat transfer model 127
  5.5 Mechanical losses 129
  5.6 Indirect losses 134
    5.6.1 Exhaust backpressure pumping losses 134
    5.6.2 Additional weight 134
6 Conclusions and future work 137
  6.1 Conclusions 139
  6.2 Future work 142
7 Bibliography 145

Nomenclature

Latin symbols

A	area
a,b	dimensions
B	cylinder bore
c	coefficient
C_d	discharge coefficient
cfmep	crankshaft friction mean effective pressure
C_L	clearance
C_m	flow parameter
c_p	specific heat capacity at constant pressure
c_x	drag coefficient
D	diameter
Ds	machine specific diameter
F	force
f	friction coefficient
g	gravitational acceleration
H	height
h	enthalpy
ht	heat transfer coefficient
J	moment of inertia
k	thermal conductivity
L	valve lift
l	length
m	mass
$\dot{m}$	mass flow rate
n	number of parts
N	rotary speed
Ns	machine specific speed
Nu	Nusselt number
p	pressure
P	power
Q	energy
R	radius
Re	Reynolds number
rfmep	reciprocating friction mean effective pressure
S	stroke
S1, S2, S3	pressure sensors
Sp	mean piston velocity
T	temperature
TR	Transmission Ratio
v	velocity

V	volume
$\dot{V}$	volumetric flow
vfmep	valvetrain friction mean effective pressure
W	width
x	distance
y, z	calculation group
ZT	figure of merit

Greek symbols

α, δ, θ	angles
γ	heat capacity ratio
ε	roughness
ζ	resistance coefficient
η	efficiency
λ	air-fuel equivalence ratio
μ	dynamic viscosity
π	pressure ratio
ρ	density
τ	torque
ω	rotational speed

Subscripts

0	at reference conditions
1	start of compression
2	end of compression
3	start of expansion
4	end of expansion
aero	aerodynamic drag
bc	bearing crankshaft
br	bearing connecting rod
bv	bearing valvetrain
C	cold
c	cycle
cA	cycle for the exhaust gas enthalpy at ambient temperature
comb	combustion
cr	critical
disp	displaced
down	downstream
dr	driving
E	engine
FD	final drive
fr	friction
front	vehicle frontal

fuel	fuel
GB	gear box
H	hot
h	hydraulic
HE	heat exchanger
HT	heat transfer
in	inlet
is	internal valve seat
lim	limiting value
loc	local
max	maximum
min	minimum
ml	mechanical losses
oh	oscillating hydrodynamic friction
om	oscillating mixed friction
os	outlet valve seat
out	outlet
p	piston
pinch	pinch point temperature difference
pl	pumping losses
r	reference
r0, r1, r2,r3	related to polynomial degree
rf	roller follower friction
roll	rolling
s	specific
st	valve stem
TR	transmission ratio
up	upstream
v	volumetric
val	valve
vc	between valve and cylinder
veh	vehicle
vv	between two valves
wh	wheel

Acronyms

ABC	Air Brayton Cycle
AFR	Air Fuel Ratio
BDC	Bottom Dead Center
CA	Closing Angle
CR	Compression Ratio
ECE	Energy Conversion Efficiency
ECU	Electronic Control Unit
EGR	Exhaust Gas Recirculation

ERE	Energy Recovery Efficiency
EVO	Early Valve Opening
HE	Heat Exchanger
HP	High Pressure
ICE	Internal Combustion Engine
LHV	Lower Heating Value
LP	Low Pressure
LVC	Late Valve Closing
MD	Main Duration
NEDC	New European Driving Cycle
OA	Opening angle
OECE	Overall Energy Conversion Efficiency
OEM	Original Equipment Manufacturer
ORC	Organic Rankine Cycle
RD	Ramp Duration
RPM	Revolutions Per Minute
RR	Ramp Ratio
TDC	Top Dead Centre
TEG	Thermo Electric Generator
TR	Transmission Ratio
VD	Valve Duration
WHR	Waste Heat Recovery

1 Introduction

Contents

1.1 Background 1
1.2 General motivation 4
1.3 Objectives 7
1.4 Methodology 8

1.1 Background

Internal Combustion Engines (ICE) are commercially available for almost 150 years. In this chapter a short historical review of inventions that had a big influence on Internal Combustion Engine efficiency will be shown, with the accent on automotive application.

In 1824 Nicolas Léonard Sadi Carnot published his only publication Reflections on the Motive Power of Fire. He concluded that there is a limit of power that can be extracted from a heat source, he suggested what would be the way to achieve it and suggested that it doesn´t depend on working fluid used. At that time the dominant heat engine was the steam machine, Internal Combustion Engines were not reliable and efficient. However, it all changed when Nikolaus Otto and Eugen Langen presented their atmospheric ICE at the 1867 World´s Fair in Paris and won the Gold Medal because their engine had the efficiency double that of other engines of that time. Otto/Langen engine is called atmospheric because it did not compress the air before the combustion. It had the efficiency of 12% and the power of 0.5 HP [1]. It was very popular but in few years it reached its technical limit with the maximum power of 3 HP, indicated efficiency of 16% and brake efficiency of 12%.

Otto was working on improving the cycle and in 1876 he patented and constructed an engine that had a compression stroke before combustion being the first four stroke Internal Combustion Engine built. Adding the compression stroke before the combustion improved the engine brake efficiency to 14% [2].

It was a year 1892 when Rudolf Diesel released patents of his cycle in various countries, trying to achieve Carnot cycle and reach efficiencies as high as 80% by compressing the air up to 250 bar. The engine that he constructed in 1897 had the efficiency of 26% which was much lower than he first planned but much higher than the other engines of that time. The main reasons for success of the Diesel engine were its high efficiency because of high compression ratio and the possibility to use heavy liquid fuels. The Otto engines of that time had very limited compression ratio of around 4, because of the knock caused by the use of fuels with low knock resistance and bad control of the start of combustion.

In order not to infringe Otto´s patent rights, there were several attempts to make a different cycle keeping the advantage of compression before the combustion. Dougald Clerk in 1878 designed the first two stroke engine with in-cylinder compression and got a patent for it in 1881. Apart from making a new kind of engine, Clerk also wrote the great book about the engines of that time [3]. The Author provides a small table, presented here as Table 1.1, to illustrate the evolution of the engine efficiency with time and the rise of compression pressure:

Year	Compression pressure	Indicated efficiency
1882-88	2.6	17%
1888-94	4.6	21%
1894	6	25%

Table 1.1. Clerk´s table of engine efficiency in function of the compression pressure

At the time this book was published the most efficient engine had indicated efficiency of 28% at 6.2 bar compression pressure. The Otto engines of that time used coal gas as fuel which has good resistance to knock so raising the compression pressure wasn´t a problem.

Once Otto, Diesel and two stroke engines were discovered and were made functional there were more challenges in adapting those engines for automotive application. Probably the most important persons in early development of personal vehicles powered by ICE were Karl Benz, Gottlieb Daimler and Wilhelm Maybach. In order to make a functional vehicle they had to overcome various problems not specific for stationary engines: the engine had to be small and light, reliable, with controlled load, cooling, easy starting etc. The fuel could no longer be coal gas because of the small energy density so instead liquid fuels had to be used. This resulted in need to solve new problems like the evaporation of fuel, mixing with air, knock resistance etc.

The progress of ICE is well described in Clerks 1910 edition of his book about engines [4]. The book focuses now not only on gas and oil engines but on petrol engines as well. There is a reference to a Daimler 3.3 litre, 4 cylinder petrol engine with indicated efficiency of 26% at the moderate compression ratio of 3.85. Petrol of that time had a low octane number so it wasn’t possible to use higher compression ratio. The most efficient gas Otto engine of that time, a big stationary engine, had the indicated efficiency of 36.8% and brake efficiency of 32.2%. For a large 500 HP Diesel engine it states the brake efficiency of 31.7%. Also, the progress in knowledge is evident with much better understanding of combustion, thermal and mechanical loses.

Discoveries that followed in the next 100 years improved significantly the engine efficiency and their usability in automobiles. Bosch invented a high-voltage magnetic ignition that solved the problem with ignition. Maybach invented the nozzle carburettor that atomized the fuel allowing a higher percentage of petrol to be vaporized that allowed practically any mixture quantity. In 1921 Thomas Midgley Jr. and T.A. Boyd discovered that tetraethyl lead can be used as antiknock additive that allowed higher compression ratios resulting in higher efficiencies. In 1920s Bosch developed an airless diesel injection pump, diesel engines first started appearing in heavy commercial vehicles followed by light commercial vehicles, and ultimately automobiles, with Mercedes 260D in 1934 being the first car with a diesel engine in serial production. In 1905 Alfred Büchim the head of diesel engine research at Gebrüder Sulzer, patented the turbocompressor. In commercial vehicles, the massive application of turbocharging started in 1960s while the first turbocharged serial production car was Mercedes 300SD in 1978, with the brake efficiency of 32.6%.

The energy crises in 1970s and rising public awareness of environmental problems led to a demand for more fuel efficient engines with lower exhaust pollution emission. Measures inside the gasoline engine were not sufficient to reduce the pollution to satisfy legal requirements. After-treatment had to be used so three-way catalytic converters (3WC) were introduced. Carburettors could not provide precise control of fuel air ratio so electronically controlled fuel injection was developed. Soon, electronics took over engine control not only for gasoline but for diesel engines as well. In 1983, the first electronic injection with lambda control and 3WC hit the market, followed by the first diesel electronically controlled fuel injection pumps the next year. The next improvement came in the form of direct injection. Massive usage of direct injection in automobile diesel engines started in 1980s because it offered better efficiency as a consequence of lower heat and flow losses then prechamber injection. For the gasoline engines it took a bit more and started in late 1990s.

Since the introduction of pollution emission legislation (1992 in Europe) improvements of engine efficiency were somewhat limited due to the negative effects on pollution emission that various techniques for efficiency improvement have.

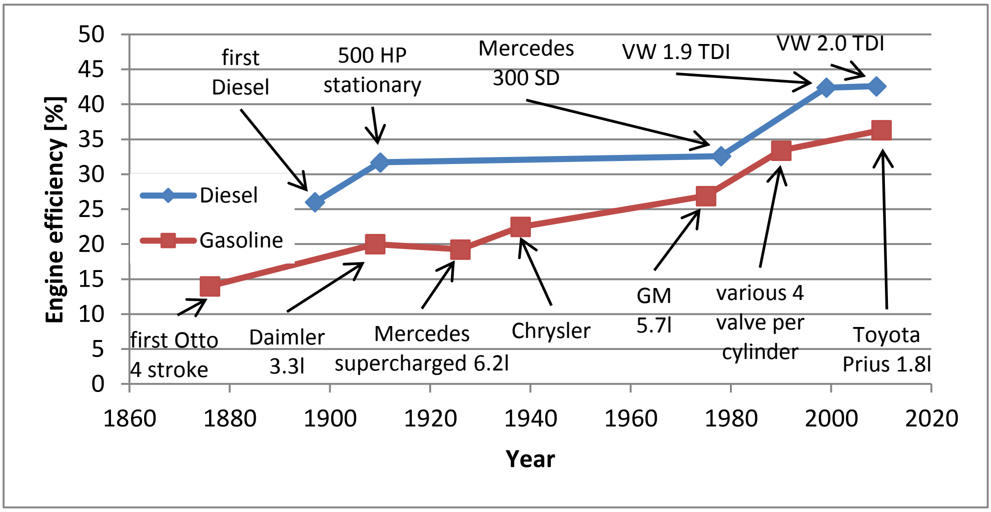

Figure 1.1. Evolution of maximum brake efficiency for car engines

Figure 1.1 shows the evolution of maximum engine efficiency for automobile application. As a summary of this brief historical review of the inventions that had the most significant influence on engine efficiency it can be concluded that in recent years, despite vast technological advances, the efficiency increase is very slow.

Nowadays, the maximum brake efficiency of the gasoline and diesel engine for automobile application is around 36% and 42% respectively. Efficiency is much lower in non-optimal conditions such as low speed and low load. Figure 1.2 represents simplified energy balance for both engine types.

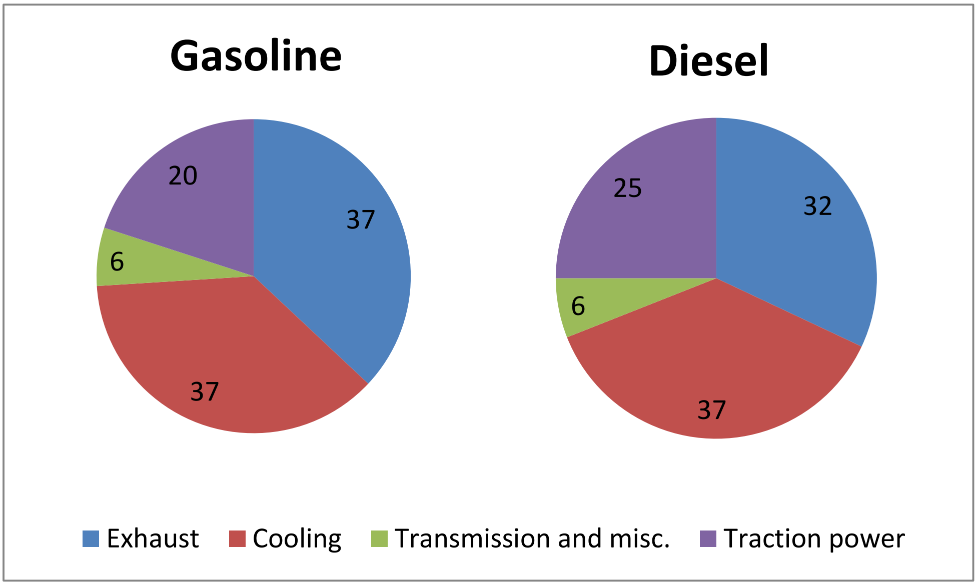

Figure 1.2. A typical energy balance of the gasoline and diesel engine [5]

Energy that is wasted as heat of exhaust gases is high in both cases. Converting part of the exhaust heat into traction power would improve engine efficiency would and decrease CO2 emission.

1.2 General motivation

During the 140 years of development, the Internal Combustion Engines were put to different challenges. Although, some of the challenges remain the same, they still have to compete with other machine types in efficiency, reliability, size, etc.

Car manufacturers, like any private company in capitalism, are primarily oriented toward making the profit as high as possible. To maximize the profit they have to lower the costs and increase the sales. Developing and producing more efficient engines does not help in reducing the costs and it could help in selling more cars only if the customers are interested in buying more fuel efficient vehicles. Of course, the customer interest to buy some car will depend strongly on the car price. Demand depends strongly on the market, fuel price, people mentality, government subventions for low fuel consumption vehicles etc. But, for sure, the best motivation for manufacturers to make more efficient and environmental friendly vehicles is imposing harder legal legislation. The first voluntary agreement in the European Union was signed in 1998 between the European Commission and European Automobile Manufacturers Association ACEA, with the objective to achieve an average of 140 g/km of CO_2 for passenger vehicles by 2008. Similar agreements were made with Japanese and Korean associations JAMA and KAMA but they had one more year to achieve the same emission goal [6]. This goal represented the 25% reduction from the 1995 level of 186 g/km. Although significant reductions have been made, the agreement did not reach the goal because the average emission for the whole car market in 2008 was 153.7 g/km [7]. In December 2007, the European Commission made a proposal for regulation to legally limit CO_2 emission. Current regulation is so that car manufacturers must reach fleet average of 130 g/km in 2015 and 95 g/km by 2020 [8]. In terms of fuel consumption, the 2015 target is approximately equivalent to 5.6 litres per 100 km (l/100 km) of petrol or 4.9 l/100 km of diesel. The 2020 target equates to approximately 4.1 l/100 km of petrol or 3.6 l/100 km of diesel.

Figure 1.3 represents the state of fleet average in recent years and objectives that should be reached [9]. Although manufacturers are significantly improving the emission reaching 2020 limits is still a hard task. Using the conventional hydro carbon fuels it is only possible to lower the CO_2 emission by lowering the fuel consumption. As fuel consumption is inversely related to engine efficiency, improving engine efficiency lowers the CO_2 emission.

Figure 1.4 shows that only hybrid vehicles and few vehicles powered only by diesel engine already accomplished 2020 norms in 2013 while there are no vehicles powered only by gasoline engine that fulfil these norms [10]. Some smaller cars will reach 2020 limits only powered by ICE, but those bigger and more powerful will probably need some degree of hybridisation. Even so, improving engine efficiency is the key to keep the ICE as primal or partial vehicle power source.

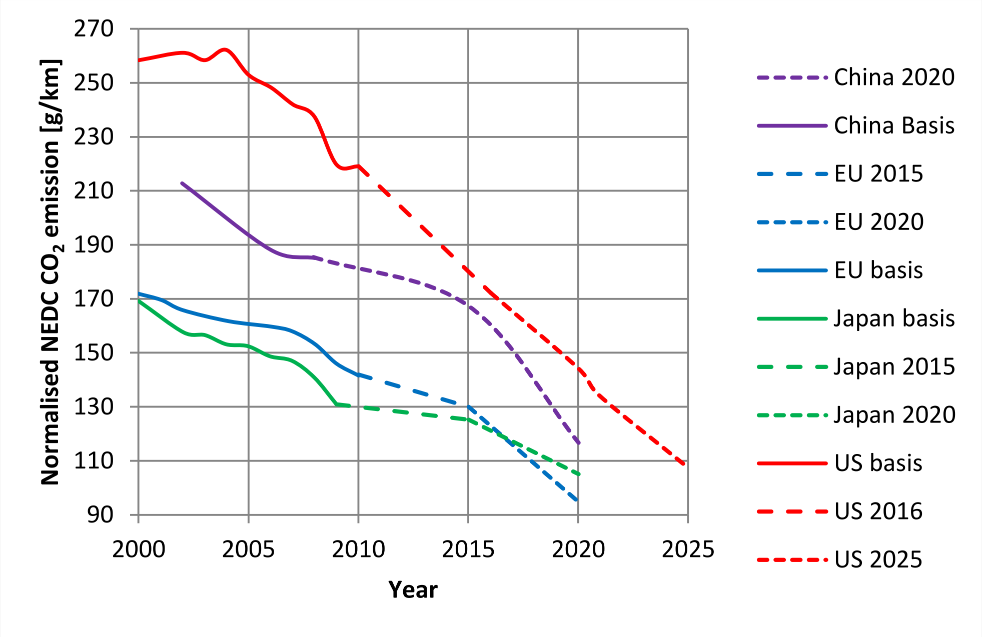

Figure 1.3. Recent fleet average CO2 emission and future legislation by year [9]

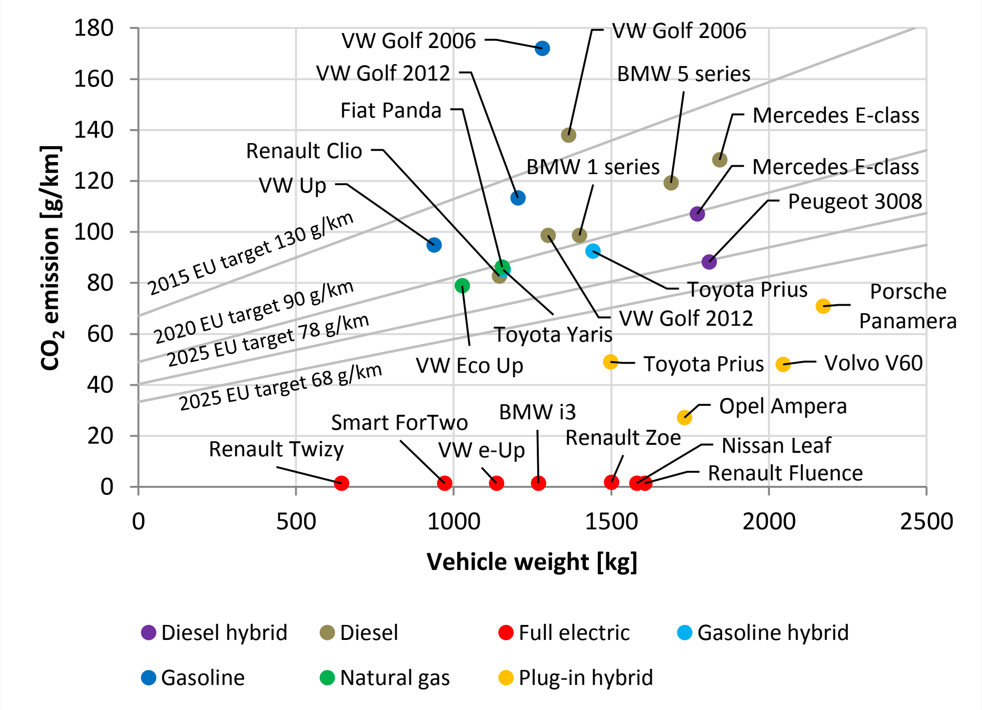

Figure 1.4. CO2 emissions for 2013 and some selected vehicles with low emission [10]

There are various ways to improve engine efficiency by extracting more mechanical power by lowering some energy loses, as showed in Figure 1.2. The present work will focus on recuperating the heat of exhaust gases in form of mechanical energy by using Air Brayton Cycle (ABC) Waste Heat Recovery (WHR). That system should be compatible with currently used technology and shouldn´t have negative effect on pollutant emission.

1.3 Objectives

The main objective of this thesis is to investigate the possibility of applying a Brayton bottoming cycle to recover the heat of exhaust gases to be used as mechanical energy on the ICE shaft. Exhaust gases are a big source of wasted energy. In turbocharged engines, pressure difference between exhaust gases leaving the cylinder and atmosphere is well used but gases still leave the turbine at a temperature significantly higher than the ambient. The idea is to use this heat and convert it into mechanical energy. The ABC heat recovery system could be a good solution for applying this idea. It consists of a compressor that admits the ambient air, compresses it and moves the compressed air to the heat exchanger where it adsorbs the heat of exhaust gases. Heated compressed air is then expanded in air expander up to almost ambient pressure, and later is expelled back to the ambient. To complete the main objective several sub-objectives had to be defined:

1. Determine the amount of energy available for recovery

   Automobile ICE work in very dynamic conditions. Energy of exhaust gases could vary significantly depending on user demands and road conditions. Selection of some engine operative conditions had to be made. For selected conditions, exhaust mass flow and temperature that define the energy of exhaust gases, have been analysed for typical passenger car diesel and petrol engines.

2. Determine the amount of energy that could be recovered in ideal cycle

   Ideal cycle considered isentropic compression and expansion, no heat or mass loses, perfect heat exchange efficiency, no friction etc. The analysis of ideal cycle was a good way to define the theoretical maximum that can be extracted by ABC.

3. Evaluate the most promising technology to be used in non-ideal cycle

   After the ideal conditions, real life conditions had to be considered. This required several technologies to be assessed, in order to search for the most promising design of the compressor, expander and heat exchanger.

4. Study non-ideal cycle in stationary conditions

   The most promising technology from the previous sub-objective was tested for stationary points. The amount of recuperated energy was evaluated along with basic machine parameters to be able to extract maximum power for each engine operating point.

1.4 Methodology

At first, a bibliographic revision was completed for several WHR technologies in order to compare them, explore their state of the art and determine why it was interesting to further study the Brayton cycle.

In order to investigate the main objective described in section 1.3, it was first necessary to do a bibliographic revision of state of the art for using ABC as bottoming cycle for waste heat recovery. Bibliographic study was done for many ABC applications in order to get the wider knowledge base, considering that some conclusions from other applications could be applied also to automotive application which is the prime target of this thesis.

After the bibliographic revision, following methodology was used to deal with the individual sub-objectives:

1. The amount of energy of exhaust gases depends on engine operating point that is engine speed and load. Some engine operative conditions had to be taken as representative. The current European legislation uses New European Driving Cycle (NEDC) as a representative cycle of typical driving in both urban and extra urban conditions. Although, its successor World harmonized Light vehicle Test Procedure is almost ready for application, NEDC cycle was used in the present work. For the engine stationary conditions, points from NEDC when vehicle speed is constant have been used. The amount of energy of exhaust gases was represented by mass flow and temperature of the gas at those points. One gasoline and one diesel engine were selected as representative typical car engines and mass flows and exhaust temperatures were measured on a test bench.
2. After determining the amount of energy of exhaust gases, the amount of energy that could be recovered in ideal cycle for stationary conditions was studied. To lower the number of variables, engine operative point was first fixed and all the parameters that affect the cycle had to be determined. Those parameters were then analysed individually. This allowed finding the optimal values for this engine operating point. Later, optimal values were determined for all selected engine operating points. The ideal cycle analysis was useful to determine the system's maximum and to eliminate more variables from the preliminary study. Nevertheless, for real life application, a non-ideal cycle must be considered.
3. Evaluating the most promising technology, for a non-ideal cycle, considered the study of existing compressor and expander machines that have a highest efficiency for given working conditions. Various technologies had to be assessed to search for the ones that can provide sufficient efficiency. The reference working condition was chosen to be one stationary point that

has a lot of energy of exhaust gas, and that is present in NEDC cycle. After choosing the technology that has good efficiency, at the reference working condition, it was important to check how it performs at other working conditions.

4. Study of the non-ideal cycle in stationary conditions started with the basic thermodynamic analysis, considering mass and heat transfer to be instantaneous, which was a very simplified approach. This was later improved by making a 0D model where these processes where modelled much more realistically. Because pressure waves can have important influence on system behaviour the model was further improved by using a 1D model of the heat exchanger and the tubes that connect it to the compressor and expander machine. The effect of pressure pulses synchronization on recuperated power was studied. A non-ideal cycle model was tested for selected engine stationary points. Computer model was made in LMS Imagine.Lab AMESim software. It is very powerful software for simulation of multi-domain systems. It contains various physical domain libraries like: pneumatic, mechanical, hydraulic, thermal, electric, signal processing etc. It also contains different application libraries like: internal combustion engines, aerospace, cooling etc. Components from those libraries can be combined to form multi-domain systems. For those reasons, it was thought that Amesim is a good tool to create a computer model of the heat recovery system.

2 Literature review

Contents

2.1 Introduction 13
2.2 Thermoelectric Generator.. 14
2.3 Rankine Cycle 18
2.4 Stirling cycle... 22
2.5 Brayton cycle... 25
2.6 Summary 30

2.1 Introduction

There are various technologies available that could be used to recuperate a part of wasted energy of exhaust gases. Some of them will be discussed in this chapter with their positive and negative sides.

Toom [11] divides exhaust gas energy recuperation on various power flows, out of which the two most important are: thermal and kinetic. For each of these flows Toom presents several solutions for waste heat recovery. These are represented in Figure 2.1and Figure 2.2 after eliminating some solutions that are thought to be inappropriate for automobile application.

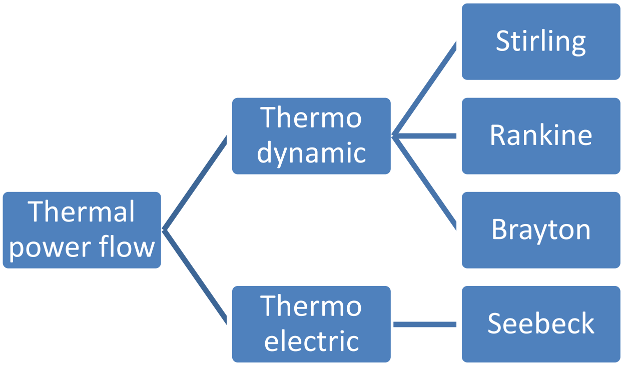

Figure 2.1. Thermal power flow WHR solutions

Thermal power flow solutions use the high temperature of exhaust gases and try to convert heat energy to other form that could be used. Thermodynamic machines at the outlet give mechanical power at the shaft that could be coupled with the engine crankshaft, to improve engine power, or the generator to produce electricity. Thermoelectric systems directly produce electricity. Electricity produced by any method could be used to charge the battery in hybrid vehicle or to run the auxiliary electrical components thereby reducing the mechanical energy used by alternator.

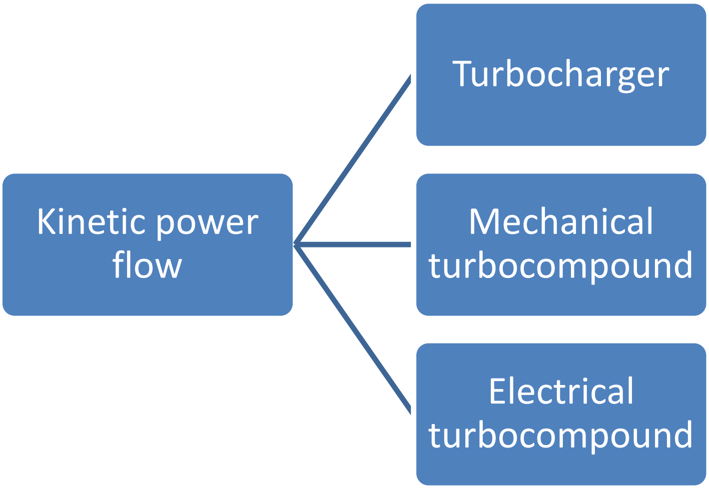

Figure 2.2. Kinetic power flow WHR solutions

Kinetic power flow solutions are much better known in automotive industry, they have been studied and used for years. Turbochargers are standard part of all diesel engines and their application on a gasoline engine is in constant growth, with the perspective of becoming the standard. Mechanical turbocompound was used in aviation since early 1940s while for heavy duty truck engines it was used the first time in early 1990s. Although, up to date, it was not used in serial car production, this technology is well known. As there is a tendency toward all car engines being turbocharged, that would leave little kinetic energy available for recovery after the turbochargers turbine. What looks like a promising solution is electrical turbocompound where the motor/generator is coupled with the turbocharger shaft. That allows recuperation of exhaust kinetic energy when there is more energy than needed to drive the compressor and to spin up the compressor in transients thereby eliminating the turbo lag.

While turbocharging is already a standard for diesel engines, it is becoming a standard also for gasoline engines driven by engine downsizing. Electrical turbocompound could be the future trend that could further improve recuperation of kinetic energy from exhaust gases. Nevertheless, that would still leave a significant energy being wasted as heat of exhaust gases. Therefore probably some form of waste heat regeneration would be necessary in the future in order to further reduce the CO2 emission. In continuation a review of most promising WHR technologies is presented.

2.2 Thermoelectric Generator

A technology that at first glance seems the easiest to apply for WHR is the thermoelectric generator, without any moving parts, directly converting temperature difference between hot and cold sides to electricity. Seebeck discovered this effect in 1821, thinking that it is a thermomagnetic effect not knowing that magnetic field is formed by generated electric current. Nevertheless, this effect today carries his name. The principle of operation is represented in Figure 2.3. The temperature difference between the hot and cold side is converted directly into electricity.

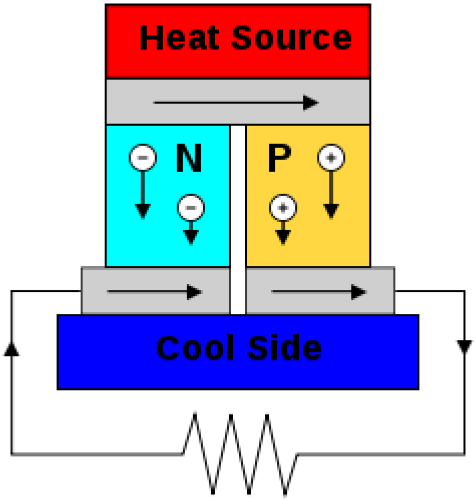

Figure 2.3. Thermoelectric generator operating principle [1]

The efficiency of the Thermoelectric Generator (TEG) to convert the heat into electricity depends on the temperatures of the hot and cold source (T_H and T_C) and dimensionless number ZT (figure of merit) being a characteristic of semiconductor materials used.

$$\eta = \frac{T_H - T_C}{T_C} \frac{\sqrt{1+ZT}-1}{\sqrt{1+ZT}+\frac{T_C}{T_H}} \tag{2.1}$$

From the Equation (2.1) it is clear that TEG efficiency is higher when ZT is higher and when the temperature difference of two sources is higher. Figure 2.4 shows the influence of these two factors on efficiency. It is assumed that T_C is 100 °C which would correspond to engine coolant being used as a cold side. It has to be noted that the cold side temperature probably would not be equal to coolant temperature. The difference between exhaust gas and hot side temperature would be even greater. These differences occur because of the imperfect heat exchangers and interface materials that connect heat exchangers and thermoelectric converters. ZT changes with temperature, for some materials it is higher with temperature rise while for others it decreases. The other problem is that not all TEG materials can stand high temperatures.

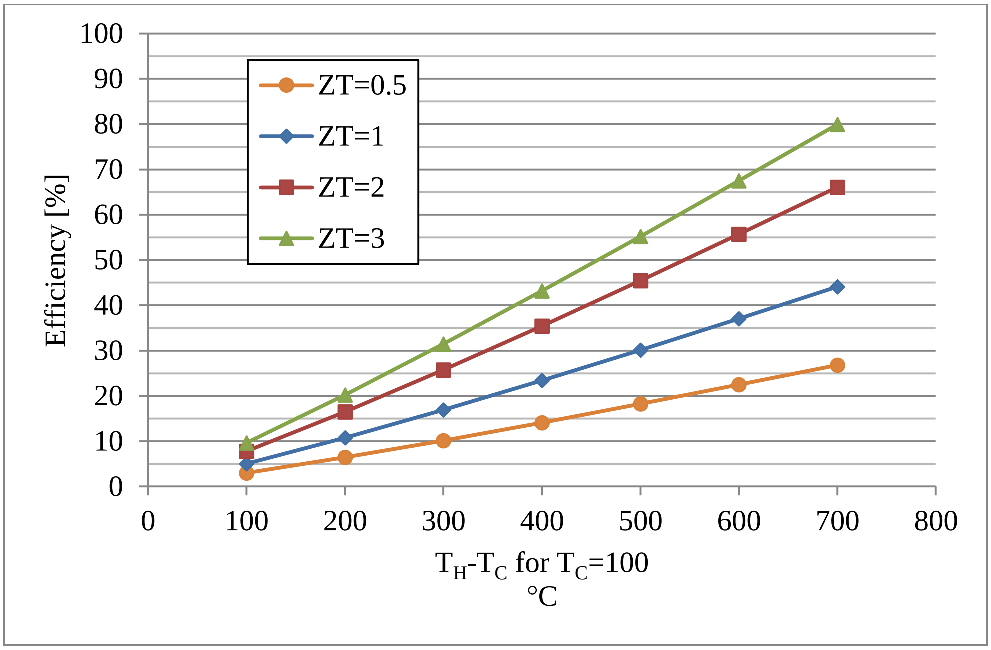

Figure 2.4. TEG efficiency as a function of ZT and temperature difference

Fairbanks [12] gives a revision of ZT values since 1940s (Figure 2.5), for materials already in use and for materials under development. Arsie et al. [13] in their 2014 article used the existing commercial Bi_2Te_3 TEGs with ZT less than 1 and expected efficiency of 1-3%, depending on hot and cold side temperatures. They applied it to Fiat Punto 1.3 l diesel engine and on the New European Driving Cycle (NEDC) they obtained a cycle average 39 W of recuperated power with maximum 410W at high vehicle speed. That would lower the CO_2 emission by 1.38 g/km on NEDC cycle. In the same article the authors say that, because of the higher temperature of exhaust gases, gasoline engine would give better results and for 1.4 l gasoline engine they presume between 60-90 W could be recovered on average. The problem of TEG is not only its low efficiency but also its power to weight ratio. Rowe et al. [14] estimates 5% efficiency and 315 W recuperated power at motorway driving condition for 1.5 l diesel engine. They find this result in accordance with the results from BMW research that obtained 200 W from 3l engine at 130km/h driving speed, and 350 W and 600 W from General Motors study on Chevy Suburban under city and highway conditions respectively. On the base of 17 different diesel cars Rowe estimated the average engine power to move 1 kg of vehicle in NEDC cycle to be 12 W. TEGs are heavy and their additional weight should be considered. Bi_2Te_3 modules used by Arsie and BMW in optimal conditions could produce 170 W per kg of TEG. Arise [13] used 80 modules each weighting 83 gr making a total of 6.6 kg, adding heat exchanger weight it easily reaches 10 kg. For a 10 kg generator that would mean 120 W of power should be recuperated just to compensate for extra weigh added. If sufficient electricity could be generated to eliminate the alternator it would lower the weight by some 5 kg. Additional weight further brings down the already low recuperated power by TEG.

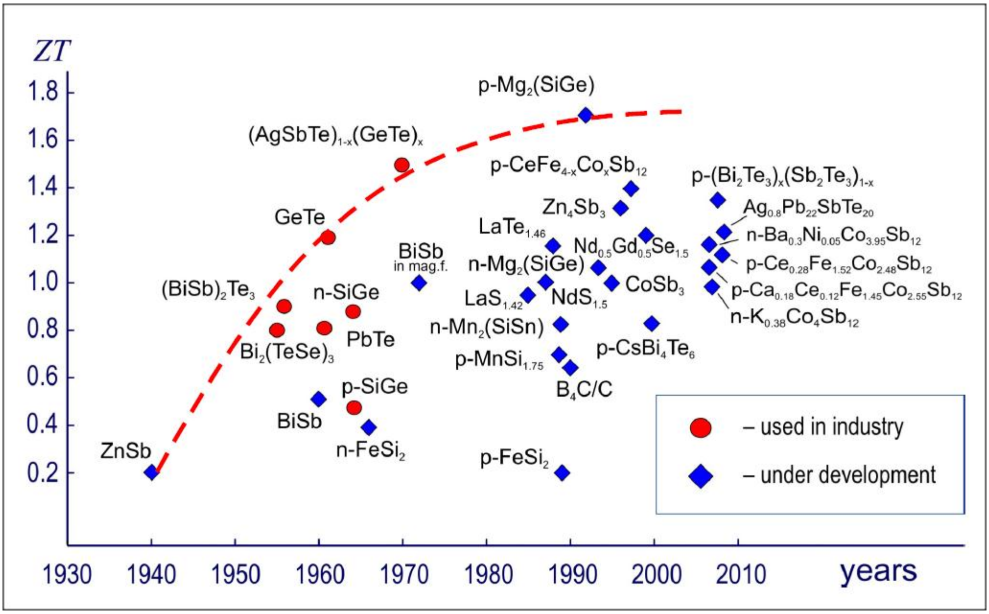

Figure 2.5. ZT increase in time with new materials [12]

Bass et al. [15] experimentally recuperated 1 kW from a 14 l diesel engine using 72 Hi-Z HZ-13 cells. Using the first heat exchanger design they were only able to recuperate 400 W, exhaust gas boundary layer was laminar and affected the heat transfer significantly. At the final version when they added swirl fins to provoke turbulent flow, they managed to recuperate 2.5 times more power just by intensifying heat transfer. High heat exchange efficiency is important at the hot side, but also at the cold side where better results are expected using engine coolant that has higher temperature but much better heat exchange.

Crane et al. [16] theoretically investigated thermoelectric heat recovery from the coolant radiator. In comparison to heat recovery from exhaust gas the advantage is better heat transfer from liquid to hot side and from air to cold side because of the much higher air mass flow and forced convection at coolant radiator. Another advantage is weight saving because the radiator is already present in the vehicle. A disadvantage is much lower temperature difference. In this case the hot side could have maximum temperature of around 120 °C, limited by the temperature of evaporation of coolant, and cold side temperature of around 37 °C (what they consider to be the temperature under the hood for warm engine). They estimate that even at 25% engine load 1 kW of electricity can be generated eliminating the need for an alternator and saving 5 kW of engine power otherwise needed to drive the alternator. At full load they estimate 2 kW of recuperated power. These results seem too optimistic and would have to be validated experimentally.

Thermoelectric generators are promising technology for Waste Heat Recuperation but currently still with insufficient efficiency and big weight. In car application the highest experimentally confirmed recuperated power was 600 W at highway speed. This performance is lower than it is expected from other WHR technologies. Price was not analysed in this study but it is another aspect this technology has to improve. Original Equipment Manufacturers (OEM) are very interested in it because of its robustness without any moving parts and its reliability. Confirmations of their reliability are Voyager I and II probes whose TEGs are still functional 38 years after the launch to deep space [17].

2.3 Rankine Cycle

Rankine cycle is a closed cycle that converts heat to mechanical energy. Traditionally, the cycle uses water as a working fluid, and when organic fluid is used the cycle is called Organic Rankine Cycle (ORC). The cycle contains four processes that are represented in Figure 2.6: 1-2 the working fluid is pumped to high pressure, as the fluid is liquid in this stage the work required by the pump is small; 2-5 the high pressure liquid enters the boiler where it evaporates at constant pressure until becoming the dry saturated vapour (point 4) or superheated vapour (point 5); 5-6 the vapour expands in the expander producing mechanical work and decreasing the temperature and the pressure of vapour; 6-1 the vapour gets condensed in condenser at constant pressure to become a saturated liquid.

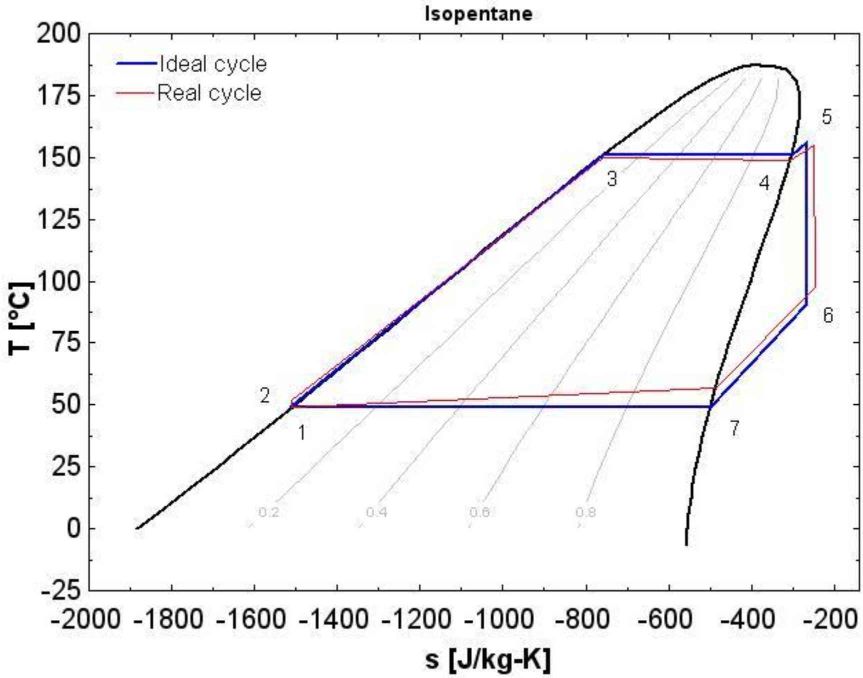

Figure 2.6. Ideal and real ORC [1]

In the ideal cycle, the pumping and the expansion is isentropic while in a real cycle there are irreversibilities in those processes and there are pressure drops in heat exchangers. The cycle could be improved by using regeneration, as the temperature after the expansion is higher than the temperature after the pump, this heat can be used to warm the fluid before entering the evaporator. Configurations with and without the regenerator are presented in Figure 2.7.

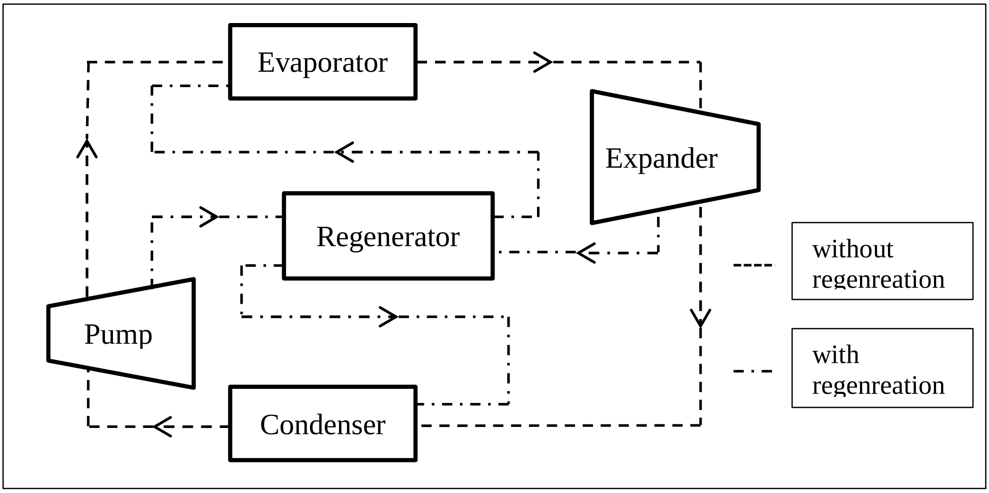

Figure 2.7. Rankine cycle schematic with and without regeneration

Rankine cycle was a well-known technology in power plants applications. ORC systems started appearing in 1970s for geothermal, solar and industrial WHR applications. About the same time, during the energy crisis, first studies were conducted for WHR of engine exhaust gas energy. For example, Patel and Doyle [18] investigated the application of ORC as a bottoming cycle on 288 bhp truck diesel engine and concluded that at peak engine power 13% more power could be achieved without the use of additional fuel. That results in 15% fuel consumption reduction. After the first energy crisis, the interest in ORC for engine WHR decreased but the interest increased recently and a lot of OEMs are considering it. Many experimental and theoretical studies have been conducted, using various types of expanders: turbine, reciprocating piston, Wankel, rotating vane etc. As this thesis is focused on car application it is interesting to analyse the studies done for this application. The main technical problem in applying bottoming Rankine cycle in automobile is the lack of space to place all the components. Like for the other WHR systems additional weight is also important as it has the negative impact on fuel consumption reduction.

Endo et al. [19] from Honda used water as a working fluid. In their experimental study they managed to improve the engine thermal efficiency from 28.9% to 32.7% at the engine condition that corresponds to the car speed of 100 km/h. The 2 litre gasoline engine they used at this point gives around 20 kW of effective power. Resulting fuel consumption reduction would be 11.6%. The evaporator was integrated with cylinder head and exhaust ports to receive the maximum heat. Fins with a catalytic material were placed inside the evaporator and it served as a catalytic converter as well. Chemical catalytic reactions further raised the temperature in the evaporator and improved the heat exchange. Integration with the cylinder head and the catalyst gives a high evaporator heat exchange efficiency of more than 90%, and a compact design results in total volume around 1.8 times higher than the standard catalytic converter, which is a good result. The expander was a swash plate with 7 pistons. At the end of the expander shaft there was an electrical generator so that the output was electricity. The authors state that the maximal thermal efficiency of the expander was 13%. They do not separate the efficiency of the expander alone and the efficiency of conversion from mechanical to electrical energy but it is reasonable to believe that mechanical power output would be considerably higher because of the inefficient conversion. Probably the expander alone could be further improved. As the overall design was compact they managed to place all the components into the engine bay of a standard car. It was possible to recuperate energy when vehicle speed was higher than approximately 40 km/h. Control for the system was developed so that in the Highway Fuel Economy Test (HWFET) it was possible to recuperate energy during the whole test even though the engine load was varying significantly.

A year later in 2008 Kadota and Yamamoto [20] continued Hondas research on Rankine cycle WHR. This time the focus was on transient behaviour in configurations with conventional engine and hybrid vehicle. Evaporator/catalyst was not integrated with the cylinder head, but was mounted just behind the exhaust manifold. The expander and the rest of the installation was the same. Thermal efficiency of the recovery system was around 10% in a wide operating range from 1 to 3 kW of recuperated power. At Japanese 10-15 Mode driving cycle the overall average engine thermal efficiency has been improved from 29.5 to 31.3% even though this cycle is not favourable for WHR because of low vehicle speed and low steam energy. These studies by Honda show a great potential and present the system almost ready for serial application, but there are some doubts about the durability of evaporator because of the high steam pressure and corrosive fluid that could lead to cracks.

Another manufacturer that put significant effort toward investigation on Rankine cycle application in cars is BMW with the series of articles [21]–[24]. They first started with a bit idealized setup, having in mind serial production, consisting of two loops: high temperature for exhaust gas and low temperature for recuperation of heat from engine coolant. Each loop had its own fluid and expander. With this idealized setup they obtained around 14% nominal fuel consumption reduction. In the other configuration, they used one loop with preheating of working fluid in the coolant heat exchanger and main evaporation in the exhaust gas heat exchanger. Maximal recuperated power was 2 kW and fuel consumption reduction of 10%. The last study considered full integration of WHR with other vehicle systems. Water was used as fluid, the expander was an impulse turbine with coupled generator producing electricity as outlet. Heat exchangers, expander and all other components were small enough to be placed on the bottom of the car. It was concluded that restrictions in power output (it could not be greater than the consumption, on board system was not capable of storing additional electric energy), increased weight, package considerations (placing the evaporator further down the exhaust line results in lower inlet temperature because of heat lost to ambient), increased cooling demand, exhaust gas back pressure, lead to significant reduction of fuel saving of only 1.3%. In comparison to the Honda study, the vapor pressure was much more modest at 7 bar. Proposed improvements included the use of toluene as working fluid, raising evaporation pressure to 15 bar, improving turbine efficiency to 60%, thermally isolating exhaust line before evaporator and reducing system weight to 15 kg. With these improvements fuel consumption reduction would be 2.3%. Even with further improvements maximum fuel saving reduction would be limited to 3.4% by the maximum electrical power demand of the vehicle. If vehicle electrical consumption was 1500W (using electrically driven power steering pump, air conditioning compressor, water pump etc.) instead of 750W used in the study, representing typical demand of BMW series 5, the fuel consumption reduction could be up to 4%. It should be noted that, like in the study by Honda, the system is only functional above certain car speed when there is sufficient heat to be recovered. Below that speed power consumed by the system is greater than the power produced and WHR should be decoupled. Better results could be expected if the system is applied to hybrid vehicle thereby power output would not be limited by on-board power demand as batteries could store the generated electrical energy.

Sprouse and Depcik [25] in 2012 gave a good review of the literature published on Rankine cycle waste heat recovery from internal combustion engines. Both heavy and light duty applications were analysed with various types of expanders, fluids and configurations (heat recovery from one or many sources: exhaust, cooling, EGR). They concluded that turbomachines are preferred for large output systems while displacement type expanders dominate small scale applications. Regarding the working fluid they did not decide on any particular one, but mention that the selection requires consideration of operating conditions, environmental concerns and economic factors. Theoretical models are often too optimistic not taking into account losses like heat transfer to the ambient or mechanical losses. Experimental studies produced roughly half the power of idealized models. Realistic expectations are in the range of 7-10% fuel economy improvement. From the economical perspective they estimate that fuel consumption reduction could pay off the system cost within 2-5 years.

One study that is not focused on car application but on heavy duty commercial vehicles (nevertheless it is interesting for this revision), is a study from Bosch [26]. The group of authors used two types of expanders: two-stage turbine and single cylinder double acting piston. The former is more interesting as it is not found in other studies. Piston rings and valves were not lubricated while crank mechanism and valve train are lubricated with engine oil. The crank drive was a Scotch yoke which permits smaller dimensions than cross-head design and stresses the piston only with longitudinal forces. The durability of Scotch yoke mechanism is questionable but it was not assessed in the study. Apart from the two expander types, five different fluids were tested: water, toluene, MM (hexamethyldisiloxane), ethanol and R245fa. Simulation model was made and confirmed experimentally on various points of European Stationary Cycle (ESC) for heavy duty vehicles. The authors of the study conclude that the most favourable solution is either a piston machine with water or ethanol as working fluids or a turbine with ethanol as a working fluid. At the optimal engine operating point, both piston and turbine with corresponding optimal working fluid augmented engine power by around 5% without additional fuel. This system could be scaled and applied to passenger cars.

There are many other studies on Rankine cycle WHR. The ones mentioned in this revision are the closest to the objective of application in automobiles. This application is specific because of several factors: limited space available for component placement, weight considerations because weight increase negatively affects, ICE efficiency drop because of backpressure at exhaust caused by placement of a heat exchanger in the exhaust line, limited working fluids that could be used on vehicle etc. The principle problems of Rankine cycle application in cars are packaging, additional fluid needed and complexity. The main advantages are its relatively good efficiency, existing and relatively non expensive technology. While the efficiency of Rankine cycle of 10% does not seem like a very good result it is almost the double than TEG with a considerable more complexity.

2.4 Stirling cycle

Robert Stirling patented his engine in 1816. It was an external combustion engine that could transform chemical energy of burned fuel into mechanical energy. The ideal cycle consists of isothermal compression 1-2, isochoric heat addition 2-3, isothermal expansion 3-4 and isochoric heat removal 4-1. The ideal cycle is represented with continuous line in Figure 2.8. In the real engine it is difficult to achieve those ideal processes [27], also the processes slightly overlap and the pressure-volume diagram assembles more to a discontinuous line on the same figure.

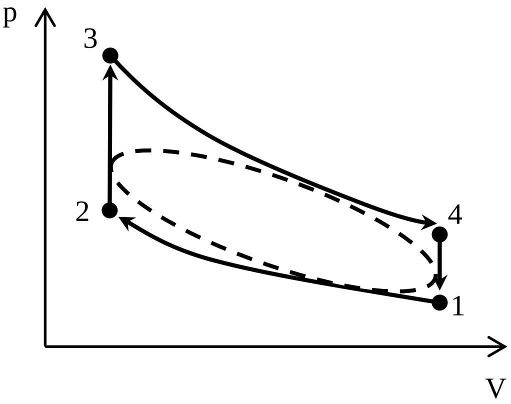

Figure 2.8. Stirling cycle p-V diagram

Apart from burning the fuel directly to provide the heat, Stirling engine can use any other heat source. That's why this engine could be used for waste heat recovery by using the heat of the exhaust gases as a hot source. Bianchi and De Pascale [28] compared three different cycles for waste heat recovery of low temperature heat sources like internal combustion engine or gas turbine exhaust gases. One of the cycles considered was Stirling cycle. Curve of the Stirling cycle efficiency as a function of temperature of the hot source that they predicted is given on the Figure 2.9.

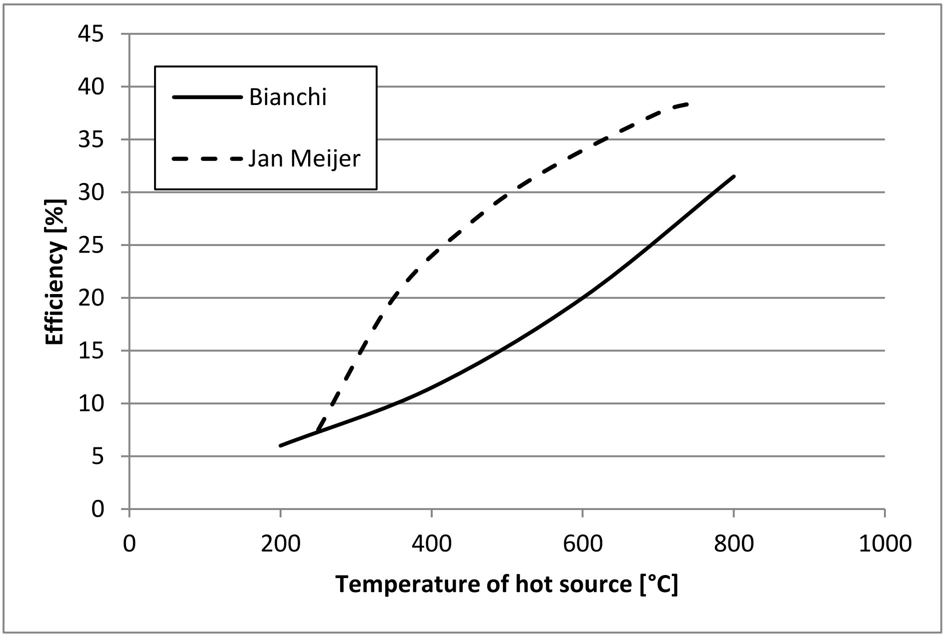

Figure 2.9. Stirling cycle efficiency as a function of hot source temperature

The basis for their prediction was the cycle efficiency of 28% at the temperature of 800 °C. Authors didn't say what was the pressure used for these calculations. On the same figure is presented also the curve of results from Jan Meijer[29] who experimentally investigated the Stirling engine that could produce 32 HP at the pressure of 140 bar and heater temperature of 750 °C. The given curve is for the fixed pressure of 140 bar that was the maximum pressure allowed and variable heater temperature. Results obtained by Jan Meijer were quite impressive taking into account that this research was conducted for his PhD Thesis in the year 1960. This thesis was a continuation of work at Philips on a development of a Stirling engine. In the 1950s Philips made the first modern Stirling engine that was produced in a larger number, around 150 units of a generator named MP1002CA that could produce 200W of electricity. Although, this engine didn't have a commercial success it was very important for further research. Another engine that had important influence on future development was the GPU 3. It was a 3 kW generator that General Motors developed for Unites States Army in 1965. In the late 1970s NASA used this engine for a research on possibility to use Stirling engine for vehicle propulsion [30]. Almost 40 years later researches still use experimental results of this engine to validate their model and compare the improvements [31], [32].

Thombare and Verma [33] gave a review of the technological development of Stirling engines. Kongtragool and Wongwises [34] did the same but putting more focus on the solar powered engines that use lower temperature difference of hot and cold heat source. From these publications it can be seen that engine efficiency and power depend on several parameters like temperatures of hot and cold sources, swept volumes, cycle pressures, heat exchanger efficiencies, working fluid characteristics etc. The efficiency is higher when: difference of temperatures of hot and cold sources is higher, efficiencies of heat exchangers are higher, regenerator efficiency is higher, flow and mechanical losses are lower etc. The power is higher when temperature difference of hot and cold sources is higher, cycle pressure is higher, engine spins faster etc. Also they reveal advantages and disadvantages of Stirling engines, the former being possibility to use various fuels, silent operation, cleaner combustion while the latter are relatively difficult power control, low specific power, bulky design.

Organ [35] in his book says that 200 years since the invention of Stirling cycle the industry still did not embrace this technology. Technological advance is slow because of proprietary exclusivity of the companies that develop the technology.

Regarding the waste heat recovery, Stirling cycle shows good potential at higher temperatures of waste heat source. During the literature review it was noted that there is the lack of literature regarding the use of Stirling cycle for WHR. Probably the biggest disadvantage of this technology, in comparison to others, is its low maturity and spreading among the car industry.

2.5 Brayton cycle

First studies of Brayton cycle as a bottoming cycle for waste heat recovery started appearing in the middle of 1980s. One of the first was a study by Bailey [36] who in 1985 compared three bottoming cycles, Rankine, Organic Rankine and Brayton for waste heat recovery of a truck “adiabatic” diesel engine exhaust gases. The engine was called adiabatic because it was thermally isolated with no water cooling thereby reducing in-cylinder heat loss. As a consequence, the temperature of exhaust gas was higher than in a typical diesel engine varying between 571 and 671 °C depending on configuration (with or without intercooler or/and turbocompound). Conclusion was that ORC was most efficient with 15% improvement of specific fuel consumption followed by Rankine with 14 and Brayton cycle with 8% improvement. The improvement of Brayton cycle could be 10% if two-stage compressing with intercooling is used. The author doesn’t give information about the efficiencies of machines and heat exchangers for any cycle although it can be calculated that Brayton cycle HE efficiency was 93.5 %. Later it will be demonstrated that those values along with exhaust gas temperature have a great influence on cycle comparison.

About the same time (1985 in US, 1986 in Europe) Farrell files a patent application for air bottoming cycle for heat recovery of industrial gas turbine [37]. In 1992 Wicks et al. [38] investigated the ideal air bottoming cycle. According to them combustion engines should not be compared to Carnot cycle because temperature of the exhaust gas as a heat source is not constant. Exhaust gas is rather a finite size hot reservoir whose temperature drops from maximum to ambient temperature. According to authors the ideal cycle would be triangular consisting of isothermal compression, heat addition and isentropic expansion as it is represented on the Figure 2.10. As such, the cycle actually does not represent the Brayton cycle but it is an interesting air bottoming cycle. Authors further concluded that triangular cycle is better suited for bottoming cycle than for topping cycle where it would require too high pressure ratio. Realization of isothermal compression could be approximated by using various intercooling stages. While for the stationary industrial application this could be possible for vehicle application it would be very hard because of limited packaging space and complexity.

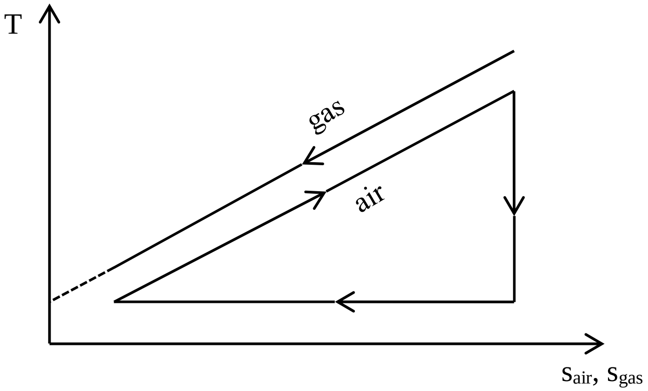

Figure 2.10. Ideal bottoming cycle by Wicks

Bolland et al [39] in 1996 considered Air Brayton Cycle (ABC) for gas turbine bottoming cycle on oil platforms. They concluded that air mass flow rate of the ABC is determined by fixing the $\dot{m}c_p$ratio between the cold and hot side to unity in order to minimize the heat transfer area. This was the first study to consider ratio of mass flows of topping and bottoming cycles. Other important conclusions were that there is an optimal compression pressure that gives maximum efficiency and it depends on number of intercoolers. Without intercooler optimal pressure ratio was around 4 and combined topping/bottoming efficiency was 43% while for 1 intercooler optimal pressure ratio was around 6 with combined efficiency around 45.5%. Further increasing of number of intercoolers doesn't bring as much benefit. Using two-stage compressing with intercooling in vehicle application could be hard to implement due to the small size requirements but it is still interesting to see the effect of cooling during compression on optimal pressure ratio and efficiency. Turbine polytropic efficiency was estimated at 90% while for the heat exchanger and compressor it was not explicitly given. They estimated that efficiency would improve from 36.1% for basic gas turbine to 46.2% for combined cycle.

Another group of authors that was studying ABC for power plant application was Kaikko et al [40] in 2001. They came do similar conclusions as Bolland about mass flows of air and exhaust gas, optimal pressure ratio and number of intercoolers. But, they also conducted sensitivity studies to demonstrate the influence of specific parameters on efficiency. It was shown that the temperature of the exhaust gas has the biggest influence followed by the efficiencies of compressor and expander. Heat exchanger efficiency was the least influential. Furthermore, the article gives comparison of ABC and ORC as bottoming cycles for two kinds of topping cycles: gas turbine and diesel engine. Basic characteristics of bottoming and topping cycles used in the study by Kaikko are given in Table 2.1.

Air Brayton Cycle	Organic Rankine Cycle	Gas Turbine	Diesel Engine
Compressor efficiency 91%	Turbine efficiency 80%	Power 7.8 MW	Power 16.8 MW
Turbine efficiency 86%	Feed pump efficiency 50%	Exhaust temperature 534 °C	Exhaust temperature 400 °C
Heat Exchanger efficiency 93%	Condenser temperature difference 7.5 °C		

Table 2.1. Basic characteristics of bottoming and topping cycles

For gas turbine, reductions of CO_2 estimated with ABC and ORC were 22.4% and 24.1% respectively. For diesel engine, reductions of CO_2 were more modest at 6.2% and 7.2%. As in the study by Bailey, the ORC was more efficient for both topping cycles but authors state that for the temperatures of exhaust higher than 680 °C Brayton cycle would be more efficient.

The industrial application of Brayton cycle reviewed in these last few publications doesn’t impose strict limitations like its application in passenger vehicles. It considers few compression stages with intercooling, big heat exchangers, any kind of machines not paying attention to size and weight. Nevertheless, principal conclusions about the parameters affecting the cycle efficiency are valid for both applications.

Song et al. [41] simulated Brayton cycle coupled with a heavy duty 11 liter diesel engine. What was interesting in this study was the Brayton machine selection, there was no separate compressor but the same engines compressor was used where part of its outlet was directed to Brayton cycle and the rest to the engine inlet. For the expander, separate turbine was coupled to electric generator. Significant mass flows needed for Brayton cycle affect the coupling between the engine and turbo compressor. Authors investigate how different turbine and compressor mass flow multipliers would affect the system performance. At design condition WHR turbine had the efficiency of 80% while heat exchanger efficiency was 95%. Compressor efficiency and temperature of exhaust depended on engine operative point. While engine speed was variable all simulation points were at full load. Authors conclude that fuel economy improvement could be 2.6% and 4.6% at high and low engine speed respectively. While this configuration could be interesting for the engines that work at stationary conditions, for passenger vehicles engines that work in very dynamic conditions compressor efficiency would be problematic at part load.

Xu et al. [42] introduced an interesting concept to separate the Overall Energy Conversion Efficiency (OECE) to Energy Recovery Efficiency (ERE) and Energy Conversion Efficiency (ECE) in order to compare different bottoming cycles. ERE represents how good is the heat transfer from hot to cold fluid while ECE describes how good is the conversion from heat of the cold fluid to mechanical or electrical energy. The bottoming cycles compared were saturated vapour Rankine cycle, overheated Rankine cycle and Brayton cycle. For the Brayton cycle, apart from the standard cycle, the cycle with heat regeneration and the cycle with isothermal compression were considered. The target application was for a passenger car with the exhaust temperature of 800 K. As in the studies by Kaikko and Bolland, they concluded that for ABC there is an optimal compression pressure, in this case around 5 bar. Separating efficiencies allows easier recognition of influences on optimal compression pressure. As it can be seen from the illustration on Figure 2.11 ERE decreases with compression pressure because temperature after the compression is higher and less heat can be recovered while ECE increases with compression pressure.

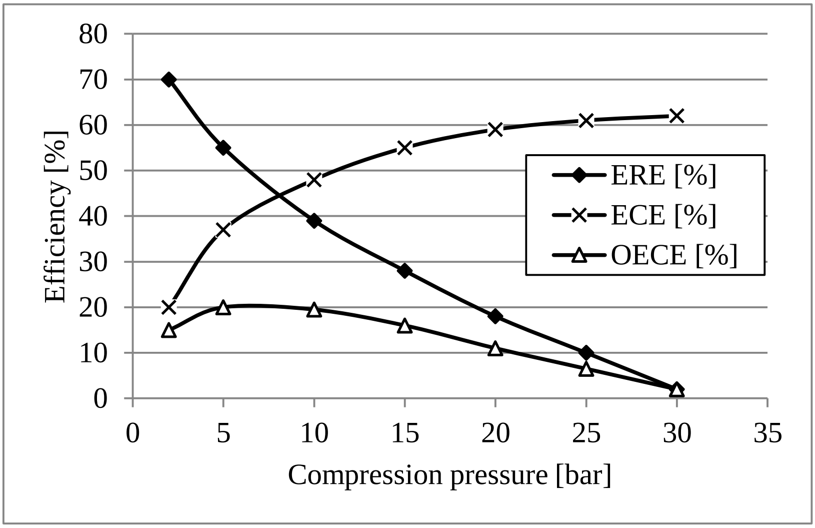

Figure 2.11. Brayton cycle efficiencies by Xu et al.

Maximum to minimum overall efficiencies obtained were: Brayton cycle with isothermal compression, Brayton cycle with regeneration, standard Brayton cycle, superheated Rankine cycle, saturated vapour Rankine cycle. Although Brayton cycle with isothermal compression gave the best result its practical application is considered very hard because too much heat would have to be extracted from cylinder which cannot be done just by heat transfer. Injection of water or other liquid with high latent heat into the cylinder could allow isothermal compression but its application on passenger cars is questionable because of the need to carry on board another fluid and complexity. The classification of cycle efficiencies was highly influenced by boundary conditions which were beneficial for Brayton cycle: high exhaust temperature and isentropic compressions and expansions.

Regarding other kinds of publications there is an interesting patent by Toyota [43]. It introduces an accumulator to store the pressurized air when heat receiving capacity of air is small or exhaust heat is too little for cycle to produce sufficient energy. Pressurized air could be later used for classic Brayton cycle being passed through heat exchanger and expanded in expander or being directed to engine inlet to rise the engine charge and therefore power when needed or director to catalyst inlet as a secondary air source to improve catalyst reaction for example at cold start when mixture is rich. The latter two applications are illustrated on Figure 2.12 as dashed and dotted lines respectively. From the same figure it can be seen that compressor and expander are separate reciprocating pistons.

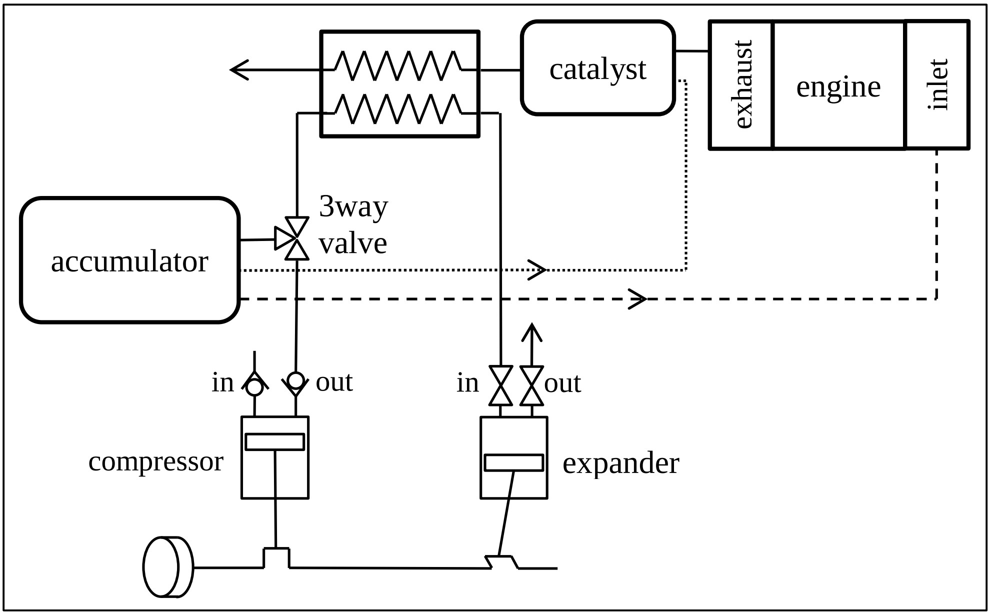

Figure 2.12. Schematic of Toyota patent for Brayton cycle

Other important aspect of this patent is that it considers the way to reduce pumping losses when cycle should not be operative i.e. low engine speed low load points. The way to do it is to close the compressor outlet valve to eliminate compressor work and to close the expander outlet to reduce pumping losses. The 3 way valve should connect in all possible combinations two out of three volumes: compressor, accumulator, heat exchanger. Compressor inlet and outlet valves are automatic reed valves while the expander valve should have controllable timing of aperture and closing. Electronic Control Unit (ECU) should control valves operation based on information from accumulator pressure sensor, exhaust temperature, engine speed etc. This system is more complex than standard Brayton cycle but it could eliminate its drawback to be unfunctional at low speed low load engine working condition.

Thevenod filed patent applications for two inventions on Brayton cycle for WHR. What is common in both patents is the innovative use of the same reciprocating piston machine for both compression and expansion. It works as a four stroke engine where two strokes are dedicated to charge and discharge of a low pressure loop while other two are for charge and discharge of a high pressure loop.

In the first patent [44] low pressure loop is connected to the ambient so it is an open Brayton cycle. In the second patent [45] the low pressure loop could be connected to ambient or closed loop. In the closed low pressure loop pressure could be higher than atmosphere, the patent suggests it to be 1 to 10 bar. As a consequence pressure of the high pressure loop is proportionally higher which results in better efficiency. Also, in the second patent, inventor contemplates using an accumulator but in comparison to Toyotas patent not for passing the pressurized air to engine or catalyst inlet but to raise the pressure in the low pressure loop. Timing of the high pressure loop valves can be controlled so that the mass flow rate entering is higher than mass flow rate leaving the high pressure loop thereby raising the pressure and working as engine brake. The pressurized air can be stored in accumulator to be used later.

After conducting the literature review it was concluded that there are very few publications on what seems to be a promising WHR technology.

2.6 Summary

In this chapter, the literature review for technologies that seem more promising for waste heat recovery of exhaust gases energy in passenger cars was given. Thermoelectric generators (TEGs) have principal advantage of being very simple but despite the ongoing research and improvements they still have low efficiency and high cost. For the moment, until more efficient TEGs are being developed, the main aim of their application could be to eliminate the need for alternator thereby lowering the fuel consumption and emissions. If TEG is applied to heat recovery from engine coolant it could be compatible with other technology being used for exhaust gas heat recovery. In contrast to TEG, Rankine cycle is the most complex technology from the ones considered but with a highest efficiency. Although for high exhaust gas temperature applications (gasoline engines) Brayton cycle could be competitive, at low temperatures (diesel engines) Rankine cycle (using organic fluid) is a clean winner. Nevertheless, Rankine cycle application has significant disadvantages in the need to use another fluid, having this fluid at high pressure and high temperature which could cause breakdowns and leakages and the need for two heat exchangers that complicate components packaging. Selecting the right fluid is also a challenge. The fluid need to poses good thermodynamic characteristics to provide efficient cycle but at the same time to have low freezing point, high flash point, low Ozone Depletion Potential (ODP), low Global Warming Potential (GWP), low toxicity etc. All this makes Rankine cycle application complicated. Stirling cycle could provide good efficiency but even though it is the subject of research for many years, technological maturity is not at the high level. It has a relatively complicated mechanism and packaging could be a problem. It was considered that Brayton cycle could be a better choice than Stirling because efficiency is similar but it could use the technology that vehicle manufacturers are more familiar with like a traditional crankshaft and alternating piston.

	Efficiency	Packaging and weight	Costs	Control	Maturity
TEG	-	+	-	+	-
Rankine	+	-	-	-	+,-
Stirling	+	-	-	-	-
Brayton	+,-	-	+	+	-

Table 2.2. Comparison of WHR technologies

All of the mentioned technologies show the potential but the literature review revealed that in the case of Brayton cycle there is a significant lack of publications and it was considered that it deserves more investigation which was defined as the objective of this thesis.

3 Thermodynamic analysis

Contents

3.1 Introduction 35
3.2 Engine energy levels... 35
  3.2.1 Gasoline engine 38
  3.2.2 Diesel engine 39
3.3 Cycle description 40
  3.3.1 Ideal cycle 43
    Mass flow effect 44
    Pressure ratio effect 46
  3.3.2 Machine selection... 50
    Compressor selection 50
    Expander selection 52
    Conclusion.. 53
  3.3.3 Non-ideal cycle 53

3.1 Introduction

Literature review on different technologies for WHR was presented in the previous chapter. It was explained why the Brayton cycle is considered to be the appropriate choice. Literature review for this cycle revealed the basic parameters that influence cycle efficiency. In this chapter the cycle will be explained more in detail. Firstly, the ideal cycle with isentropic compression and expansion processes and very efficient heat exchanger will be presented. Later on, the type of machines that could be applied for this application will be discussed, and their efficiencies will be estimated in order to analyse the cycle with the realistic values of isentropic efficiency. Two types of heat sources for energy recovery will be considered: gasoline and diesel engine of a passenger car.

3.2 Engine energy levels

In order to recuperate some part of energy of the exhaust gas, it is important to know the amount of the energy available. The energy level of the exhaust gas coming from the Internal Combustion Engine is determined by the mass flow rate and temperature, and these values will depend on engine operative point. As ICE has a wide operative range, some working points had to be selected for further analysis.

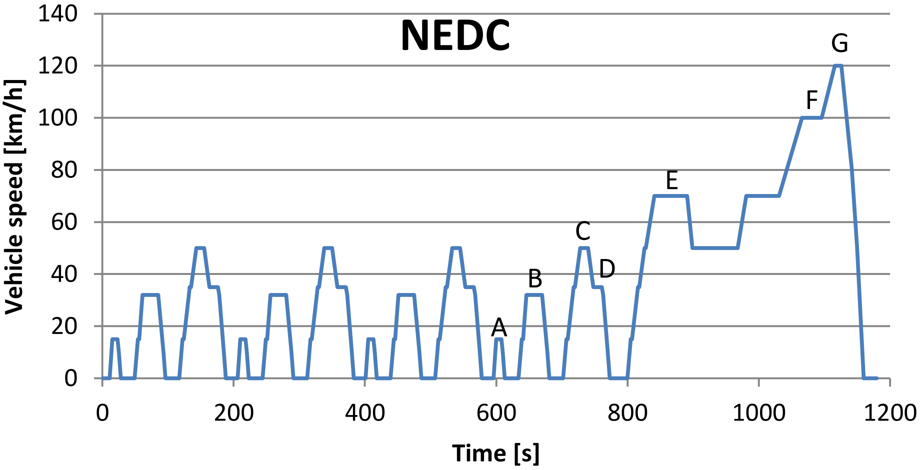

Figure 3.1. NEDC points

The New European Driving Cycle (NEDC) that represents the vehicle speed as a function of time is shown in Figure 3.1. Points from the NEDC marked with letters A-G have been selected as a reference engine operating points. It means that those constant vehicle speeds were taken and for each of them separate stationary test measures were taken to have well established values for temperature and mass flow. Values from NEDC transient cycle could not be used directly because stationary period of each point is not long enough for the temperature and mass flow to stabilize. The vehicle speed and transmission gear for each point, as it is defined in UN/ECE regulation No 83 [46], is presented in Table 3.1

Point	*Vehicle speed [km/h]*	*Transmission Gear*
A	15	1
B	32	2
C	50	3
D	35	3
E	70	5
F	100	5 or 6
G	120	5 or 6

Table 3.1. Vehicle speed for NEDC points

For the points F and G, if the vehicle transmission has 6 gears, the 6th gear should be used for these points. To determine engine working point (rotary speed and load) for a given vehicle speed some vehicle characteristics have to be known.

If it is assumed that there is no slipping between the wheel and the ground or anywhere else inside the transmission path then the engine rotary speed would be related to the vehicle velocity by:

$$\omega_E = v_{veh} \frac{60}{2\pi R_{wh}} TR_{GB} TR_{FD} \tag{3.1}$$

where $\omega_E \left[\frac{rev}{min}\right]$ is the engine rotary speed, $v_{veh} \left[\frac{m}{s}\right]$ is the vehicle speed, $R_{wh}[m]$ is the wheel radius, TR_{GB} is the gearbox transmission ratio and TR_{FD} is the final drive transmission ratio.

Wheel radius is calculated by:

$$R_{wh} = \frac{1}{2} D_{rim} + \frac{H}{100} W \tag{3.2}$$

where $D_{rim}[m]$ is the rim diameter, $H[\%]$ is the height of the tire expressed as percentage of tire width $W[m]$.

Engine torque, representing the engine load, will depend on resistances to vehicle motion and it is calculated by:

$$\tau_E = (F_{dr} + F_{aero}) R_{wh} \frac{1}{TR_{FD}} \frac{1}{TR_{GB}} \frac{1}{\eta_{TR}} \tag{3.3}$$

where $\tau_E[Nm]$ is the engine torque, $F_{dr}[N]$ is the driving force, $F_{aero}[N]$ is the aerodynamic drag force and η_{TR} is the total efficiency of transmission(gear box and final drive).

Driving force is calculated by:

$$F_{dr} = \left(m_{veh} + 4\frac{J_{wh}}{R_{wh}^2}\right)gf \tag{3.4}$$

where $m_{veh}[kg]$ is the vehicle mass, $J_{wh}[kgm^2]$ is the wheel moment of inertia, $g = 9.81\frac{m}{s^2}$ is the gravitational acceleration and f is the rolling friction coefficient.

Aerodynamic drag force is calculated by:

$$F_{aero} = \frac{1}{2}\rho_{air}c_x A_{front}v_{veh}^2 \tag{3.5}$$

where $\rho_{air}\left[\frac{kg}{m^3}\right]$ is the density of ambient air, c_x is the aerodynamic drag coefficient and $A_{front}[m^2]$ is the vehicle active frontal area.

Some parameters were considered to be constant regardless of the vehicle type, vehicle speed or engine type and are presented in Table 3.2.

Parameter	*Value*
$J_{wh}[kgm^2]$	0.8
f	0.01
$\rho_{air}\left[\frac{kg}{m^3}\right]$	1.2
η_{TR}	0.9

Table 3.2. Constant vehicle parameters

Two types of engines will be considered: gasoline and diesel. The choice of diesel and gasoline engines for further study was primarily determined by the engines available at CMT-Motores Termicos (CMT) at that moment. Nevertheless, both engines are used in European D-segment large passenger cars, which could be the target platform for WHR application.

Engine efficiency was calculated by:

$$\eta_E = \frac{P_E}{Q_{comb}} \tag{3.6}$$

where P_E is the engine power measured on the test bench and Q_{comb} is the energy obtained by combustion of fuel defined by:

$$Q_{comb} = LHV \cdot \dot{m}_{fuel} \quad \text{for} \quad \lambda < 1$$
$$Q_{comb} = LHV \cdot \frac{\dot{m}_{air}}{AFR} \quad \text{for} \quad \lambda > 1 \tag{3.7}$$

where LHV is the lower heating value of fuel, AFR is the stoichiometric ratio of air and fuel, λ is the equivalence ratio (λ<1 rich mixture, λ>1 poor mixture). The values of LHV and AFR for each fuel were taken from [2].

3.2.1 Gasoline engine

Gasoline engine that was chosen as a representative was Ford EcoBoost 2 litre turbocharged engine. It is a modern engine with direct fuel injection and double wall exhaust manifold. Its main characteristics are given in Table 3.3.

Parameter	*Maximum Values*
Displacement [dm^3]	2
Power [kW]	153
Revolutions [rev/min]	6500
Torque [Nm]	308
Mass flow [g/s]	179
Exhaust temperature [°C]	908

Table 3.3. Gasoline engine characteristics

To obtain the engine rotational speed and load for selected NEDC points, the vehicle whose parameters would be used in equations (3.1)-(3.5) had to be selected. The selected vehicle was Ford Mondeo with important characteristics presented in Table 3.4.

Parameter	*Maximum Values*
Vehicle mass m_{veh}[kg]	1569
Frontal area A_{front} [m^2]	2.33
Aerodynamic drag coefficient c_x	0.29
Tire dimension	205/55-R16
1st gear ratio	3.818
2nd gear ratio	2.15
3rd gear ratio	1.407
4th gear ratio	1.029
5th gear ratio	1.188
6th gear ratio	0.971
Final drive transmission ratio TR_{FD}	3.933 (gears 1-4) 2.682 (gear 5,6)

Table 3.4. Main characteristics of gasoline engine vehicle

After calculating engine rotational speed and load for selected NEDC points tests were done on an engine test bench to determine exhaust gas temperature and mass flow. The values obtained are given in the Table 3.5.

Point	Engine speed [rev/min]	Effective Power [W]	Engine efficiency [%]	Exhaust temperature [°C]	Exhaust mass flow [g/s]
A	1891	758	4.36	499	6.17
B	2271	1866	8.40	543	7.89
C	2322	3632	13.67	559	9.44
D	1626	2111	10.78	520	6.96
E	1872	6714	22.94	559	10.41
F	2186	14531	28.12	664	18.37
G	2623	22556	29.66	733	27.01

Table 3.5. Gasoline engine values for NEDC points

The exhaust temperatures given in Table 3.3 and Table 3.5 are the temperatures after the three way catalytic converter.

3.2.2 Diesel engine

The selected diesel engine was Ford/PSA DV5 1.5 litre turbocharged engine, with intercooled variable geometry turbocharger and diesel particulate filter placed in the same case with diesel oxidation catalyst and closely coupled to the exhaust manifold. Main engine characteristics are presented in Table 3.6.

Parameter	*Maximum Values*
Displacement [dm^3]	1.5
Power [kW]	81
Revolutions [rev/min]	4500
Torque [Nm]	278
Mass flow [g/s]	110
Exhaust temperature [°C]	668

Table 3.6. Diesel engine characteristics

As for the gasoline engine, a particular vehicle had to be selected for the diesel engine as well. It was Citroen C5 whose values are presented in Table 3.7

Parameter	*Maximum Values*
Vehicle mass m_{veh} [kg]	1503
Frontal area A_{front} [m^2]	2.25
Aerodynamic drag coefficient c_x	0.3
Tire dimension	225/60-R16
1st gear ratio	3.417
2nd gear ratio	1.841
3rd gear ratio	1.167
4th gear ratio	0.823
5th gear ratio	0.673
Final drive transmission ratio TR_{FD}	4.063

Table 3.7. Main characteristics of diesel engine vehicle

Engine speed and load were calculated, and then those engine operating points were tested on the engine test bench to obtain exhaust temperature and mass flow. The results are presented in Table 3.8.

As it is well known and demonstrated in this case, diesel engine has much lower exhaust gas temperatures than the gasoline engine. As shown in the literature review, the exhaust gas temperature is very important for the WHR efficiency. In continuation it will be shown how important it is for Brayton cycle.

Point	Engine speed [rev/min]	Effective Power [W]	Engine efficiency [%]	Exhaust temperature [°C]	Exhaust mass flow [g/s]
A	1633	726	11.30	125	11.32
B	1877	1798	17.31	148	16.60
C	1859	3521	24.60	191	15.20
D	1301	2034	24.46	148	9.52
E	1501	6551	34.44	254	13.70
F	2144	14274	34.75	354	24.23
G	2573	22223	36.08	324	53.04

Table 3.8. Diesel engine values for NEDC points

3.3 Cycle description

The basic bottoming Brayton cycle is represented in Figure 3.2 and it consists of the following processes: compressor air intake from the ambient, isentropic compression of air from ambient pressure to pressure p_2 (1-2), isobaric heat addition with temperature rise to temperature T_3 (2-3), isentropic expansion, from pressure p3 to ambient pressure (3-4), expulsion of air at temperature T_4 to the ambient.

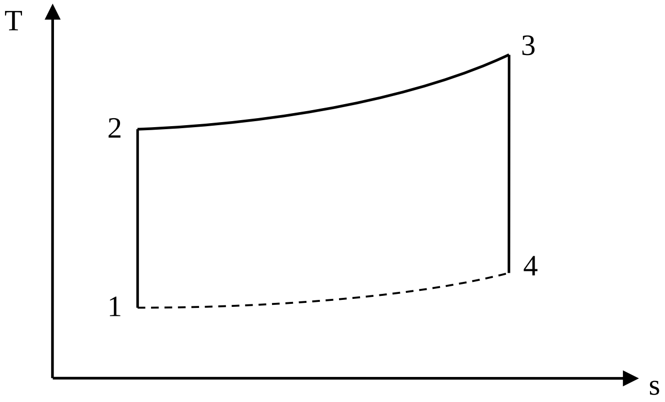

Figure 3.2. Basic Brayton cycle T-s diagram

This basic cycle is idealized. Compression and expansion processes are isentropic without any irreversibility. Heat exchange is almost perfectly efficient and without pressure losses. There are no frictions or other mechanical losses. All the processes are instantaneous. Furthermore, it is considered that exhaust gas has the same characteristics as air, although in continuation it will be referred to as exhaust gas to separate the two flows. Air is considered to be ideal gas. The cycle is schematically represented in Figure 3.3. As shown, the heat exchanger should be placed either after the exhaust aftertreatment or they could be combined in one unit like Honda did in the previously mentioned study [19].

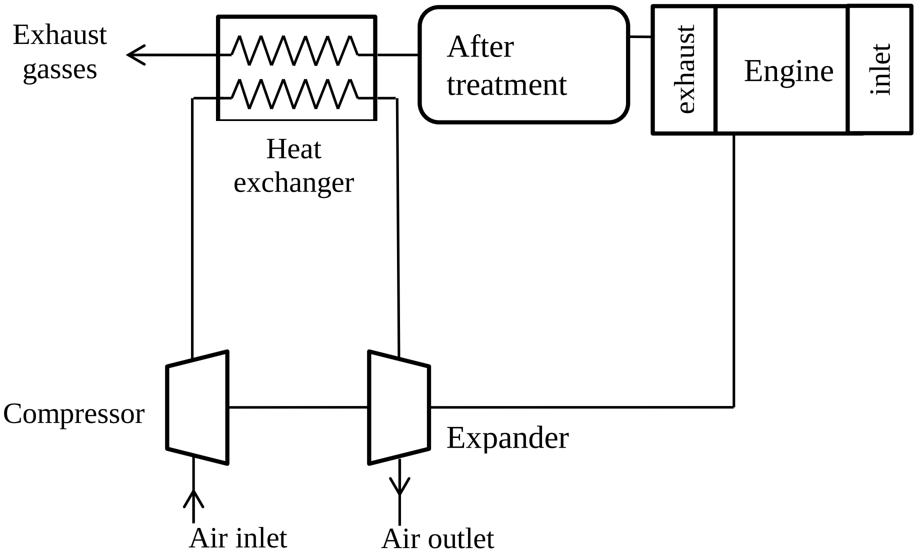
Exhaust gasses
After treatment
exhaust
Engine
inlet
Heat exchanger
Compressor
Expander
Air inlet
Air outlet

Figure 3.3. Schematic representation of basic Brayton cycle

The amount of heat that is exchanged in the heat exchanger is limited by the temperature difference of two gases. Some authors refer to this temperature difference as pinch point [47]. Selected temperature difference is **10 K**. This small temperature difference results in high heat exchanger efficiency.

The temperatures of air and gas in the heat exchanger depend on mass flows of air and gas. If the mass flow of air is lower than mass flow of exhaust gas, the pinch point will be between temperature T_3 and the temperature of the gas at the heat exchanger inlet $T_{gas,in}$. If the mass flow of air is larger than the mass flow of gas, then the pinch point will be between temperature T_2 and exhaust gas temperature at the outlet of heat exchanger $T_{gas,out}$. This is illustrated in Figure 3.4.

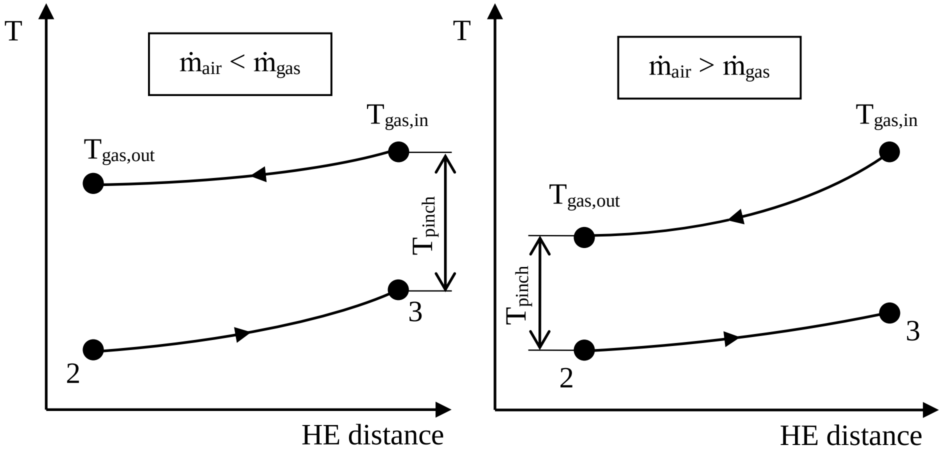

Figure 3.4. Pinch point depending on the ratio of gasses

By defining the pinch point this way, the amount of heat exchanged will depend on engine operating point (temperature and mass flow of exhaust gas) and mass flow of air.

Air is considered to be an ideal gas, so the enthalpies are functions of temperatures for corresponding points. Temperature T_1=288 K is the known temperature at the start of compression. Temperature at the end of compression T_2 depends on temperature T_1 and pressure ratio p_2/p_1. The pressure at the start of compression p_1=1 bar is known, while the pressure at the end of compression p_2 is a variable. Temperature T_3 at the end of heat exchange depends on the pressure at the heat exchanger $p_2=p_3$ and the pinch point.

From the definition of pinch point, for $\dot{m}_{air} \leq \dot{m}_{gas}$, temperature T_3 is calculated by $T_3=T_{gas,in}-10$. Enthalpy and temperature of the exhaust gases at the outlet of HE are calculated form the heat exchanger energy balance:

$$\dot{m}_{air} \cdot (h_3 - h_2) = \dot{m}_{gas} \cdot (h_{gas,in} - h_{gas,out}) \tag{3.8}$$

For the $\dot{m}_{air} > \dot{m}_{gas}$ enthalpy at heat exchanger outlet $h_{gas,out}$ is defined by the temperature at heat exchanger outlet $T_{gas,out}=T_2+10$ and temperature T_3 is calculated from the equation (3.8).

Temperature T_4 is calculated considering that the pressure $p_4=p_1$ and that the expansion is isentropic from the pressure p_3.

The cycle is completely defined by: the engine operating point, pressure at the end of compression p_2 and the mass flow of air. As exhaust gas mass flow is fixed for engine operating point, the flow ratio of gases $\dot{m}_{air}/\dot{m}_{gas}$ can be used instead of mass flow of air.

The recuperated power from the cycle is equal to:

$$P = \dot{m}_{air}[(h_3 - h_4) - (h_2 - h_1)] \tag{3.9}$$

For a non-ideal cycle, enthalpies h_2 and h_4 depend on isentropic efficiency of compressor and expander. For simplicity, it will be assumed that isentropic efficiency of both machines is the same η.

$$h_2 = h_1\left(\frac{\pi^y}{\eta} - \frac{1}{\eta} + 1\right) \tag{3.10}$$

$$h_4 = h_3(1 - \eta + \eta\pi^z) \tag{3.11}$$

where:

$$y = \frac{\kappa - 1}{\kappa} \qquad z = \frac{1-\kappa}{\kappa} = -y \qquad \pi = \frac{p_2}{p_1}$$

Substituting equations (3.10) and (3.11) in (3.9):

$$P = \dot{m}_{air}\left[h_3\eta(1 - \pi^z) + \frac{h_1}{\eta}(1 - \pi^y)\right] \tag{3.12}$$

Expressing h_3 from (3.8) and replacing it in (3.12) the following is obtained:

$$\begin{aligned} P &= \eta\dot{m}_{gas}\left(h_{gas,in} - h_{gas,out}\right)(1 - \pi^z) \\ &\quad + \dot{m}_{air}h_1\left[\pi^y\left(1 - \frac{1}{\eta}\right) + \pi^z(1 - \eta) + \eta + \frac{1}{\eta} - 2\right] \end{aligned} \tag{3.13}$$

3.3.1 Ideal cycle

The ideal cycle assumes that air has ideal gas properties and that both compression and expansion are isentropic. Unknown air properties were then numerically calculated using the NIST database [48]. For the engine operating point G, the recuperated power as a function of pressure p_2 and ratio of gases is represented in Figure 3.5 and Figure 3.6 for previously chosen diesel and gasoline engines, respectively. These figures show that the maximum recuperated power is more than double for the gasoline engine (6.2 kW for gasoline, 2.8 kW for diesel). To analyse the results it is useful to fix one parameter and see how changing the other affects the recuperated power. For the fixed ratio of gases m_{air}/m_{gas} there is an optimal pressure p_2 that gives the maximum power. The optimal pressure p_2 for the gasoline engine is much higher than for the diesel engine (around 10 bar and 3.5 bar respectively). Moreover, for fixed pressure p_2 recuperated power rises with the rise of ratio of gases until it reaches the value of 1, after which it remains constant, as shown in the figures.

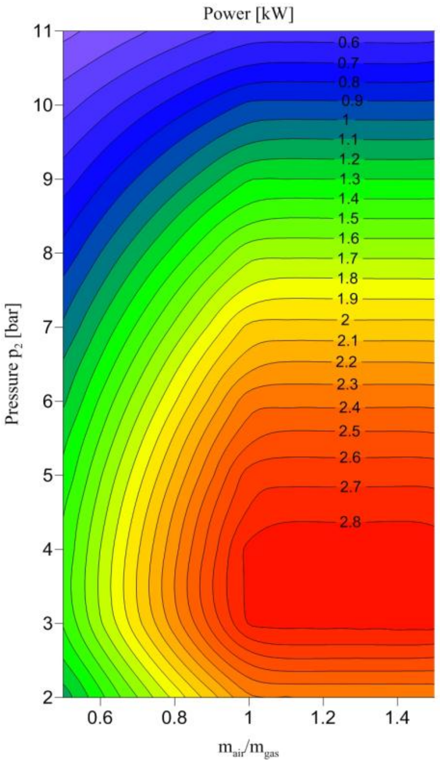

Figure 3.5. Diesel engine op. point G

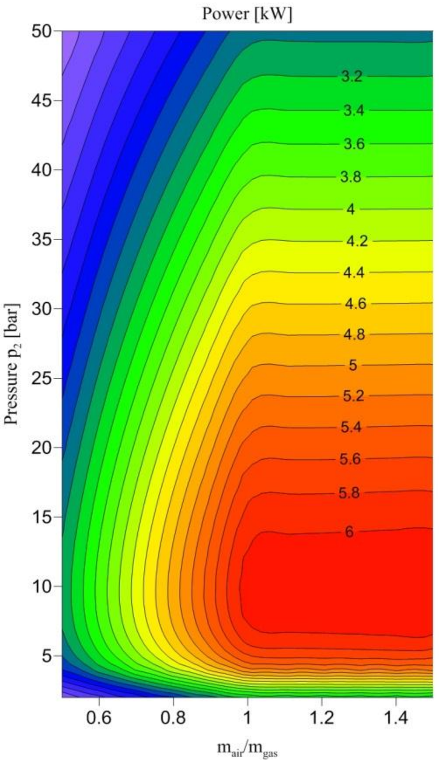

Figure 3.6. Gasoline engine op. point G

A part from numerical analysis, to understand the cycle better it is useful to study it analytically.

Mass flow effect

To analyse the effect of air mass flow on recuperated power, pressure p_2 was fixed and with it enthalpy h_2 was also fixed. For the point 3 the definition of pinch point should be considered again.

For set pressure p_2, for any $\dot{m}_{air} \leq \dot{m}_{gas}$ the temperature T_3 is constant ($T_3=T_{gas,in}-10$), because pinch point imposes the air temperature at point 3. The cycle is fully defined, and for any point where mass flow of air is less than mass flow of gas the power rises with the rise of air mass flow.

For $\dot{m}_{air} > \dot{m}_{gas}$ pinch point defines the temperature and enthalpy of gas at the heat exchanger outlet and temperature T_3 can be calculated from the heat exchanger balance. If mass flow of air rises, the temperature T_3 drops.

The effect of flow ratio of gases could be observed on T-s diagram as well. Three cycles for fixed pressure p_2=10 bar, fixed engine operating point G for gasoline engine and variable ratio of gas flows $\dot{m}_{air}/\dot{m}_{gas}$ are represented in Figure 3.7.

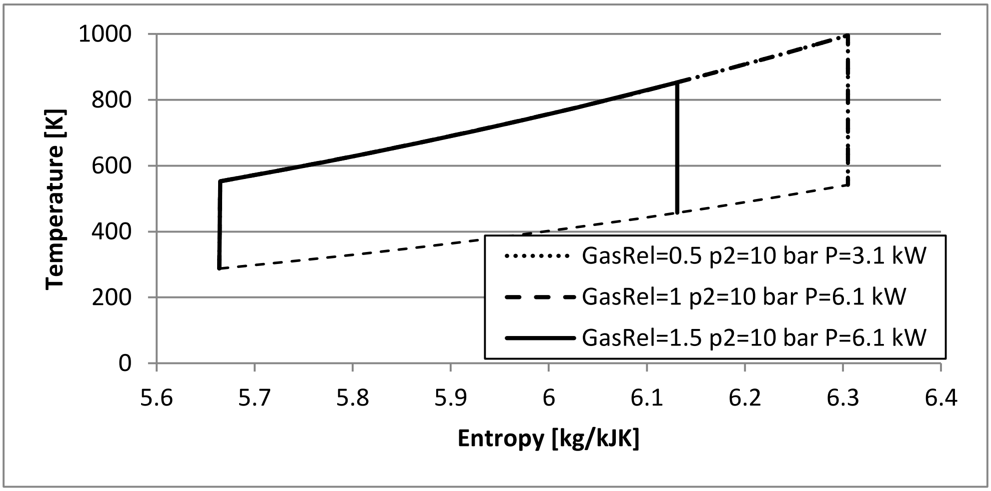

Figure 3.7. T-s diagram for fixed pressure p_2 and variable ratio of gas flows, engine operating point G, p_2=10 bar

For cycles with $\dot{m}_{air} \leq \dot{m}_{gas}$ (dotted and discontinued lines in Figure 3.7) the cycles are exactly the same, and thus overlap in the figure, with the power proportional to air mass flow. On the other hand, for the cycle with $\dot{m}_{air} > \dot{m}_{gas}$ temperature T3 decreases.

Another way to look at how temperature T_3 and temperature of gas at the heat exchanger outlet change by varying air mass flow could be by looking at temperatures of air and gas along the heat exchanger. This is represented in Figure 3.8, where position 0 represents the inlet of air in the heat exchanger (outlet of gas) and position 1 the outlet of air in the heat exchanger (inlet of gas).

For $\dot{m}_{air} = \dot{m}_{gas}$ the lines of air and gas temperatures are parallel. For $\dot{m}_{air} > \dot{m}_{gas}$, the temperature of the air rises slower than the temperature of the gas drops, this decreases temperature T_3 and enthalpy h_3. According to Figure 3.6 this enthalpy drop is proportional to air mass flow rise because the power is kept constant. This can be proven analytically by analysing the equation (3.13). For $\dot{m}_{air} > \dot{m}_{gas}$, enthalpy $h_{gas,out}$ is constant. For the ideal cycle η=1 so that a parenthesis next to the $\dot{m}_{air}$ is equal to zero, meaning that recuperated power does not depend on air mass flow and is equal to:

$$P = \dot{m}_{gas}\left(h_{gas,in} - h_{gas,out}\right)(1 - \pi^{z}) \tag{3.14}$$

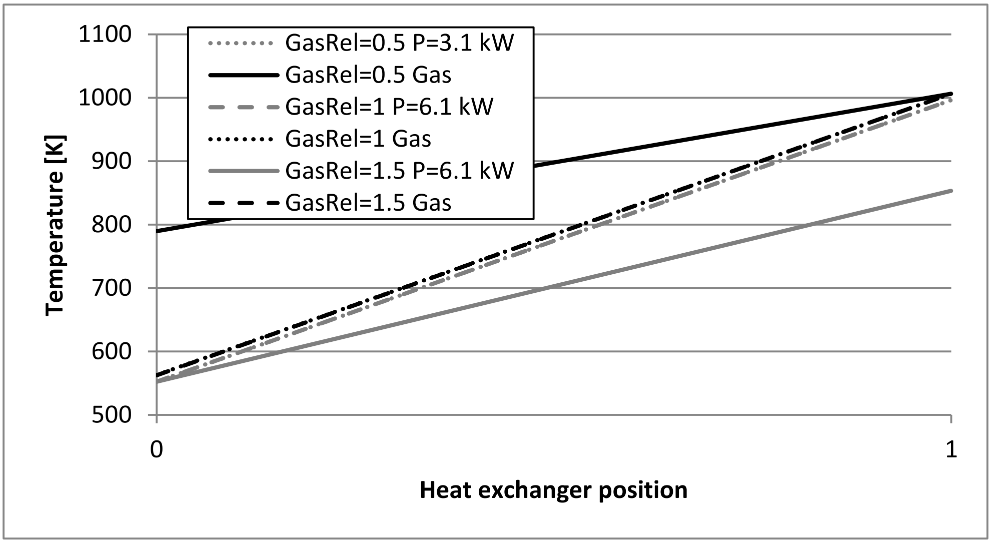

Figure 3.8. Temperatures of air and gas at Heat Exchanger inlet and outlet, engine operating point G, p_2=10 bar

Pressure ratio effect

In order to study the effect of pressure ratio p_2/p_1, the air mass flow should be fixed. Three cycles with same air/gas mass flow ratio and different pressure ratio are presented in Figure 3.9

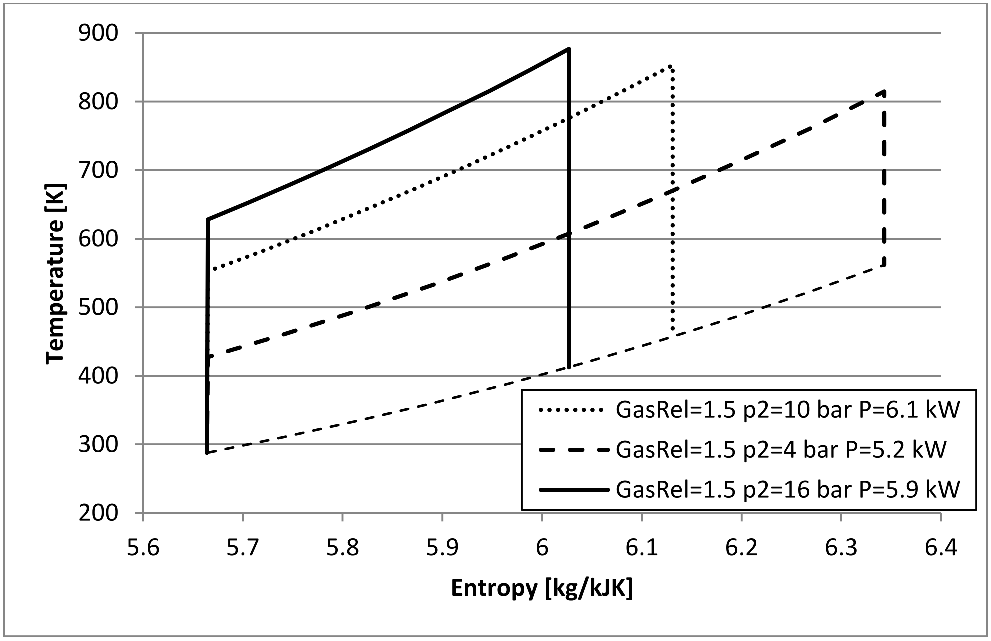

Figure 3.9. T-s diagram for fixed air mass flow and variable pressure p_2, engine operating point G, gas flow ratio 1.5

The optimal pressure ratio that gives the maximum power is the one that will have the biggest area on the T-s diagram. A more precise way to find the optimal pressure is to analyse it analytically. For $\dot{m}_{air} \leq \dot{m}_{gas}$, enthalpy h_3 is constant and does not depend on air mass flow. To find the pressure ratio that gives the maximum power, the partial derivative of the equation (3.12) should be equalled to zero:

$$\frac{\partial(P)}{\partial(\pi)} = 0 \tag{3.15}$$

To obtain:

$$\pi = \left(\frac{h_3}{h_1}\right)^{1/2y} \eta^{1/y} \tag{3.16}$$

For $\dot{m}_{air} \leq \dot{m}_{gas}$, temperature T_3 is constant and the optimal pressure p_2 (that gives the maximum power) is also constant.

As it was shown before, for the ideal cycle it can be considered that air mass flow should be equal or higher than exhaust gas mass flow. Fixing the $\dot{m}_{air} = \dot{m}_{gas}$ other NEDC points can be analysed to find the optimal pressure p_2 for each point. This is represented in Figure 3.10 for the diesel engine and Figure 3.11 for the gasoline engine. Pressure was varied for all NEDC points to find the optimum pressure that gives maximum power that is marked with red crosses in those figures. The optimal pressure in the heat exchanger changes with the engine operating point. Heat recovery system should allow control of the heat exchanger pressure in order to recuperate the maximum power for all engine operating points. It could be seen that the optimum pressure generally rises with the rise of the exhaust temperature (exhaust gas temperature rises from point A to point G). For the diesel engine, the temperature of the point F is higher than temperature of point G, thus the higher optimum pressure, although mass flow for point G is much higher, thereby resulting in higher recuperated power.

Moreover, it is evident that the amount of recuperated power is much smaller for the diesel than for the gasoline engine, as a consequence of the lower temperature of exhaust gases.

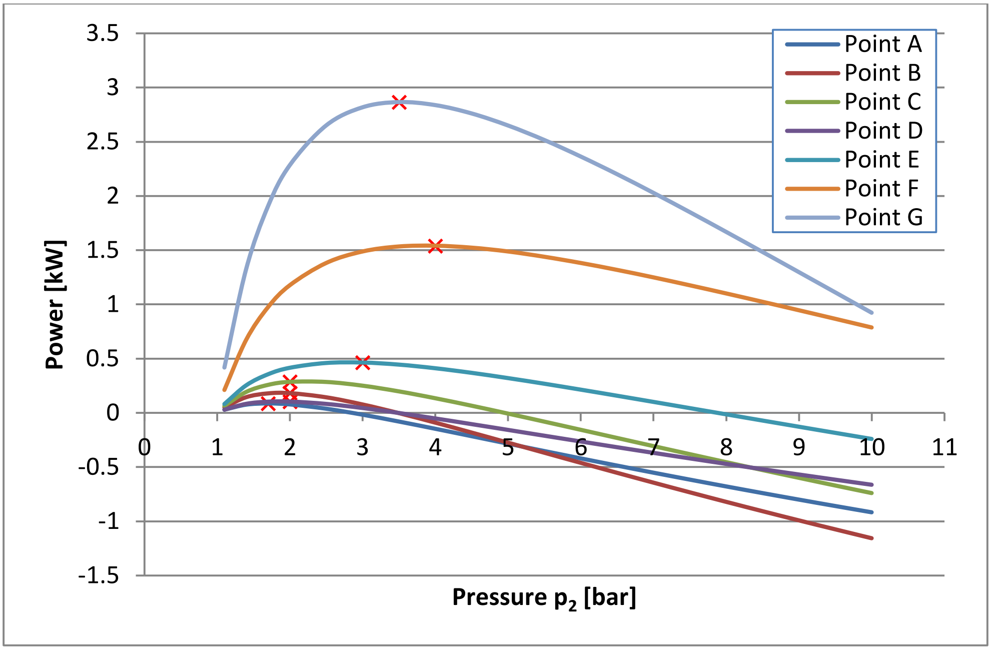

Figure 3.10. Recuperated power as a function of pressure ratio for diesel engine

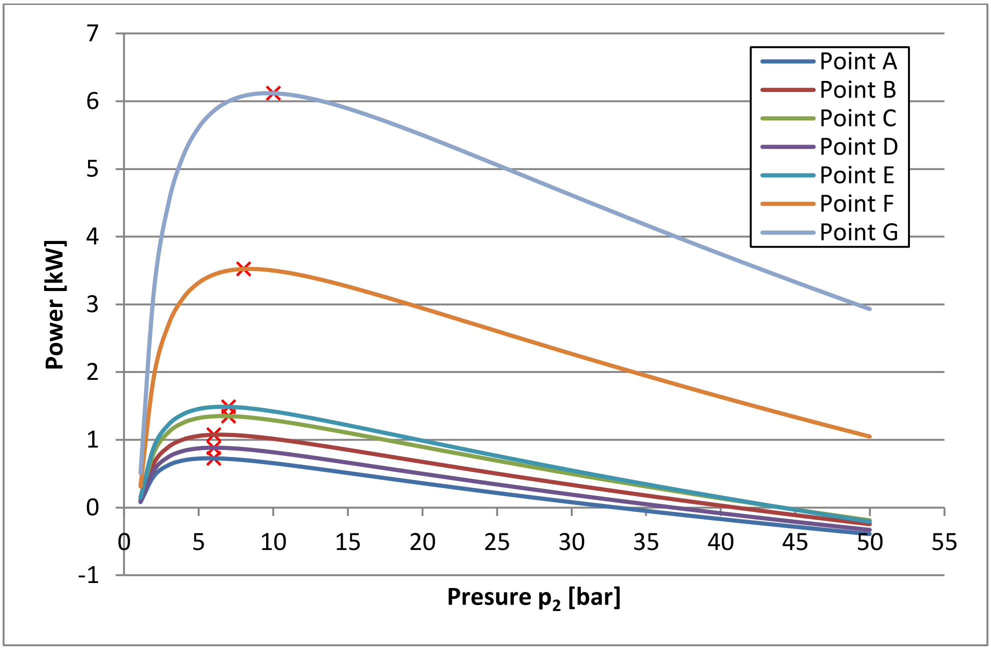

Figure 3.11. Recuperated power as a function of pressure ration for gasoline engine

3.3.2 Machine selection

As it was theoretically shown, it is possible to recuperate power from all selected engine operating points. Mechanical, heat transfer or charge losses that are not included in the previous calculation could waste a lot of the recuperated power and even generate power losses to the engine. That is why it is more reasonable to consider the Waste Heat Recuperation from the points where the engine has a higher exhaust temperature and mass flow, and it is possible to recover a higher amount of wasted energy.

To simplify the machine selection process, nominal operative point will be point G of the gasoline engine when vehicle speed is constant at 120 km/h and exhaust conditions are good for heat recovery. This corresponds to normal highway driving conditions. From the thermodynamic analysis for this point, for heat exchanger pressure of 10 bar that gives the maximum power and $\dot{m}_{air} = \dot{m}_{gas}$, the specific enthalpies of air and volumetric flows are:

Start of compression	h_1=288.4 kJ/kg	$\dot{V}_1$=0.02233 m^3/s	Δh=268.9 kJ/kg
End of compression	h_2=557.3 kJ/kg		
Start of expansion	h_3=1042 kJ/kg		Δh=495.6 kJ/kg
End of expansion	h_4=546.4 kJ/kg	$\dot{V}_4$=0.04199 m^3/s	

Table 3.9. Compression and expansion parameters for point G

Table 3.9 shows the values of enthalpy (h) for each cycle point, the enthalpy difference (Δh) for compression and expansion, and volumetric flows ($\dot{V}$) at the start of compression and end of expansion.

Compressor selection

The recuperated power directly depends on the machine isentropic efficiency. For that reason, when different machine designs have been used, the zones with highest efficiencies were targeted.

Barber-Nichols diagram [49] was used for the compressor machine selection. Three potential compressor machines are used in this diagram: alternating piston, rotary piston and radial compressor. In order to define the characteristics of these compressor machines, two numbers should be defined: the specific diameter (D_s) and the specific speed (N_s):

$$D_s = \frac{D \cdot \Delta h^{0.25}}{\sqrt{\dot{V}_1}} \tag{3.17}$$

$$N_s = \frac{N\sqrt{\dot{V}_1}}{\Delta h^{0.75}} \tag{3.18}$$

For the alternating piston, the range of rotational speed (N) is set to 1000-6000 rpm, which corresponds to engine speed range and the range of diameter (D) from 50-200 mm. Maximum diameter was set assuming that this is the maximum size that could fit in the space available under the hood. Although compressor speed does not have to correspond to engine speed, it is convenient to avoid gearing between the engine and the compressor. Knowing the volumetric flow $\dot{V}_1$ and enthalpy difference Δh from Table 3.9, the specific speeds Ns and specific diameters Ds can be calculated. The optimal point was chosen so that the compressor speed is the same as the engine (2623 rpm), and to obtain the maximum efficiency. The resulting diameter is 115 mm that gives 80% isentropic efficiency.

For the rotary piston and radial compressor, the Ns and Ds ranges are selected to form the zone where efficiency is higher than 70%. Optimal points are placed where efficiency is the highest 80%.

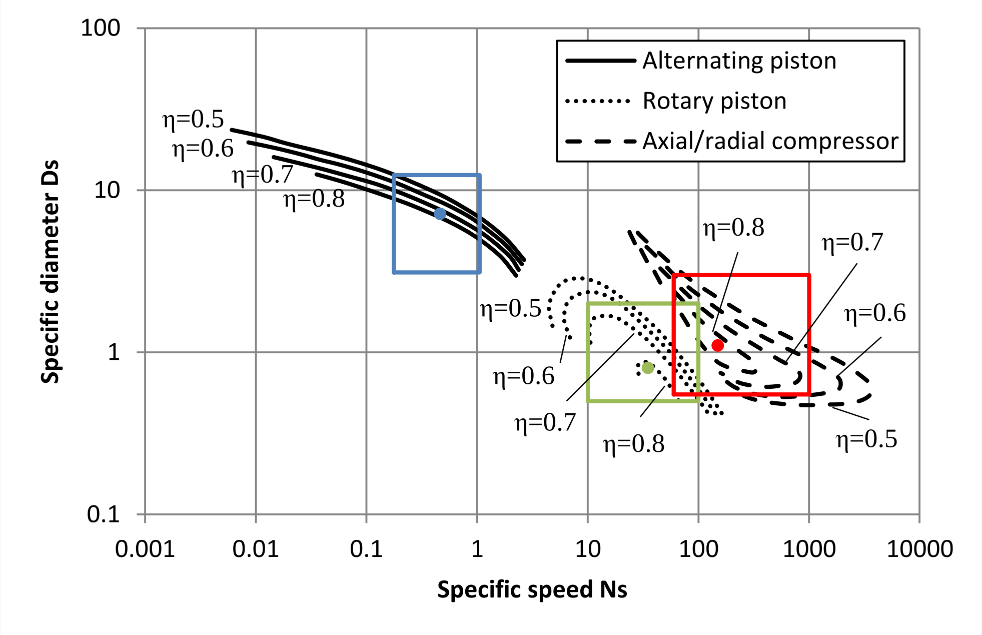

Figure 3.12. Barber-Nichol diagram for compressor

Figure 3.12 shows the Barber-Nichols diagram for compressor selection. Squares represent the selected range of Ns and Ds while dots represent the selected optimal points for each machine type.

Machine type	D min [mm]	D max [mm]	D opt [mm]	RPM min	RPM max	RPM opt
Alternating piston	50	200	115	1000	6000	2623
Rotary piston	8.05	32.20	12.88	56791	567908	198768
Axial/Radial compressor	8.85	48.30	17.71	340745	5679076	851861

Table 3.10. Compressor rotary speeds and diameters

Speed ranges obtained in Table 3.10 for both rotary and radial compressor are too high. Optimum speed values are beyond what the current technology permits. For that reason, a more feasible solution is the alternating piston. Moreover, this technology is similar to internal combustion engines, what makes it more attractive for vehicle manufacturers.

Expander selection

For the expansion machine selection, a similar procedure to the one used on compressor was applied. Again the same limitations have been applied on all types of machinery. Figure 3.13 shows the Barber-Nichols diagram for expander selection.

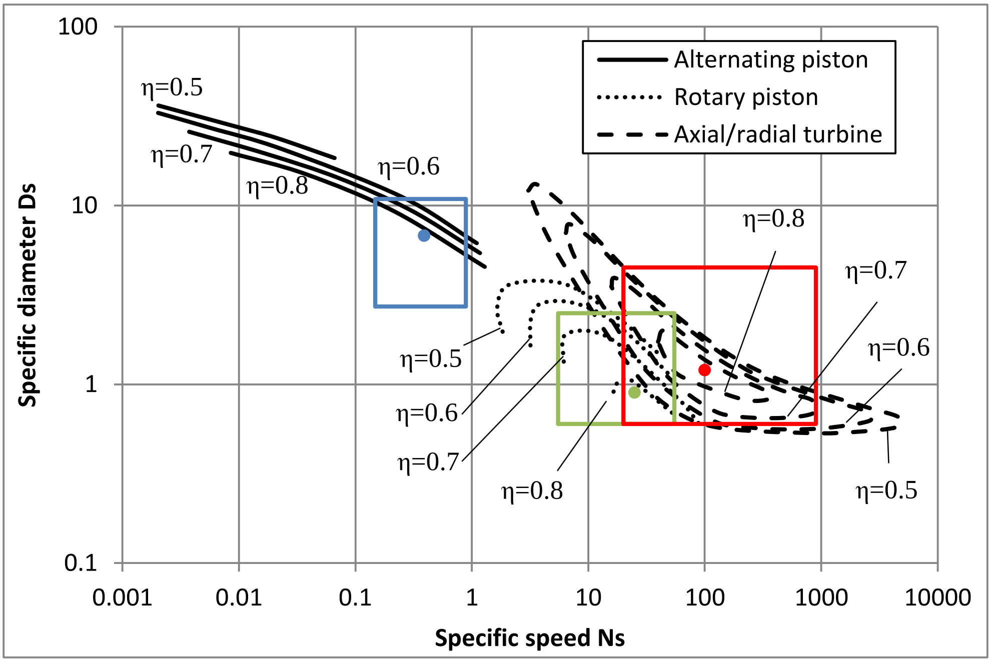

Figure 3.13. Barber-Nichols diagram for expander

Rotary machinery offers smaller dimensions, but the rotary speed is too high for the current technology. Alternating piston with 125 mm diameter and isentropic efficiency of 80% is selected for the expansion machine.

The values obtained are presented in Table 3.11. Once more the situation is similar, rotary and radial turbine have a rotary speed too high, while the reciprocating piston is big but still possible to fit in the engine bay or below the vehicle.

Machine type	D min [mm]	D max [mm]	D opt [mm]	RPM min	RPM max	RPM opt
Alternating piston	50	200	125	1000	6000	2623
Rotary piston	11.03	45.99	16.55	37111	371112	168687
Axial/Radial turbine	11.03	82.79	22.07	134950	6072747	674750

Table 3.11. Expander rotary speeds and diameters

Conclusion

According to this analysis, it seems that for both compressor and expander machine, the most promising machine type is the alternating piston. Furthermore, for both machines the optimal values of rotating speed and piston diameter are similar. This implies that the same piston machine can be used for both processes of compression and expansion. That is why the same piston diameter of **120 mm** was chosen for both machines. Furthermore, the optimal machine rotating speed is very similar to the internal combustion engine speed for the analysed working point (120 km/h), so that machine could be coupled with the engine directly without a gearbox.

3.3.3 Non-ideal cycle

For the non-ideal cycle isentropic efficiency of the compressor and the expander is no longer 100% like it was for the ideal cycle. As it was shown before, similar efficiencies can be expected for the compressor and the expander alternating piston machine. Because of that, and the simplicity, it was decided that the compressor and the expander have the same efficiency $\boldsymbol{\eta=0.8}$. This value was chosen as a maximum value from the previous study. Pinch point temperature difference of 10 degrees was the same as for the ideal cycle. Recuperated power was again first studied numerically, by varying the values for ratio of gases and pressure p_2. The plots of the recuperated power as a function of pressure p_2 and ratio of gases are presented in Figure 3.14 and Figure 3.15. The recuperated power decreases significantly with the drop of isentropic efficiency. Those figures were obtained considering air to be the ideal gas and calculating the unknown values the same way as for the ideal cycle. For the non-ideal cycle with $\dot{m}_{air} > \dot{m}_{gas}$ the power is no longer independent of $\dot{m}_{air}$. By analysing the equation (3.13) and the parenthesis next to air mass flow

$$\left[\pi^{y}\left(1-\frac{1}{\eta}\right)+\pi^{z}(1-\eta)+\eta+\frac{1}{\eta}-2\right] \tag{3.19}$$

it can be concluded that for any $\pi>1$ and $0<\eta<1$ the value of the parenthesis will be negative, thereby with the increase of air mass flow the power will decrease. The equation (3.16) clearly shows that the optimal pressure decreases with the decrease of the isentropic efficiency and enthalpy h_3. Enthalpy h_3 is lower when the exhaust gas temperature is lower. Thereby, for the diesel engine, the optimal pressure p_2 is lower than for the gasoline engine. Also, for the gasoline engine operating points with lower exhaust temperature, the optimal pressure p_2 is lower than for point G when the gas temperature is high. For the optimal mass flow, it is clear that the ratio of mass flows should be close to 1.

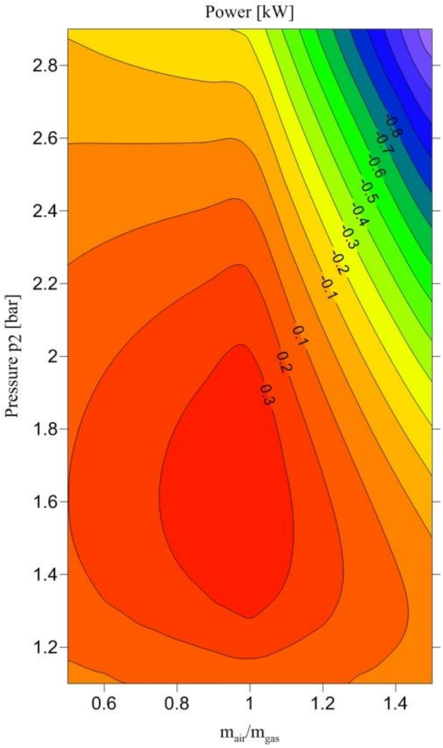

Figure 3.14. Diesel engine operating point G, η=0.8

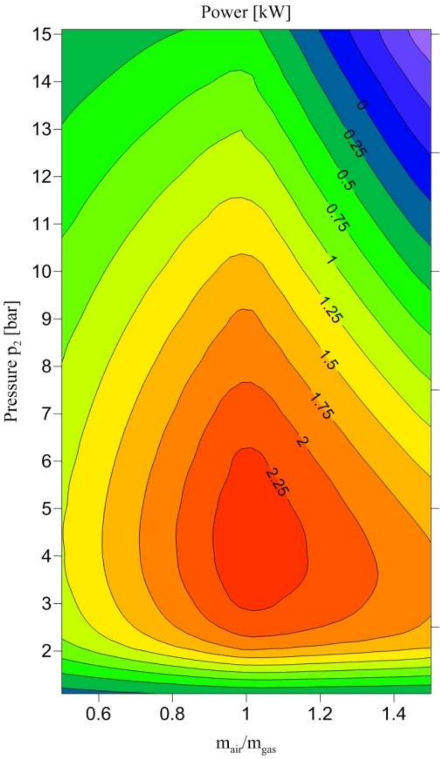

Figure 3.15. Gasoline engine operating point G, η=0.8

Similar to the ideal cycle, the recuperated power for all NEDC points was studied non-ideal cycle as well. Mass flow of air is set to be equal to mass flow of gas for each point, and the power as a function of pressure in the heat exchanger was analysed. Figure 3.16 shows that in case of the diesel engine, the recuperated power is very small, 397 W in the best case. As this study did not include mechanical loses, pumping loses nor various other cycle loses it could be expected that in the real machine it would not be possible to extract any power. Situation is better for the gasoline engine were maximum recuperated power was 2461 W. Figure 3.17 shows that theoretically it could be possible to extract power from all points. However, because of the same presumptions like for the diesel engine, useful power for the real machine could probably be extracted only for last two points F and G. That is, the machine would work well only during the extra urban and highway driving.

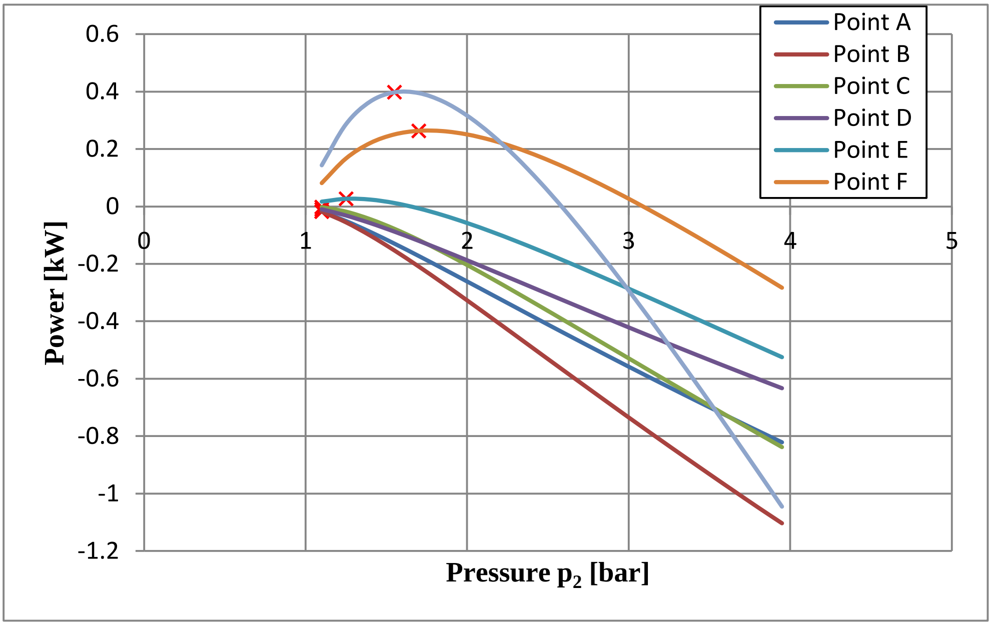

Figure 3.16. Recuperated power for diesel engine and WHR isentropic efficiency 80%

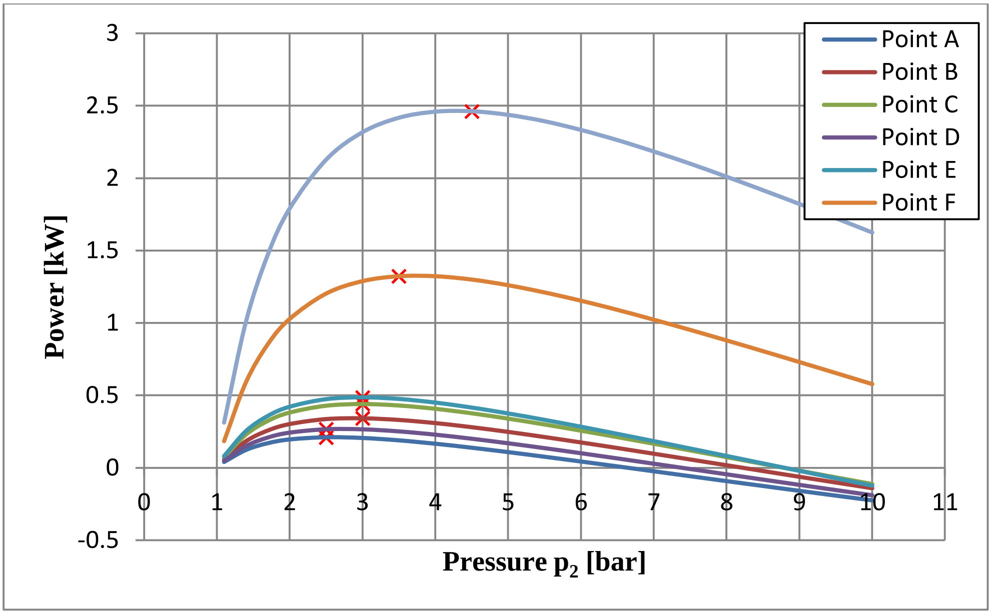

Figure 3.17. Recuperated power for gasoline engine and WHR isentropic efficiency 80%

It should be noted that the isentropic efficiency of 80% that was set for all NEDC points, was chosen based on the machine selection analysis that considered only the point G. It is possible that the efficiency this high cannot be achieved for other NEDC points.

Heat exchanger efficiency is defined by:

$$\eta_{HE} = \frac{T_3 - T_2}{T_{gas,in} - T_2} \tag{3.20}$$

Pinch point of 10 degrees results in very high heat exchanger efficiency. For the point G of gasoline engine and the pressure ratio that gives the maximum power, heat exchanger efficiency is 98%. This is probably a value too high for a reasonable size heat exchanger. Figure 3.18 shows how heat exchanger efficiency influences the recuperated power for point G of the gasoline engine. Maximum power and optimal pressure decrease proportionally to heat exchanger efficiency.

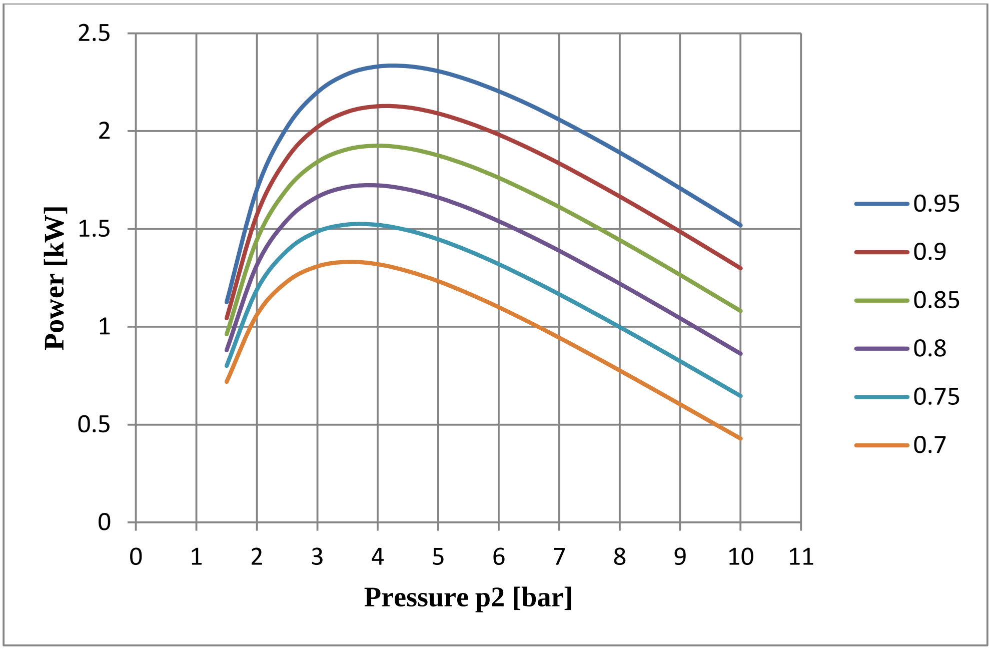

Figure 3.18. Point G of gasoline engine and varying heat exchanger efficiency

It could be interesting to see how each of the three efficiencies (compressor, expander and heat exchanger) affects the cycle. For the gasoline engine operating point G, one of the efficiencies was set to 0.8 while the others were 1. This was repeated for each efficiency and represented in Figure 3.19, along with the curve when all efficiencies are equal to 1. It can be seen that the biggest power decrease is when the expander efficiency is 0.8, meaning that this efficiency has the highest influence on the total cycle efficiency. Compressor and heat exchanger efficiencies have similar effect up to around 4.5 bar. At higher pressures the compressor efficiency is more important.

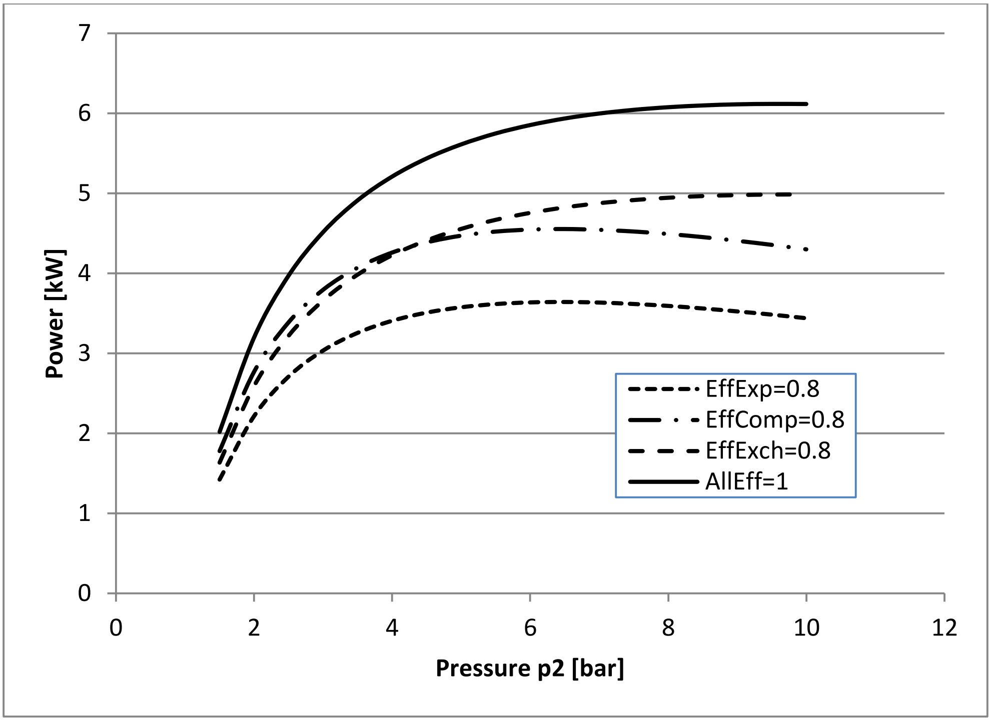

Figure 3.19. Influence of different efficiencies on the cycle, gasoline engine operating point G

Overall cycle efficiency is an important parameter for the comparison of different cycles. One way to define the cycle efficiency is as a ratio of recuperated power and power transferred from the exhaust gas to the heat exchanger:

$$\eta_c = \frac{P}{P_{HE}} = \frac{P}{\dot{m}_{gas}\left(h_{gasIn} - h_{gasOut}\right)} \tag{3.21}$$

where h_{gasIn} and h_{gasOut} are specific enthalpies of exhaust gas at heat exchanger inlet and outlet respectively.

At the maximum power for gasoline engine operating point G, the cycle efficiency is η_c=15.88%.

The other way is to define the cycle efficiency as a ratio of recuperated power and difference of enthalpies of the exhaust gas at HE inlet and enthalpy of exhaust gas at ambient temperature:

$$\eta_{cA} = \frac{P}{\dot{m}_{gas}\left(h_{gasIn} - h_{gasAmb}\right)} \tag{3.22}$$

where h_{gasAmb} is the specific enthalpy of exhaust gas at ambient temperature.

At the maximum power for gasoline engine operating point G cycle efficiency is η_{cA}=11.92%. Comparing with the other WHR technologies reviewed in Chapter 2, this efficiency represents a good result. Maximum recuperated power was also thought to be a good result and it was considered that the cycle should be further investigated.

4 Heat exchanger

Contents

4.1 Introduction 63
4.2 Heat exchanger efficiency 64
4.3 Pressure drop 67
4.4 Pressure wave transmissivity 75

4.1 Introduction

Heat exchanger is an important part of the Brayton cycle heat recovery system. Its main function is to add energy to the working fluid by taking the heat from the exhaust gas. Thereby, its main characteristic in this cycle is its ability to take the heat from the exhaust gas and pass it to the air. This ability is called heat exchanger efficiency. Moreover, heat exchanger efficiency is closely related to other two important characteristics of heat exchangers: pressure drop and size. In order to increase the heat transfer coefficient some obstacles can be introduced on the gas path, increasing not only the heat transfer coefficient, but also the friction losses in the ducts of the exchanger and consequently augmenting the pressure drop in the exhaust line. Higher pressure drop means more engine pumping losses, which lowers ICE efficiency. Similar thing happens with the size. If the heat exchanger is bigger, there is more area for heat exchange and the exchanger is more efficient but also heavier, which negatively affects the engine consumption, and requires more space for packaging.

Apart from heat exchanger efficiency, pressure drop and size there is another important heat exchanger property: pressure wave transmissivity. Pressure wave transmissivity tells us which part of the input pressure wave is transmitted and which part is reflected when pressure wave reaches the heat exchanger. This property will be further explained later when it is described how it was measured on a special pressure pulse installation at CMT.

It was important to know, or correctly estimate, heat exchanger characteristics that would be implemented in the heat recovery system. The partner company in this research, Valeo Systemes Thermiques (in continuation Valeo), provided a prototype of the heat exchanger that would be adequate for this application. In fact, not only did Valeo develop and produce this prototype, it also conducted one part of the experimental testing of the heat exchanger performance. The mentioned prototype was a gas-gas, cross flow, plate-fin recuperator. The overall heat exchanger dimensions, including the flanges, were 311x282x103 mm. Figure 4.1 shows the photo of a heat exchanger on the pulse test bench. The flanges of the air inlet and outlet are connected to the test installation while the exhaust flanges are free. It can be seen that the exhaust passes directly through the heat exchanger while the air flow has to make two 90 degrees turns.

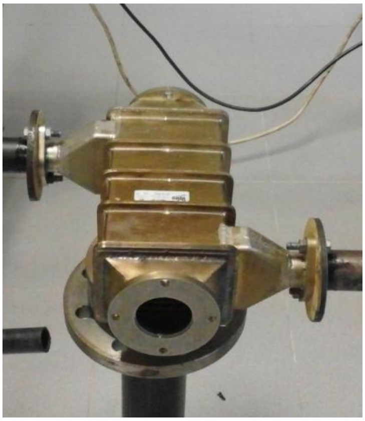

Figure 4.1. Photo of the heat exchanger

4.2 Heat exchanger efficiency

From the definition of heat exchanger efficiency it is easy to see what values should be measured to determine its efficiency: temperatures of air at the inlet and outlet, temperature of exhaust gas at the inlet of heat exchanger.

$$\eta_{HE} = \frac{T_{air,out} - T_{air,in}}{T_{gas,in} - T_{air,in}} \tag{4.1}$$

Valeo used an experimental facility to estimate heat exchanger efficiency. Figure 4.2 shows the schematic of the heat exchanger test installation. The schematic shows that gasoline engine was used as a source of hot gas. In this facility, several parameters were measured: temperature of gas at the outlet, mass flows of exhaust gas, mass flow of air, pressures at the air inlet and outlet, pressures at the gas inlet and outlet Different combinations of engine rotational speed and load allow different possible gas mass flows and temperatures, but they do not allow for any provisional combination of mass flow and temperature of exhaust gas. For example, same mass flow could be achieved with different rotational speed by changing the engine load. This would result in different gas temperature, but the range of possible temperatures is limited. Anyhow, only two points were used for gas side inlet. At the air side, compressor was used to supply air at desired pressure. Air passed through electrical resistance that heated the air to desired temperature. Air mass flow was adjusted by the valve. All tested points are presented in Table 4.1 where one row represents one tested point.

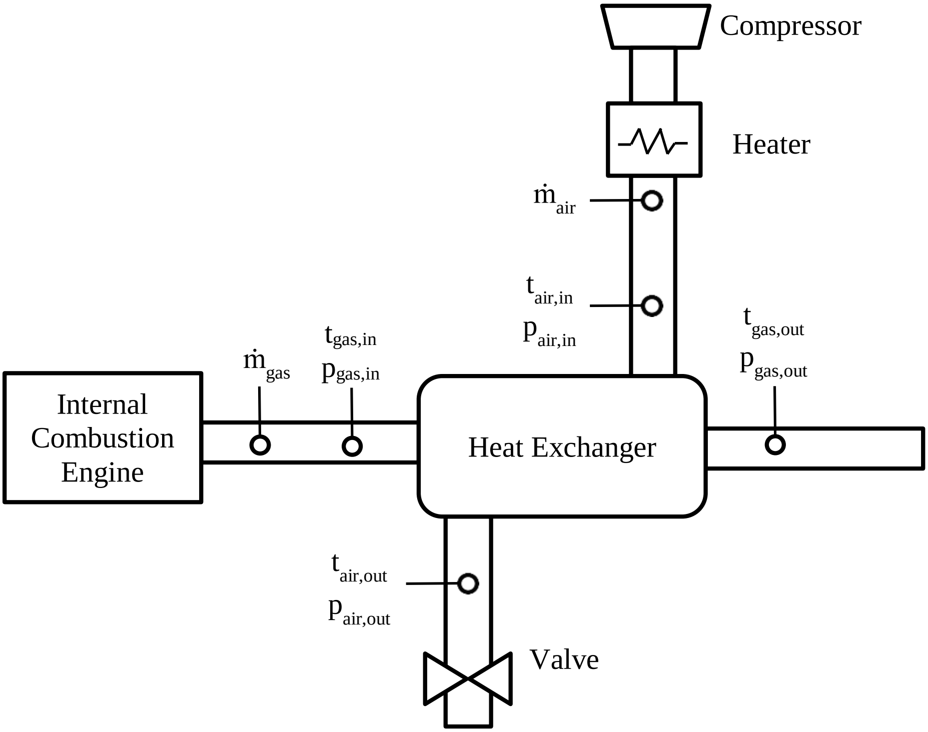
Compressor
Heater
ṁ air
t air,in
p air,in
t gas,out
p gas,out
t gas,in
p gas,in
ṁ gas
Internal Combustion Engine
Heat Exchanger
t air,out
p air,out
Valve

Figure 4.2. Schematic of the heat exchanger test installation

point	gas			air			AirGas ratio	Efficiency
	mass flow [g/s]	Tin [°C]	Tout [°C]	mass flow [g/s]	Tin [°C]	Tout [°C]		
1	19.8	505	358	10.0	200	473	0.51	89.51
2	19.5	504	358	10.0	200	473	0.51	89.80
3	19.7	493	270	20.0	200	426	1.02	77.13
4	19.8	493	270	19.9	200	426	1.01	77.13
5	20.3	497	234	30.0	200	382	1.48	61.28
6	20.0	498	235	30.1	200	383	1.50	61.41
7	19.6	504	231	30.1	200	381	1.53	59.54
8	19.6	504	231	30.0	200	381	1.53	59.54

Table 4.1. Tested heat exchanger points

Figure 4.3 shows the plot of heat exchanger efficiency as a function of AirGas ratio for all measured points. The ratio of air to gas mass flows (AirGas ratio) has a big influence on heat exchanger efficiency. As it was analysed in Chapter 3, when AirGas ratio is higher than 1 and rises, heat exchanger efficiency decreases.

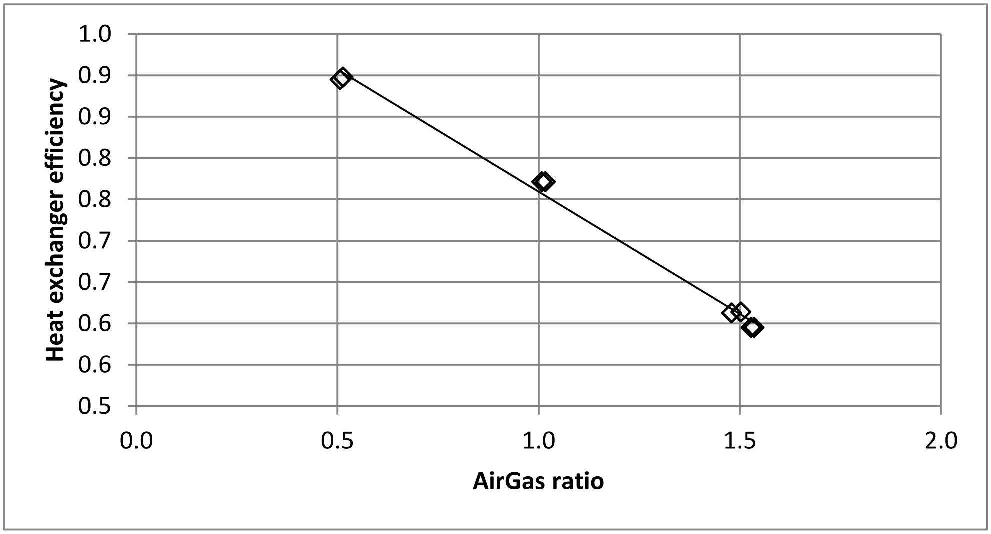

Figure 4.3. Heat exchanger efficiency as a function of AirGas ratio

It is obvious from this plot that heat exchanger efficiency decreases always with the rise of AirGas ratio, not only when AirGas ratio is higher than 1. In Chapter 3 it was demonstrated that optimal AirGas ratio should be around 1. Nevertheless, that was the case for the simple cycle and heat exchanger efficiency defined by pinch point. For the more complex model of WHR machine and heat exchanger it should be checked what is the optimal AirGas ratio.

Figure 4.3 shows that heat exchanger efficiency changes with AirGas ratio in a very linear way in the range of AirGas ratio 0.5÷1.5. This linearity was approximated with the equation:

$$\eta_{HE} = -0.2956\, AirGas + 1.055 \tag{4.2}$$

Heat exchanger efficiency defined by equation (4.2)was used in the model of the heat recovery system.

4.3 Pressure drop

Pressure drop represents the difference of pressure between two points along the fluid flow. For the heat exchanger, these two points were heat exchanger inlet and outlet. Pressure drop is a consequence of the friction forces acting upon fluid flow. Friction forces appear all along the fluid flow in the channels, fittings, joints etc. Pressure drop creates pumping losses and it should be minimized. Nevertheless, a compromise is often made, because many elements that increase the heat transfer, like fins inside the channels, negatively affect pressure drop. On the gas side, an additional pressure drop in the exhaust line causes ICE pumping losses because the engine has to use more energy to pump the exhaust gasses out. Those pumping losses should be calculated and subtracted from the power recuperated in the Air Brayton Cycle (ABC) in order to take into account the overall energy recovered. On the air side, the piston will have to use more energy to push the air through the heat exchanger. Pressure drop on the air side of the heat exchanger should be included in the machine model.

Figure 4.2 shows that pressures were measured at the inlet and outlet of both gas side and air side. The measured pressure drop (dP) is presented in Table 4.2, along with the temperatures at inlet and outlet, temperature differences (dT) and mass flows.

point	Gas side					Air side				
	mass flow [g/s]	Tin [°C]	Tout [°C]	dT [°C]	dP [kPa]	mass flow [g/s]	Tin [°C]	Tout [°C]	dT [°C]	dP [kPa]
1	9.1	316	201	116	0.23	9.9	200	275	76	0.14
2	9.1	316	201	115	0.23	10.0	200	276	76	0.13
3	9.1	315	193	122	0.23	20.0	200	247	47	0.45
4	9.1	315	193	122	0.23	20.0	200	246	47	0.44
5	9.2	316	193	122	0.21	30.0	200	232	32	0.94
6	9.2	316	193	122	0.21	29.9	200	232	32	0.94
7	9.2	315	202	114	0.24	10.1	200	276	76	0.007
8	9.1	315	202	114	0.24	10.0	200	276	76	0.007
9	19.8	505	358	148	0.78	10.0	200	473	273	0.2
10	19.5	504	358	147	0.78	10.0	200	473	273	0.2
11	19.7	493	270	223	0.68	20.0	200	426	227	0.61
12	19.8	493	270	223	0.68	19.9	200	426	226	0.61
13	20.3	497	234	262	0.63	30.0	200	382	182	1.2
14	20.0	498	235	263	0.63	30.1	200	383	182	1.18
15	19.6	504	231	272	0.61	30.1	200	381	181	1.2
16	19.6	504	231	273	0.61	30.0	200	381	181	1.21
17	19.5	504	258	247	0.65	20.1	200	404	205	0.61
18	19.3	505	258	247	0.65	20.1	200	405	205	0.61
19	19.4	505	257	248	0.65	20.1	200	404	204	0.61
20	19.3	505	257	248	0.65	20.1	200	404	204	0.62

Table 4.2. Pressure drop for tested points

In order to obtain a theoretical model to predict the pressure drop through the heat exchanger, the work of Kakac and Liu [50] has been considered. This work suggests that pressure drop calculation for plate-fin heat exchanger is made of few terms: the first term represents the entrance effect, the second term is the acceleration effect, the third term is the core friction and the forth term is the outlet effect. Nevertheless, the authors mention that the third term, core friction, generally accounts for more than 90% of the total pressure drop. The equation for core pressure drop is derived from the Darcy-Weisbach equation:

$$\Delta p = f\frac{l}{D_h}\frac{\dot{m}^2}{2\rho A^2} \tag{4.3}$$

where f is the friction coefficient, l is the length, A is the area, D_h is the hydraulic diameter, ρ is the density and $\dot{m}$ is the mass flow.

Friction factor is the function of Reynolds number and relative roughness (rr). Figure 4.4 shows the Moody diagram [51] of friction factor. It shows that when the flow is laminar, the friction coefficient depends only on the Reynolds number. In the transitional phase, when the flow turns from laminar to turbulent, friction factor depends both on Reynolds number and relative roughness. When the Reynolds number is high, and the flow is turbulent, friction coefficient is only the function of relative roughness.

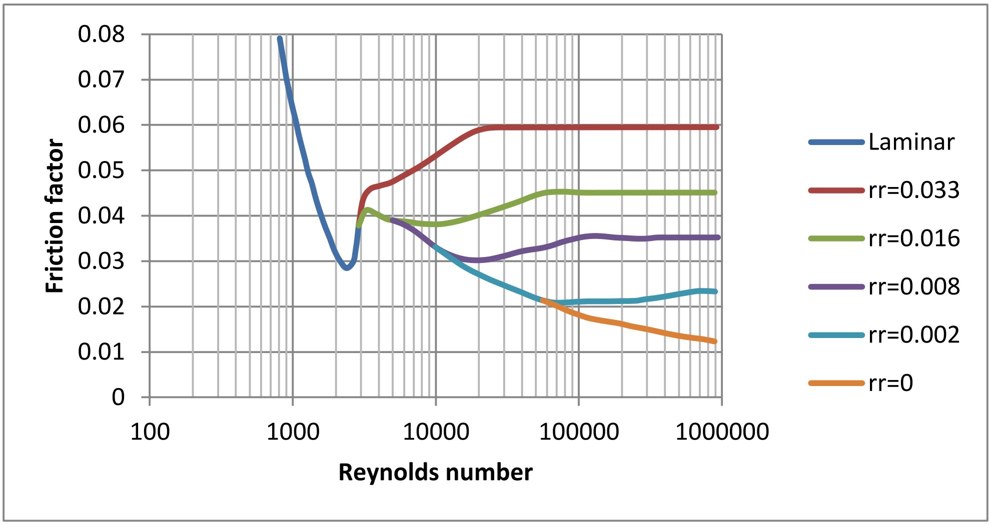

Figure 4.4. Moody diagram

Test results show that the pressure drop depends highly on the temperature difference. This could be seen for both air and gas side in Figure 4.5 and Figure 4.6. For fixed mass flow, inlet temperature was also kept constant or at least that was the intention. For some points there is an insignificant drift. Although not shown in Table 4.2, the inlet pressure was also kept constant. Thereby, for fixed mass flow, pressure drop difference comes from the temperature difference.

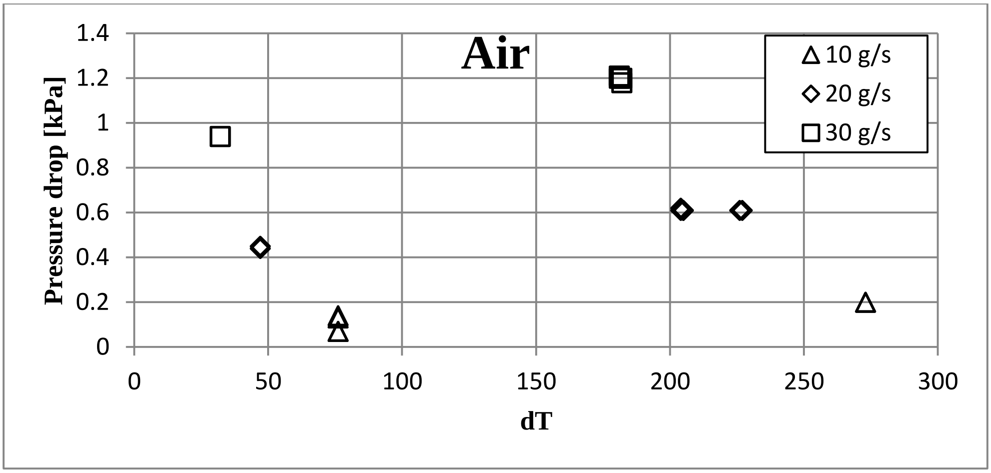

Figure 4.5. Pressure drop as a function of the temperature difference, air side

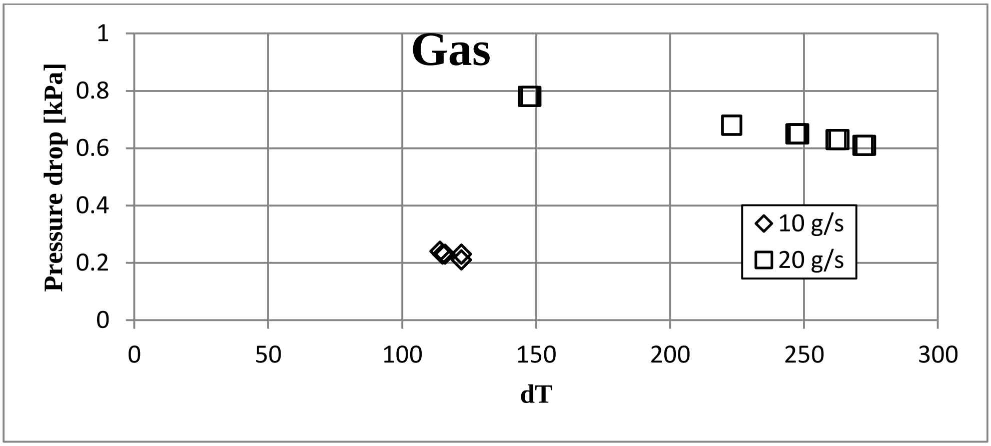

Figure 4.6. Pressure drop as a function of the temperature difference, gas side

To take into account the added heat in the tube because of the heat transfer, density used in equation (4.3) was the arithmetic mean value of inlet and outlet density.

The simulation model supposed equal distribution of mass flow to all channels. The pressure drop would be then equal in all channels. By this hypothesis, the pressure drop for the whole core would be equal to the pressure drop of each channel. Thereby, it was calculated the pressure drop for one channel.

Hydraulic diameter was calculated by:

$$D_h = \frac{2ab}{a+b} \tag{4.4}$$

Where a,b are the height and the width of the channel.

Dimensions of the air channel were 3x1.5 mm and dimensions of the gas channel were 5x2 mm. The effective dimensions of the channels, after discounting the wall thickness, were 2.8x1.3 mm for the air and 4.8x1.8 mm for the gas. Hydraulic diameters of both channels can be calculated by equation (4.4).

$$D_{h,air} = 1.77\ mm \qquad D_{h,gas} = 2.61\ mm \tag{4.5}$$

The absolute roughness was selected from the [51] for the channel made of commercial steel and it was ε=0.01 mm. Relative roughness was calculated by:

$$rr = \frac{\varepsilon}{D_h} \tag{4.6}$$

The length of the gas channel was 224.4 mm while the air channel was shorter for the width of the diffuser which was 30 mm.

The results of modelled pressure drop at the gas side are plotted on the Figure 4.7 along with the measured pressure drops. In this figure dT represents the temperature difference of the inlet and outlet temperature.

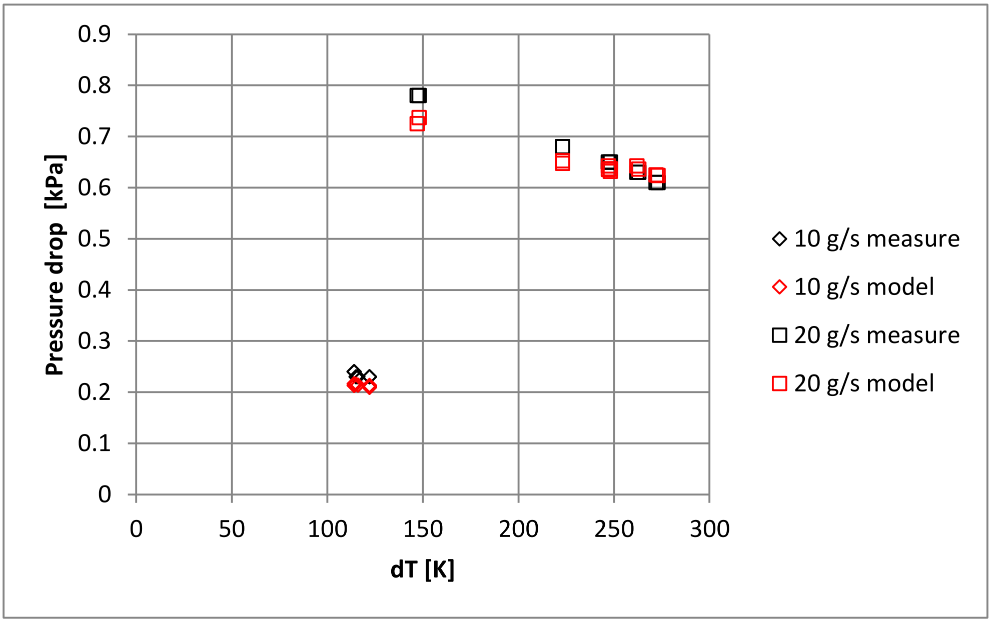

Figure 4.7. Measured and modelled pressure drop, gas side

For the gas side, the fit between the experimental measurements and simulation results is generally good. The discrepancy was less than 10 % for all points. This was considered to be a good result and proved the hypothesis that majority the of the pressure drop comes from core friction it this case.

At the gas side, apart from the heat exchanger core there were two other parts that influence the flow: inlet divergent diffuser and outlet convergent diffuser.

Nevertheless, the change of section in those diffusers was not very big. It was considered that pressure drop in those components was not significant and it was not applied in the model. At the air side, the change of section was bigger and it could have more influence on total pressure drop. But, the biggest difference at the air side was that the flow had to change the direction two times. First, at the entrance, flow turns 90 degrees and then at the outlet it changes the direction again for 90 degrees. Those flow bends had to be included in the model.

Pressure drop in diffuser or bend is determined by:

$$\Delta p = \zeta \frac{\dot{m}^2}{2\rho A^2} \tag{4.7}$$

where ζ is the total resistance coefficient and other parameters are the same as in equation (4.3).

Total resistance coefficient represents the sum of local resistance and friction resistance to the flow:

$$\zeta = \zeta_{loc} + \zeta_{fr} \tag{4.8}$$

Nevertheless, friction resistance was neglected in this case because of short diffuser length.

Diffuser was modelled according to Idelchik [51] that defines the resistance coefficient for a diffuser as a function of diffuser angle and ratio of inlet (A_{in}) and outlet (A_{out}) areas.

$$\zeta = f\left(\alpha, \frac{A_{in}}{A_{out}}\right) \tag{4.9}$$

For a transition from circular to rectangle (inlet diffuser), diffuser angle α was calculated by:

$$\alpha = 2\tan^{-1}\left(\frac{2\sqrt{\frac{a \cdot b}{\pi}} - D}{2l}\right) \tag{4.10}$$

where a=30 mm and b=80 mm are the width and the height of the rectangular area, D=33 mm is the diameter of the circular area and l=40 mm is the length.

For the outlet diffuser when transition is from rectangular to circular shape, diffuser angle was calculated by:

$$\alpha = 2\tan^{-1}\left(\frac{D - 2\sqrt{\frac{a \cdot b}{\pi}}}{2l}\right) \tag{4.11}$$

Resistance coefficient was then interpolated from the table that Idelchik gives to estimate the friction factor as a function of diffuser angle and area ratio.

It should be noted that friction coefficient does not depend on flow parameters like Reynolds number. Thereby resistance coefficient was only a function of geometrical dimensions and it was $\zeta_{dif} = 0.358$.

Bends were also modelled according to data from Idelchik. Again, friction part of the total resistance coefficient was considered negligible and resistance coefficient was calculated as:

$$\zeta = c_{b1} \cdot c_{b2} \cdot c_{b3} \tag{4.12}$$

where c_{b1} is the coefficient that takes into account bend angle δ, c_{b2} is the coefficient that takes into account bend radius and is defined by the ratio of bend radius and hydraulic pipe diameter R/D_h, c_{b3} is the coefficient that takes into account the shape of the profile and it is defined as the ratio of width and height a/b.

The value of bend angle was δ=90°, ratio a/b=30/80 was the ratio of rectangle diffuser side, bend radius was defined as $R=0.5D_h$ and hydraulic diameter D_h was used as a parameter for optimisation of pressure drop. The value used was $D_h=26.8$ mm. The actual geometry of this diffuser is very complex so an approximate simpler geometry with an equivalent diameter has been considered for this model. Values for coefficients c_{b1}, c_{b2} and c_{b3} were taken from the Table 4.3, Table 4.4 and Table 4.5 [51].

δ	0	20	30	45	60	75	90	110	130	150	180
c_{b1}	0	0.31	0.45	0.60	0.78	0.90	1	1.13	1.20	1.28	1.40

Table 4.3. Bend resistance coefficient c_{b1}

R/Dh	0.5	0.6	0.7	0.8	0.9	1	1.25	1.50
cb_2	1.18	0.77	0.51	0.2=37	0.28	0.21	0.19	0.17

Table 4.4. Bend resistance coefficient c_{b2}

a/b	0.25	0.5	0.75	1	1.5	2	3	4	5	6	7	8
cb_3	1.3	1.17	1.09	1	0.85	0.85	0.90	0.95	0.95	0.98	1	1

Table 4.5. Bend resistance coefficient c_{b3}

Resistance coefficient was again independent of the flow characteristics and only defined by adopted bend dimensions. The calculated value was $\zeta_{bend} = 1.406$.

Pressure drop model for the air side was compared with measured values and results are presented in Figure 4.8. The model does not predict well the pressure drop at the low mass flow (10 g/s) where discrepancy between measured and modelled pressure drop was as high as 50%. Nevertheless, those points are not very interesting for WHR because of the low potential for energy recuperation. For the mass flow of 20 g/s discrepancy was less than 15%. For the mass flow of 30 g/s discrepancy was less than 7%. It was considered that obtained results fitted well with the measured values in the mass flow range that has high waste heat recovery potential.

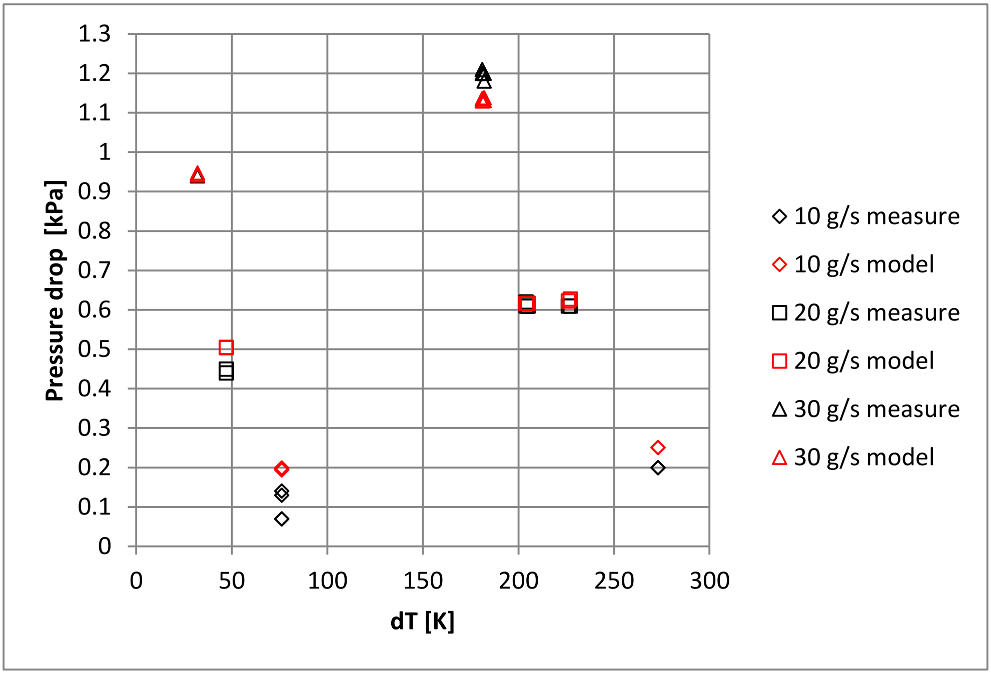

Figure 4.8. Measured and modelled pressure drop, air side

Heat exchanger model for the air side was applied in the model of the Brayton cycle system. For the gas side, the pressure drop calculation was used to calculate the engine pumping loss to push the exhaust gas through the heat exchanger.

4.4 Pressure wave transmissivity

At first, it should be explained why it is important to determine this characteristic. The alternating piston motion, along with opening and closing of valves creates a strong pulsation in the tubes that connect the cylinder with the atmosphere and the heat exchanger. While the internal combustion engines admission and exhaust is similar, the effect here could be different. For ICE, synchronising admission pulses leads to more air being admitted, which allows more fuel to be injected and burned, leading to more power. Synchronising exhaust pulses takes more product of combustion out of the cylinder, thus lowering the temperature inside the cylinder and allowing more air to be admitted. For compressor-expander machines on air Brayton cycles (ABC), the effect of synchronisation of pressure pulses has to be studied. For these machines, there is not only admission and exhaust that should be tuned, but also a high pressure loop that connects the cylinder with heat exchanger. Actually, it is the high pressure loop that is more interesting for tuning, because negative work of the high pressure loop is expected to be higher than the negative work of the low pressure loop due to the short opening period of these high pressure valves.

Figure 5.1 shows the WHR system schematic and the denomination of the tubes and valves. Pressure pulse in the high pressure loop is created when the high pressure (HP) outlet valve opens and the air starts to flow from the machine to the heat exchanger inlet tube. Wave then travels through the inlet tube and reaches the heat exchanger. At the heat exchanger inlet some part of the wave is transmitted while the other part is reflected. Reflected wave goes back toward the outlet wave and gets superimposed with the wave traveling toward the heat exchanger. Transmitted wave travels through the heat exchanger and reaches the outlet where again one part is transmitted and the other is reflected. The transmitted part goes through the outlet tube and bounces at the high pressure (HP) inlet valve.

It is important to determine the acoustic response of the heat exchanger as this will determine the pressure wave formed in the tubes that connect the heat exchanger with the machine. If pressure wave at the heat exchanger inlet tube is optimised, then low pressure peak can arrive at the time of the high pressure outlet valve of the machine opening, thereby reducing the pumping losses to pump the air from the cylinder to the heat exchanger.

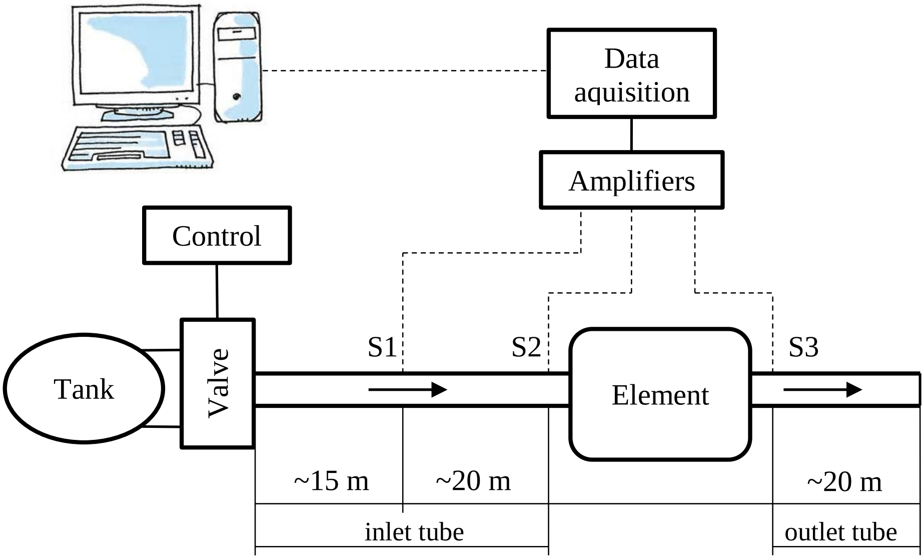

Figure 4.9. Pressure pulse test bench schematic

In order to characterize the heat exchanger transmissibility, it had to be examined on the pressure pulse test bench. Figure 4.9 shows the schematic of the pressure pulse test bench developed at CMT. The tank is charged by the externally supplied compressed air to a desired pressure. Tank volume is 50 litres and maximum pressure is 10 bar. The desired static pressure can be adjusted by a regulator that is not shown on the schematic. The maximum regulator pressure is 21 bar and the operating range is between 0 and 8.5 bar. The valve is in charge of creating a pressure pulse by rapidly opening and closing. Electronic circuit controls the solenoid voltage and is capable of opening and closing the valve in a desired period between 10 to 80 ms. The valve connects the tank with the inlet tube. Tubes with different inner diameters are available and the one that most closely fits the inner inlet diameter of the tested element should be used. Figure 4.9 also shows the lengths of the inlet and outlet tubes. The inlet tube is divided to two parts, and the first pressure sensor S1 is mounted in between them. The tube lengths are big, so that the sensor S1 could capture completely the pressure pulse generated without any reflections. Other requirement is that the tubes have to be sufficiently rigid to avoid deformations during the pressure wave propagation. The tubes were made from polyethylene that possess good rigidity and can be easily rolled up so that the installation can be more compact. The radius of the rolled tubes has to be big enough to avoid the influence of curvature on pressure wave propagation. In this case the radius was 1m.

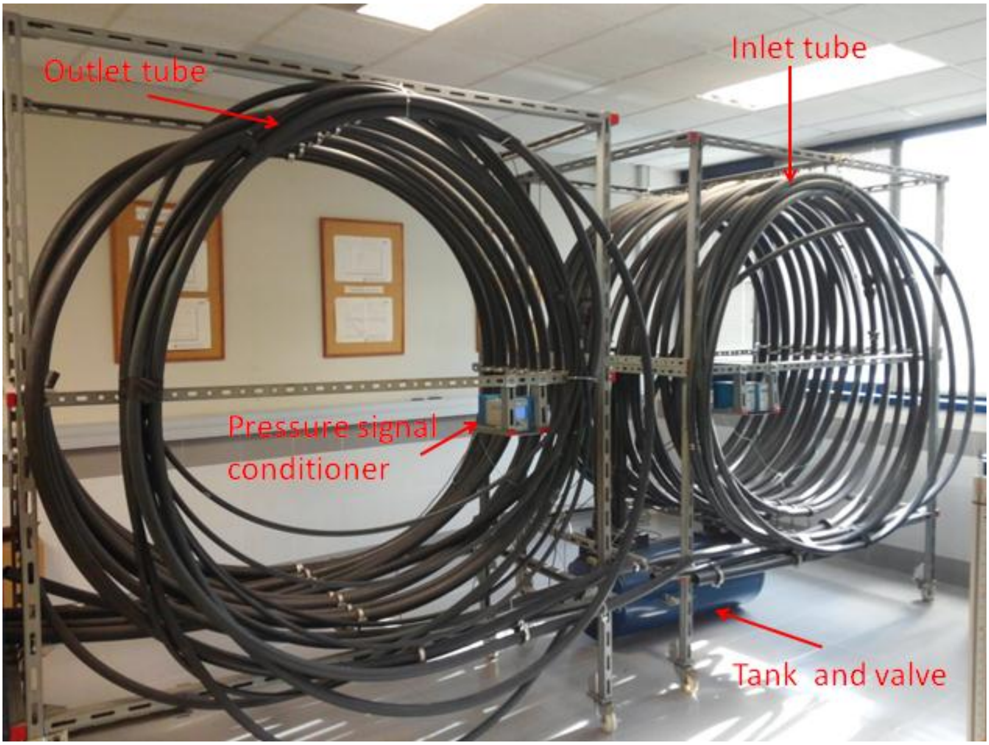

Figure 4.10. Pressure pulse test bench

The photo of the test bench is presented in Figure 4.10. The 50 litres blue pressure tank can be seen at the bottom right. The fast valve is installed at the left end of the deposit. The valve is connected to the inlet tube shown on the right side. The pressure pulse travels along the inlet tube until it reaches the element being tested that should be placed between the inlet tube on the right and the outlet tube on the left. On this photo no element was mounted. Three pressure transducers are used. The first (S1) approximately at the middle of the inlet tube, second (S2) before the tested element and third (S3) after the tested element. The photo also shows two signal conditioners for pressure sensors. Few different inlet and outlet tube sets with different diameter can also be seen. In this case, the tubes with 33mm internal diameter were used, as this was the internal diameter of heat exchanger inlet and outlet flanges.

KISTLER 7001 piezoelectric transducers were used for measuring pressures. This type of pressure transducer is considered appropriate for this application because of its good sensitivity. KISTLER 5011 charge amplifiers were used for amplification and conditioning of the signal coming from the pressure transducers. HP 3565S was used for acquisition of conditioned signals to the computer, where the acquired data was processed by commercial software LMS-CADA. The most important properties for all devices are presented in the Table 4.6.

Device	Property	Value
Kistler 7001 pressure transducer	Sensitivity	80 pC/bar
	Pressure range	0-250 bar
	Linearity	<±0.8 %
	Maximum temperature	350 °C
Kistler 5011 charge amplifier	Measuring range	±10-±990000 pC
	Sensor sensitivity	±0.01-±9900 pC/bar
	Frequency range	0-200 kHz
	Maximum error	<3% (typically <2%)
HP 3656S	Maximum sampling frequency	102.4 kHz
	Throughput	2.6 Mb/s

Table 4.6. Pulse test bench device properties

The test procedure consisted of generating the pressure pulse by fast opening and closing of the valve. The amplitude and duration of the pulse should be of the similar order of magnitude as the one expected at inlet of tested element. In this case that would be the pressure pulse generated at high pressure loop when the outlet valve opens. The amplitude of the pulse is controlled by the pressure in the tank. Two values were tested for the tank pressure: 5 bar and 7 bar. The duration of the pulse is controlled by the duration of valve opening and closing. The duration of the pulse was kept at 15 ms.

Pressure pulse travels along the inlet tube and reaches the tested element where one part of the wave gets reflected and returns toward the valve, while other part is transmitted through the element and output tube to ambient. Long tubes allow measurement of the incident, reflected and transmitted wave without the mutual interaction.

First pressure sensor is located after the valve on the sufficient distance to allow a complete development of the generated pressure pulse. Second sensor measures the pressure at the inlet of the tested element. It captures both the incident and the reflected wave. Third sensor at the element outlet measures the transmitted wave.

The methodology to test the heat exchanger was as follows. First, a straight tube is placed instead of the tested element; the internal diameter of the tube is the same as the internal diameter of the tested element inlet. Then, 10 identical tests are done with the tube and pressures are captured with sensors S1 and S2. After, the tube is replaced by the tested element and 5 tests are done measuring pressures with all three sensors. The 5 measurements of pressure from the sensor S1 for the element are compared with the 10 measurements from the same sensor for the tube, in order to find the pair that gives the closest match. The measurement of the heat exchanger, from this pair, was used for further analysis.

Figure 4.11 shows the plot of measured pressures for heat exchanger for tank pressure of 5 bar and pulse duration of 15 ms. It can be seen that the long tubes allow good separation of incident and reflected waves as there are no negative pressure peaks (during the wave propagation through the heat exchanger) that would represent the reflected waves. The first peak (S1) on the plot represents the generated pressure pulse created by fast opening and closing of the valve. The second peak (S2) represents the pressure at the heat exchanger inlet composed of superimposed inlet wave and reflected wave. The third peak (S3) represents only the wave that is transmitted through the heat exchanger. Same meaning for pressure signals from sensors S1-S3 is applied for Figure 4.12, Figure 4.13 and Figure 4.14.

Figure 4.12 shows the plot for tank pressure of 7 bar. Duration of generated pulse was maintained constant but the amplitude is higher. Consequently, all pressure peaks are higher than for 5 bar tank pressure, but there are not any other significant changes.

Heat exchanger was also tested in reverse, the inlet from the previous tests was now the outlet and vice versa. Again, tests were done for 5 and 7 bar tank pressure. The results are given in Figure 4.13 and Figure 4.14.

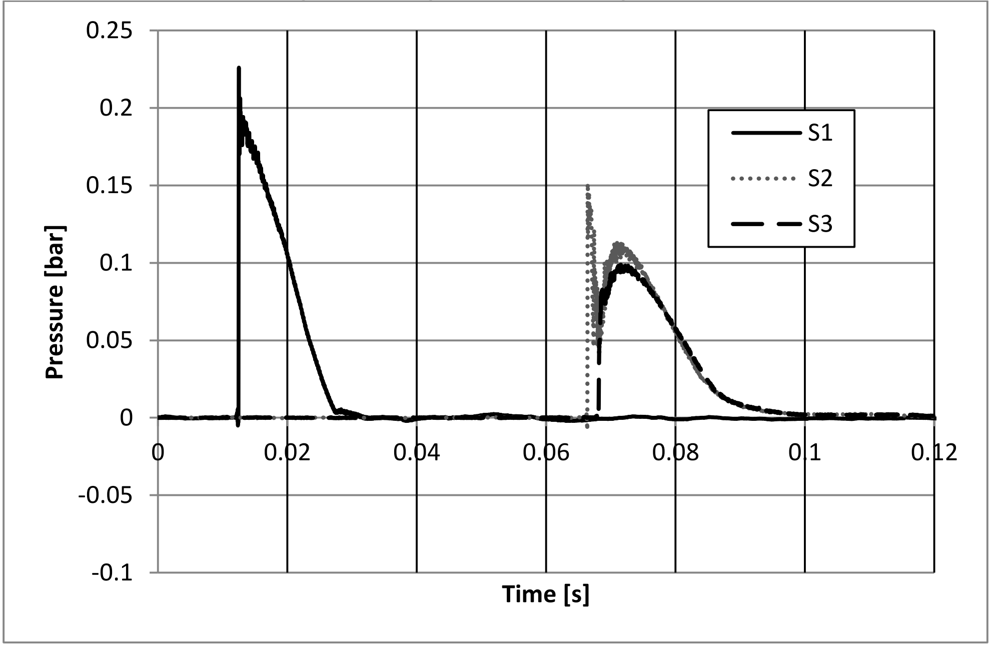

Figure 4.11. Recorded pressures for 5 bar tank pressure, direct test

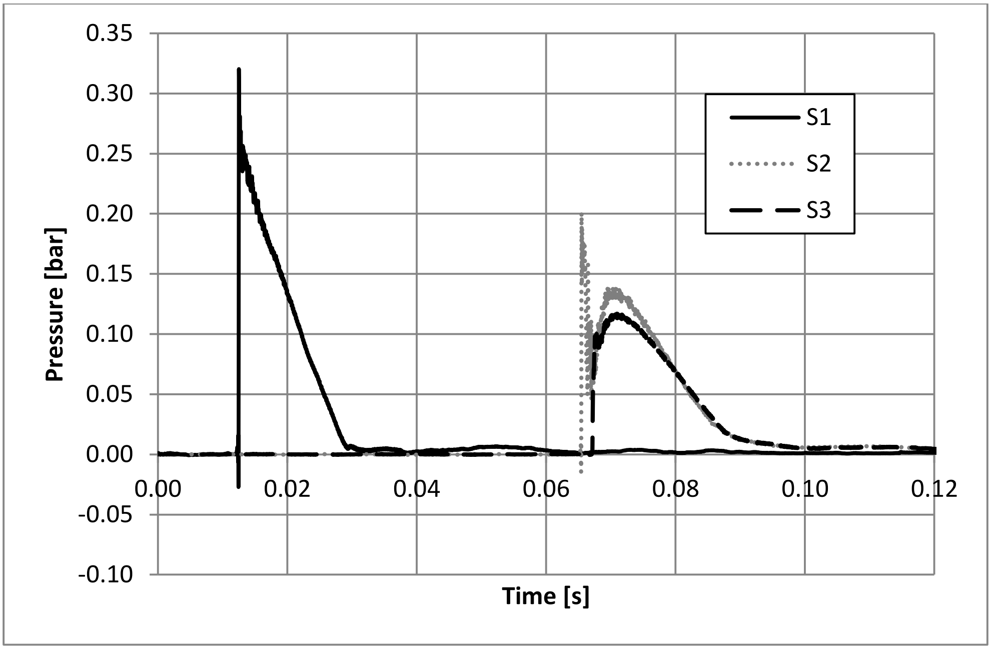

Figure 4.12. Recorded pressures for 7 bar tank pressure, direct test

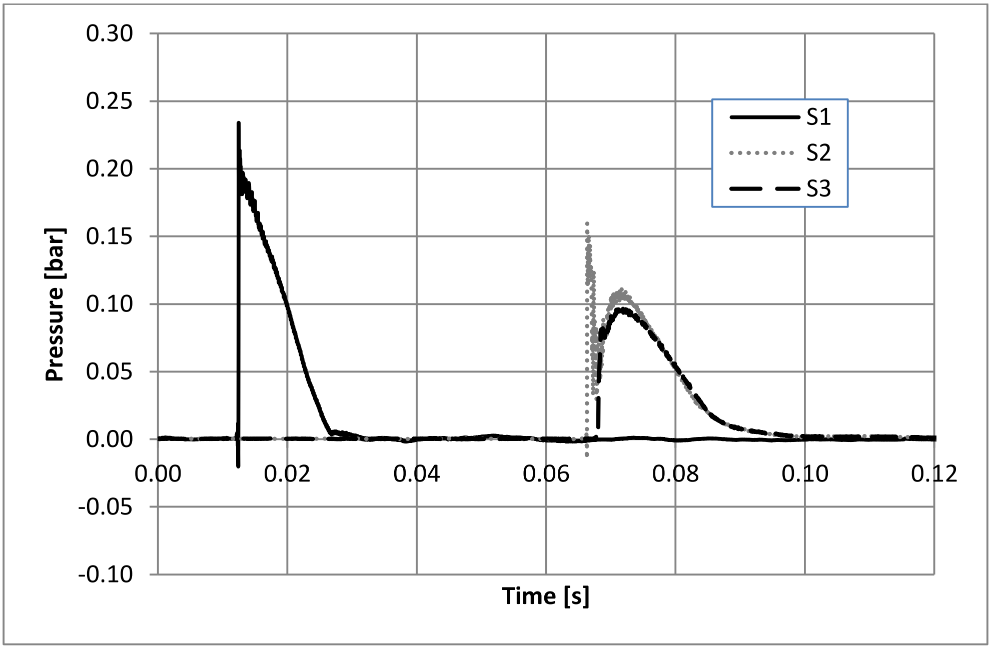

Figure 4.13. Recorded pressures for 5 bar tank pressure, reverse test

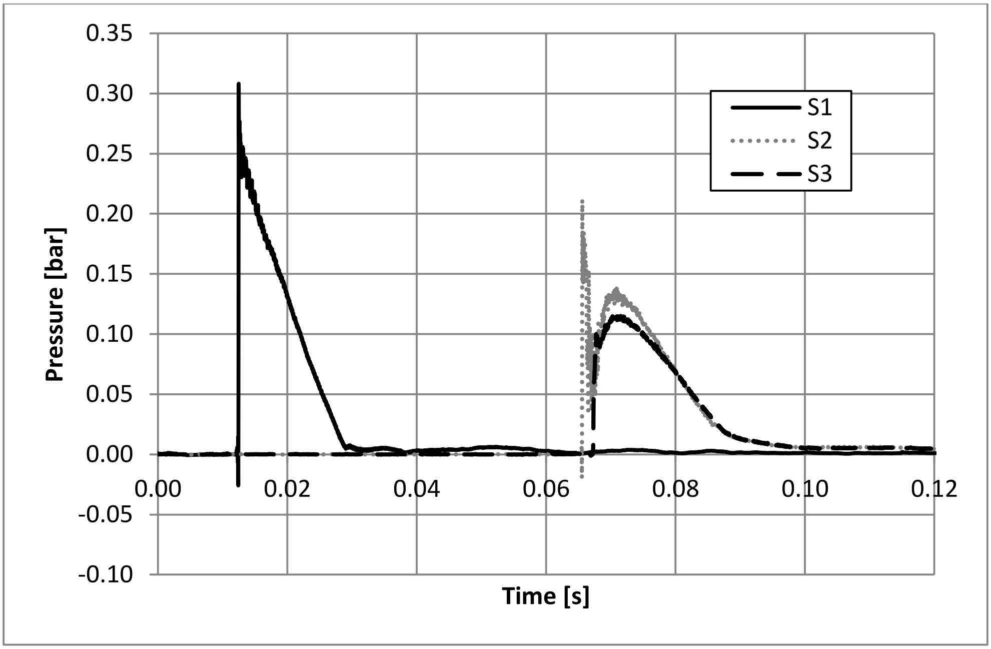

Figure 4.14. Recorded pressures for 7 bar tank pressure, reverse test

Plots for the direct and inverse test are almost identical meaning that the heat exchanger has a symmetrical acoustic response. That was the expected behaviour because of the heat exchanger geometrical symmetry. Figure 4.15 shows the heat exchanger on the test bench where its geometrical symmetry can be observed.

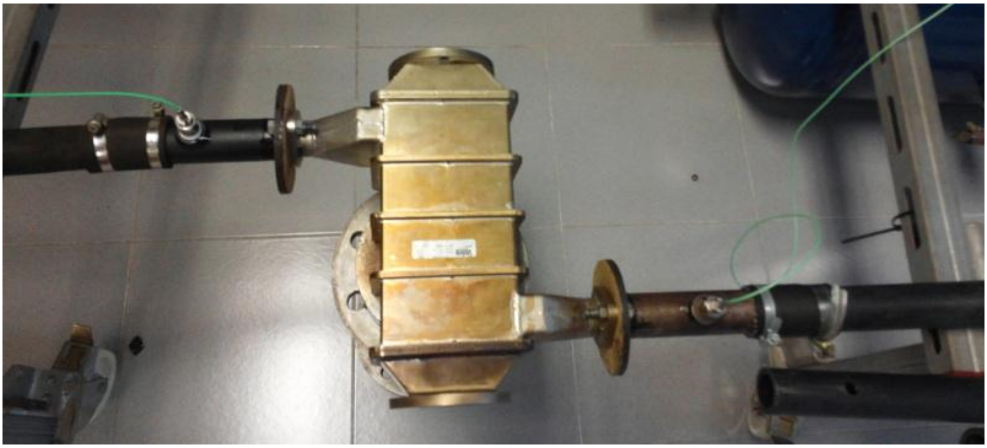

Figure 4.15. Heat exchanger on the test bench

The 1D model of the heat exchanger was made in Amesim. The model consisted of: heat exchanger core, inlet divergent diffuser, inlet bend, outlet convergent diffuser and outlet bend. The model was similar to the 0D heat exchanger model with some differences: diffusers were circular on both ends, bends had different diameters at the inlet and outlet and bend radius was different. Figure 4.16 shows the Amesim model that was used for optimisation of the parameters in order to fit the model with the experimental measurements.

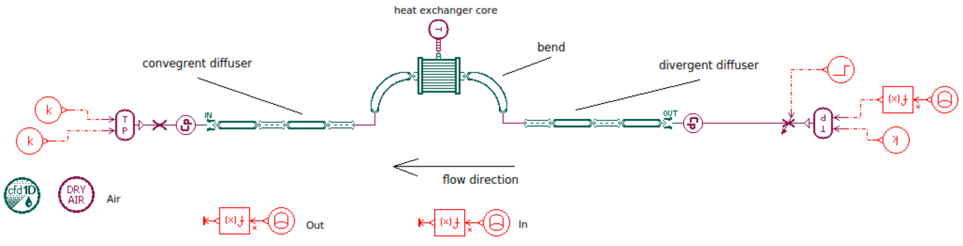

Figure 4.16. Amesim 1D heat exchanger model

Smaller diameter of diffusers was 33 mm (same as the internal diameter of the flange) and the bigger diameter was 43.6 mm which was the value of hydraulic diameter calculated by equation (4.4) for the rectangle channel with the dimensions 30x80 mm. Heat exchanger core was modelled as multiple channels where channel dimension were the same as for 0D model 2.8x1.3 mm and the total area was equal to the channel area multiplied by number of channels which was 750. Bend angle was 90 degrees. Bend had the bigger diameter equal to adjacent diffuser diameter 43.6 mm. The smaller bend diameter (adjacent to the core) and bend curvature radius were the parameters for optimisation. The values that gave the good fit with the experimental data were 30 mm for the smaller bend diameter and 110 mm for the curvature radius. The model simplified the real heat exchanger geometry but its main dimensions were respected.

The result of the optimisation is presented in Figure 4.17 and Figure 4.18, for 5 bar and 7 bar tank pressure, the measured values of pressure from sensors S1, S2 and S3 were compared with simulation results. Simulation results fit very well with the experimental measurements. 1D heat exchanger model was used in complete WHR machine model to analyse the effect that pressure wave synchronisation could have on the cycle.

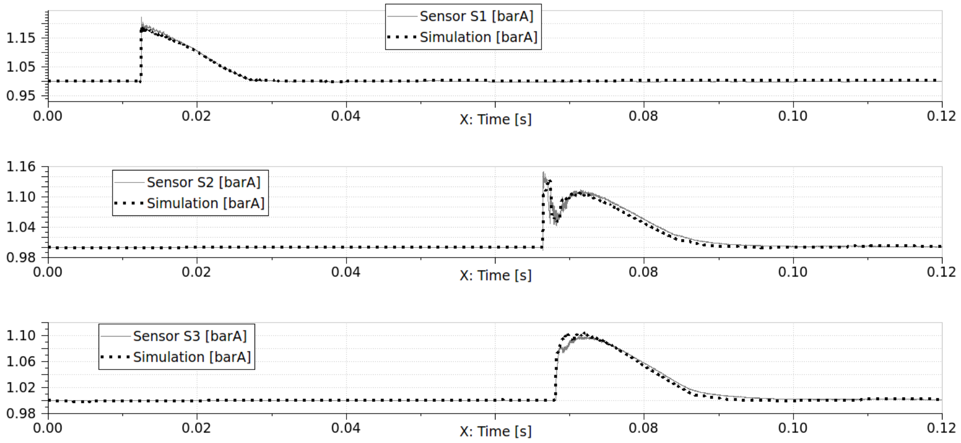

Figure 4.17. Fitting the heat exchanger model with the experimental results, 5 bar

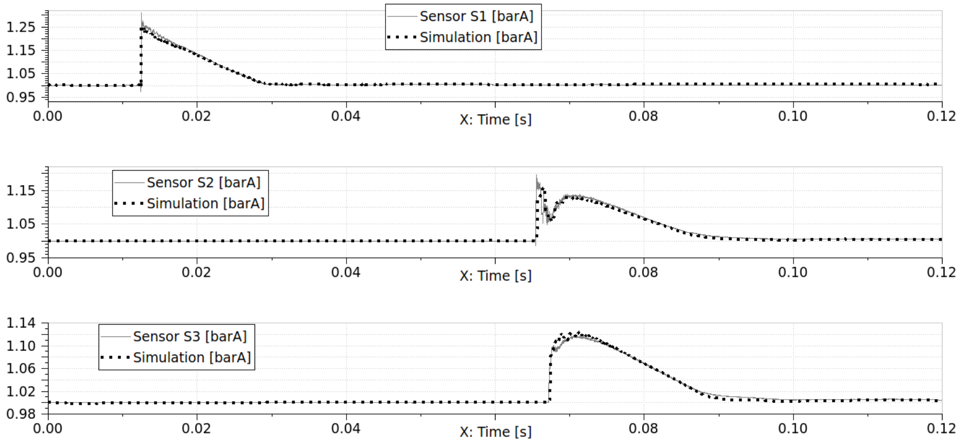

Figure 4.18. Fitting the heat exchanger model with the experimental results, 7 bar

5 Heat recovery system model

Contents

5.1 Introduction 87

5.2 Simple machine model 90

  5.2.1 Poppet valve 93

  5.2.2 Reed valve 110

  5.2.3 Camless poppet valve 117

5.3 Heat exchanger tube length 119

5.4 Heat transfer model 127

5.5 Mechanical losses.. 129

5.6 Indirect losses.. 134

  5.6.1 Exhaust backpressure pumping losses 134

  5.6.2 Additional weight... 134

5.1 Introduction

In Chapter 3 the ideal cycle was first analysed to get the idea of the theoretical maximum that could be obtained with this WHR system. Later it was considered what kind of a machine could be used for this cycle. Machine selection gave the idea of the machine efficiency so that the non-ideal cycle could be studied. In this case the only difference from the ideal cycle was that compression and expansion processes were no longer ideal but they had the isentropic efficiency of 80%. These isentropic efficiencies represent various machine losses which were not separately identified. In this chapter machine design was further considered by analysing machine elements and losses. The objective of this chapter was to study the machine elements that could be used to realise the cycle, make the computer model of the whole system and then analyse the cycle. In the first approximation machine elements should be from some existing and well known technology in order to avoid many unknows that could arise from the technology that is not well known and documented.

Some elements of the machine design were already defined in the Chapter 3:

- one cylinder with alternating piston doing both compression and expansion processes.
- piston diameter 120 mm
- machine is coupled directly to the engine without gearbox with the expected maximum rotary speed of around 7000 rpm. This value was the maximum rotary speed of the engine whose data were used in Chapter 3 which could be considered to be the typical gasoline engine.

The schematic of this Brayton cycle WHR sytem is given on the Figure 5.1. As it was already said the machine is an alternating piston sliding in the cylinder. The machine is used both as a compressor and expander and it can be coupled directly with ICE. On the figure, only the valves for connection to heat exchanger (high pressure valves) can be seen but the machine has also one or two valves for connection with the atmosphere (low pressure valves). On the same figure outlet valve is represented as reed valve and inlet valve as poppet valve although they can both be of any type. Operating principle is similar to four stroke internal combustion engine. At the start, piston is at the lowest position called Bottom Dead Centre (BDC). At this position the crank angle is 0 degrees. In the first stroke the piston goes up lowering the chamber volume and raising the pressure inside the chamber. All valves are closed and the air inside the cylinder is being compressed. This is the compression stroke that gives a negative cycle work. In some moment, before reaching the highest piston position called Top Dead Centre (TDC), High Pressure (HP) outlet valve opens and hot compressed air passes from the cylinder to the heat exchanger where it gets heated. Piston reaches the TDC (180 degrees), HP outlet valve closes and piston starts to go down augmenting the volume and lowering the pressure and temperature in the chamber. In some moment HP inlet valve opens and hot compressed air from the heat exchanger enters the cylinder. The inlet valve closes and trapped air gets expanded giving a positive cycle work. This is the expansion stroke. Piston reaches the BDC (360 degrees) and the next stroke begins. LP valves for connections with the ambient open, piston rises and pushes the air out to the ambient. This stroke is called exhaust and it ends when the piston reaches the TDC (540 degrees). Piston starts going down augmenting the volume. The Low Pressure (LP) valve (or few of them) for connection to the ambient are open and air is admitted to the chamber. This is the suction or admission stroke. Piston reaches the BDC (720 degrees) and the cycle is complete. Admission and exhaust create the negative work as piston has to move the air in and out of the cylinder. The cycle power depends on the difference between the positive and negative work of the cycle.

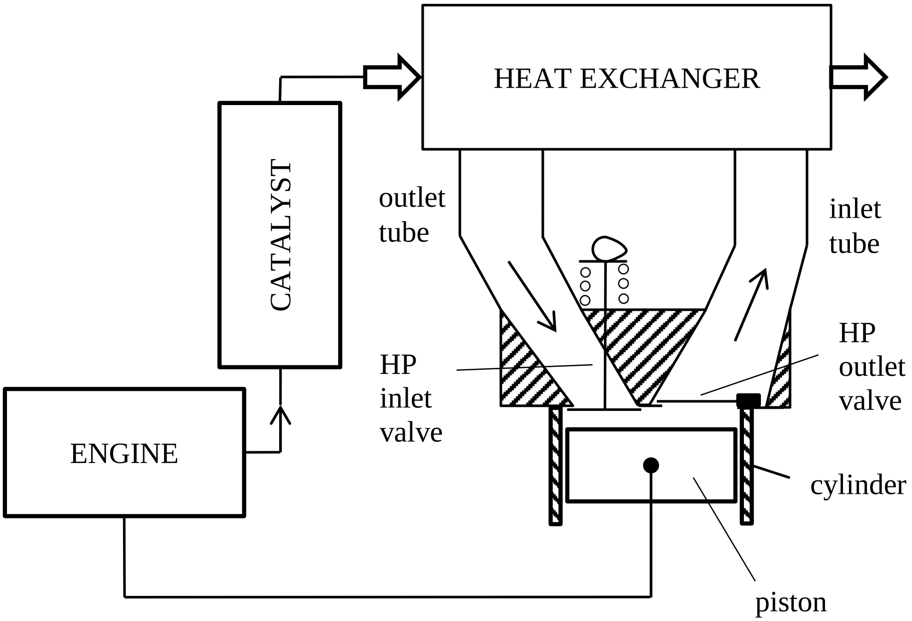

Figure 5.1. ABC schematic

As it was explained, HP outlet and inlet valves are not open at the same time, except for a short possible valve overlap around TDC. This way the flow of air through the heat exchanger is unidirectional and in the opposite direction to the exhaust gas in counter-flow heat exchanger. Valve opening duration is short, around half the time of one piston stroke, so there is not much time available to transfer all the air from the cylinder to heat exchanger. Different strategy is possible for LP valves, where both valves could open at the beginning of exhaust and stay open all the way during suction. In this case there would have to be reliefs in the piston for the valves to avoid the contact between the piston and valves when piston goes toward TDC and valves are open. This happens at the end of exhaust and beginning of suction. Or other strategy could be to close the valves at the end of exhaust and open them again at the beginning of suction. In any case, both valve would serve for exhaust and suction. Temperature of air at exhaust is higher than the temperature of ambient air so there is a risk that hot air could be sucked into the machine thereby reducing the density of admitted air and mass flow. Nevertheless, at first, it was considered that this is not the case and that fresh charge is at the ambient air temperature.

There are many machine parameters that have not yet been defined. Piston stroke is one of them. With fixed piston diameter, it is the stroke that defines the displaced volume, which in turn along with volumetric efficiency and rotational speed defines the air mass flow.

Type, number and dimensions of valves, timing of opening and closing the valves are all very important to determine the in cylinder pressure and consequently the cycle efficiency. Air passing through the valves defines the pumping losses. Those losses affect the isentropic efficiency defined in Chapter 3 and as it was shown isentropic efficiency has a big influence on cycle efficiency.

Other type of losses should also be considered. They are the consequence of friction either between the two parts in relative motion or due to the fluid friction. Mechanical losses could represent important losses and must be included in the model.

After passing through the heat exchanger, temperature of the air inside the cylinder gets much higher than the temperature of the cylinder wall thereby there is a heat transfer from hot air to colder cylinder wall. This way the part of the heat admitted from heat exchanger would not produce the work. Furthermore, for steady conditions, the heat that was passed to the cylinder wall heats the wall that later during the suction and compression stroke heats the air inside the cylinder. This further reduces the recuperated power. Heat transfer between the ambient air and heat exchanger and the ducts connecting it to the cylinder can represent an important energy loss. These parts should be thermally isolated from the surrounding air in order to reduce the heat transfer to the ambient.

All these subjects intend to treat the cycle losses that would distinguish the real cycle from the ideal one analysed in Chapter 3. This way, losses can be treated separately and not just included in one coefficient, as it was done in Chapter 3 for a non-ideal cycle using machine isentropic efficiency. Cycle losses can generally be divided in following categories:

- Air management processes: real processes are not instantaneous but require time and can overlap; most adoption of heat is partly overlapped with compression and expansion processes. These processes include the pumping losses to admit the air from the ambient, expulse the air to the heat exchanger, admit the air from the heat exchanger and expulse the air to the ambient.

- Heat losses: loss of heat from trapped air by heat transfer from air to cylinder inner wall and from the cylinder outer wall to the ambient.
- Mechanical losses: friction between the parts in relative motion that lowers the positive cycle work and generates heat.

This chapter deals with creation of the computer model of the WHR system that would include all these losses and provide a tool to estimate recuperated power.

5.2 Simple machine model

A simple machine model was made to represent air management processes. Simple machine model served as a base to apply the models of other losses. Literature review revealed a significant lack of information regarding the alternating piston use as a heat recovery machine. Nevertheless, other machines like internal combustion engines or reciprocating compressors also use alternating piston and are well tested and documented. Apart from the crankshaft-piston mechanism, heat recovery machine could also share other design elements used in these machines like valves, lubrication system, cooling system etc. Confirmed models of air management, mechanical losses or heat losses of ICE or reciprocating compressors were applied to heat recovery machine as a first approximation. Later, specific models could be developed to better adapt to the piston expander of WHR system.

System was modelled in the computer program AMESim. The main component of the system is the variable volume chamber. This volume is connected to the heat exchanger by two HP valves and to the ambient by two LP valves. Heat transfer model is applied to the chamber to represent the heat transfer between the gas inside the chamber and chamber walls. Alternating piston mechanism is connected with the chamber to provide a variation of volume. The model of the mechanical losses is connected to the alternating piston mechanism.

Cylinder volume changes as a function of crankshaft rotation. Crankshaft angle (CA) defines the linear piston displacement but it is also used as a reference for other variables. Piston displacement in turn defines the cylinder volume. Maximum cylinder volume is defined as a sum of total displaced volume (V_{disp}) and minimum volume (V_{min}):

$$V_{max} = V_{disp} + V_{min} \tag{5.1}$$

The minimum cylinder volume, also called dead volume, is the volume when piston is at TDC position. V_{disp} is the volume displaced by cylinder when it is moving from TDC to BDC. Consequently, cylinder volume is at maximum when piston is at BDC. Displaced volume is expressed by:

$$V_{disp} = \frac{D_p^2 \pi}{4} S \tag{5.2}$$

D_p is the piston diameter and S is the piston stroke. Piston diameter was already defined but the piston stoke was not. Piston stroke is an important parameter because it defines the displaced volume and thereby air mass flow capacity and machine size. For a fixed piston diameter, the bigger the piston stroke is, the higher the displaced volume would be. More air could be moved by the piston but also the machine would be longer. Air mass flow through the machine does not depend only on displaced volume but also on the machine ability to fill this volume with air. As machine admits and expulses the air through the valves it is necessary first to model the actual valves in order to estimate the air mass flow. In the Chapter 3 it was estimated that better results could be obtained if air mass flow is equal to gas mas flow. This conclusion was valid for a very simple definition of cycle and heat exchanger from Chapter 3. For a more complex model used in this chapter it had to be checked what is the optimal ratio of air to gas mass flow. Piston stroke was a variable parameter that allowed the change of air mass flow. As gas mass flow was fixed for point G, change of air mass flow directly changed the ratio of air and gas mass flows.

WHR alternating piston machine and ICE share some processes. Compression, expansion, air admission from the ambient and expulsion of the air (gas) from the previous cycle are very similar. However the main difference comes from the adsorption of heat into the system. In ICE heat is mainly introduced by combustion of fuel and air mixture while all the valves are closed. The pressure in the cylinder rises significantly and positive work is generated. In WHR air has to be pushed to the heat exchanger to get warmed up and then introduced back to the machine. During this process at least one valve for connection with the heat exchanger is opened and the generated work is negative because energy has to be spent to move the air. This can be seen in the estimated pressure-volume diagram in Figure 5.2

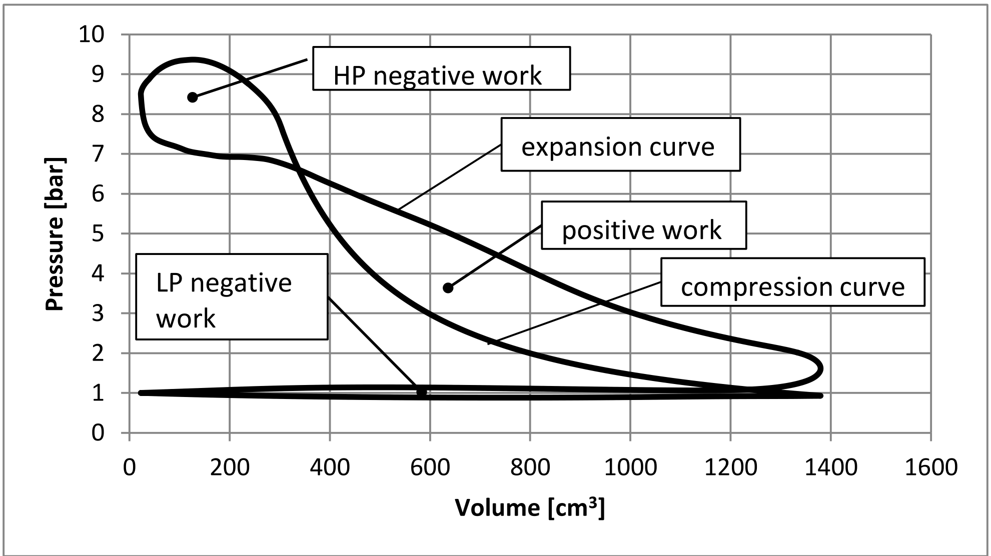

Figure 5.2. Estimated Brayton cycle pV diagram

High Pressure (HP) negative work is lower if pumping losses to move the air to and from heat exchanger are lower. These are lower if the flow resistance through the valves and heat exchanger is lower. Low Pressure (LP) negative work is lower if flow resistance in admission and exhaust to the ambient is lower. In order for the cycle to be efficient total negative work should be as low as possible. Valves represent an important flow resistance thereby valve selection and design could have a big influence on the cycle efficiency.

As admission and exhaust of the Brayton cycle machine are similar to those processes in ICE it was first considered the use of poppet valves that are typically used in the passenger car engines.

As was introduced previously, one parameter that is very important for ICE is the minimum volume (V_{min}), also called clearance or dead volume. It is important because it defines the compression ratio (CR). Compression ratio is defined as a ratio of maximum volume (sum of minimum volume and displaced volume) to minimum volume:

$$CR = \frac{V_{disp} + V_{min}}{V_{min}} \tag{5.3}$$

For ICE, compression ratio is important because it defines the pressure and temperature at the end of compression and before the start of combustion. That is because during the compression all the valves are closed and final pressure and temperature depend on their initial values and compression ratio. Compression ratio is limited to the values between 8 to 14 for gasoline engine and 17 to 23 for diesel engines [52]. In diesel engine (that uses higher compression ratio), compression ratio is limited by the maximum cylinder pressure during combustion in order not to overload engine parts. The pressure peak of the combustion is higher if the compression ratio is higher, consequently, it is a limitation parameter to design an ICE. The pressure peak of the combustion in diesel engine can reach more than 200 bar. There is no combustion in WHR and compression ratio could be higher than in ICE. For the WHR, compression ratio is not the only parameter that defines the pressure and temperature at the end of compression. That is because, at the second part of compression, HP outlet valve is opened toward the heat exchanger and this element limits the pressure rise in the machine. Thereby, as CR could be much higher for WHR than for ICE, minimal volume could be much smaller. For WHR, minimal volume is limited by the clearance between the piston and cylinder head and also by the clearance between the piston and the valve that is opened while the piston is at the TDC (if some valve should be opened while the piston is at TDC). The recommended minimum piston to valve clearance from [53] is 0.07 inch (1.77 mm). The value of 2 mm was adopted both for piston to head and piston to valve clearance. Piston to valve distance should be checked for any valve timing and if there would be a smaller distance than adopted 2 mm value then valve reliefs should be cut into piston crown surface and their volume should be calculated into minimum volume. Figure 5.3 shows that same clearance C_L is applied in all areas.

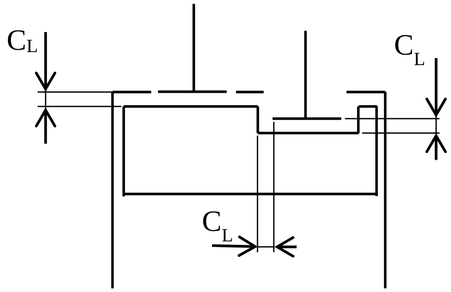

Figure 5.3. Piston to head and piston to valve clearance

5.2.1 Poppet valve

Poppet valves are for decades the standard valves used for typical four stroke internal combustion engines on vehicles. Their characteristics are well studied and known. Diameter of valves should be the highest possible to augment the flow area that allows better air flow through the cylinder. Number and diameter of valves are limited by the area of the piston. Recommendation for valve number and outer seat diameters as a function of piston diameter (Dp) for ICE. Figure 5.4 shows recommendations [54] for valve diameters and distances between the valves for four valves per cylinder. Recommendations for other valve dimensions were taken from [2].

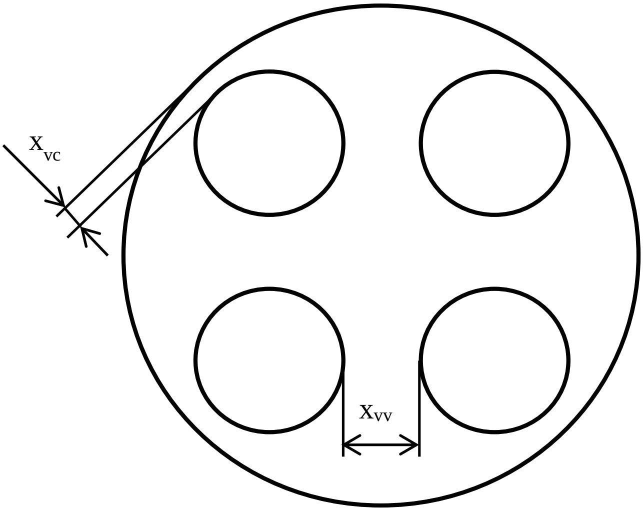

Figure 5.4. Valve dimensions recommendation; outer seat diameter (left), other dimensions (right)

For ICE valves are usually named admission and exhaust valves. For ABC machine, valves should be named differently and it is proposed here High Pressure

(HP) valves for the one that connect the cylinder with heat exchanger and Low Pressure (LP) for the valves that connect cylinder with ambient. HP valves can further be distinguished by direction of air flow looking from the cylinder. HP outlet valve is the one where air goes from cylinder toward heat exchanger and HP inlet valve is the one where air moves from heat exchanger to cylinder. HP valve denomination can be seen in Figure 5.1. For the ICE both admission and exhaust gas connect the cylinder with ambient. However, at the exhaust there is no air but products of combustion at much higher temperature. If same valves would be used first for exhaust and then for admission there would be many products of combustion being admitted with fresh air. Temperature of admitted mixture would be much higher thereby lowering the density of fresh charge. For ABC at the exhaust is pure air at the temperature much lower than for ICE. That is why it was considered that same LP valves could be used both for admission and for exhaust. Although the temperature of the exhaust for ABC is much lower than for ICE it is still higher than ambient temperature. If the temperature of the admitted air is higher density of fresh charge would be lower, mass flow through the machine would be lower and efficiency would be worse. In order not to admit hot exhaust one solution that could be used is to expel the hot air downstream of the admission in the channel with the circulation of fresh air.

In the first approximation, it was considered that machine has four valves of equal diameter. If all four valves are equal, outer valve seat diameter can be calculated by:

$$D_{os} = \frac{D_p - 2x_{vc} - \sqrt{2}x_{vv}}{\sqrt{2} + 1} \tag{5.4}$$

Where x_{vc} is the distance between the valve and cylinder and x_{vv} is the distance between two valves. Those parameters are represented in Figure 5.4.

The distance between the valve and cylinder wall (x_{vc}) was considered to be 2.5 mm. This value was taken from the book by professor Gordon Blair [55] where it was concluded that smaller values would cause a drop of valve discharge coefficient because of valve masking effect. If x_{vv}=0.12D_p is kept from recommendations for ICE then resulting valve outer seat diameter for piston diameter 120 mm is D_{os}=39.19 mm. The round value of 39 mm was accepted. Valve inner seat diameter is then calculated from recommendation by:

$$D_{is} = \frac{D_{os}}{1.1} \tag{5.5}$$

In the same book professor Blair gives experimental results of measured discharge coefficients of poppet valves for different gasoline engines: 50 cm^3 (50cm^3/cylinder) moped engine, 600 cm^3 (125 cm^3/cylinder) sport motorcycle engine and 2000 cm^3 (500 cm^3/cylinder) average car engine. He concluded that, although engines are very different there are no big differences in discharge coefficient maps. Two discharge coefficient maps from that book where used in this work as a reference maps for inflow and outflow and are shown on the Figure 5.5 and Figure 5.6 respectively. Discharge coefficient from the map is the function of two parameters: pressure ratio and valve lift ratio. Pressure ratio represents the ratio of pressures on each side of the valve. Valve lift ratio represents the ratio of valve lift and maximum valve lift L_{max}.

$$LR = \frac{L}{L_{max}} \tag{5.6}$$

Valve lift ratio defined this way has an advantage of being dimensionless and ranging from 0 to 1. This is useful for creation and comparison of discharge coefficient maps for different valves.

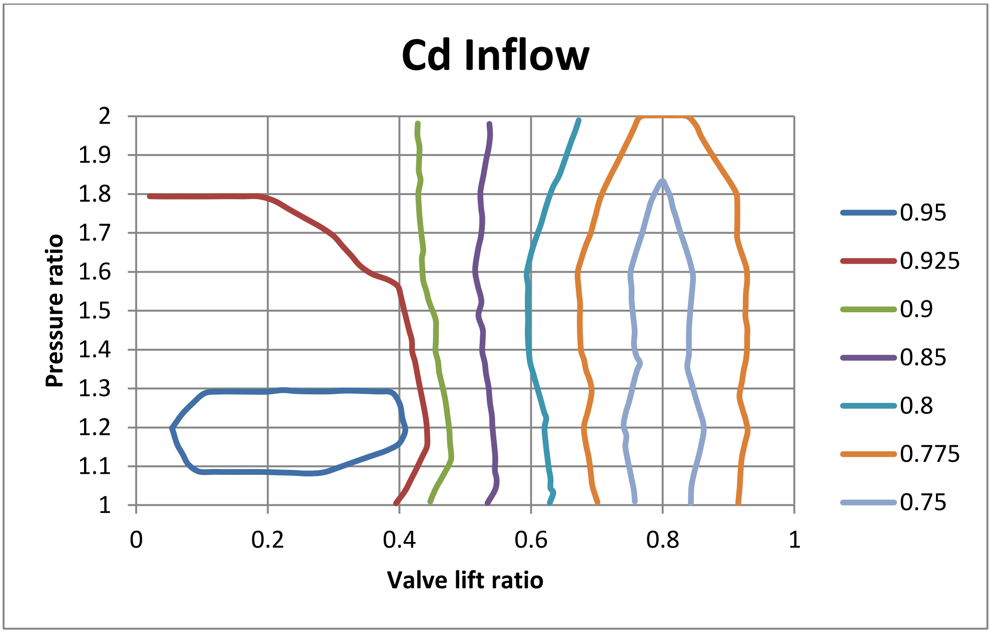

Figure 5.5. Inflow discharge coefficient map [55]

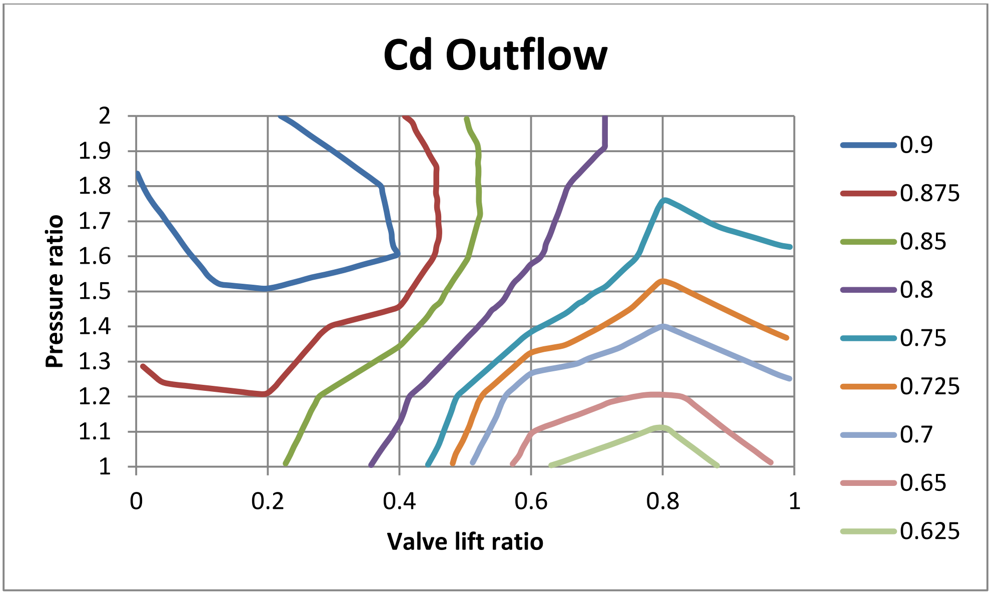

Figure 5.6. Outflow discharge coefficient map [55]

The reference valve area according to Blair should be more precisely calculated than it is traditionally calculated by valve curtain area equation $\pi D_{is}L$. At low valve lift distance x is normal to valve seat while at the high lift that is no longer the case. Limiting valve lift when distance x is no longer normal to valve seat is determined by:

$$L_{lim} = \frac{D_{os} - D_{is}}{\sin 2\varphi} \tag{5.7}$$

Where φ is valve seat angle. On the left side of Figure 5.7 is represented low valve lift while on the right is high valve lift.

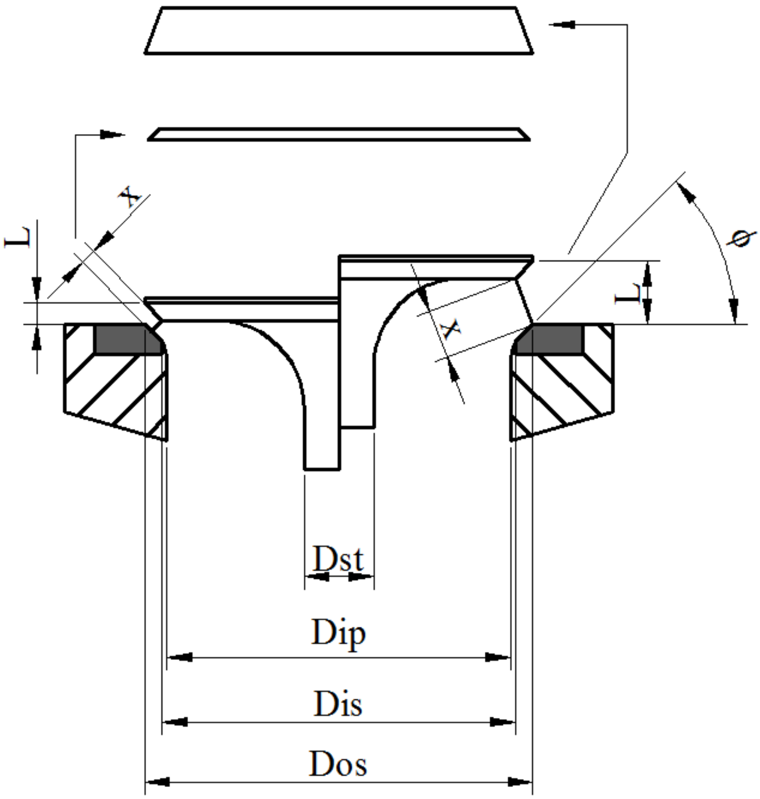

Figure 5.7. Valve curtain area calculation

Reference valve area for low valve lift when $L \leq L_{lim}$ can be calculated by:

$$A_r = \pi L \cos\varphi (D_{is} + L \sin\varphi \cos\varphi) \tag{5.8}$$

While for high valve lift when $L > L_{lim}$ it is:

$$A_r = \pi \left(\frac{D_{os} + D_{is}}{2}\right) \sqrt{\left(L - \frac{D_{os} - D_{is}}{2} \tan\varphi\right)^2 + \left(\frac{D_{os} - D_{is}}{2}\right)^2} \tag{5.9}$$

Massflow through the valve was estimated by:

$$\dot{m} = A_r \cdot C_d \cdot C_m \frac{p_{up}}{\sqrt{T_{up}}} \tag{5.10}$$

Where p_{up} and T_{up} are the pressure and the temperature upstream of the flow, C_d is the discharge coefficient and C_m is the flow parameter. When the flow is subsonic, the flow parameter C_m is the function of pressure ratio p_{dn}/p_{up} and when the flow becomes sonic flow parameter is constant. Type of the flow is determined by critical pressure ratio p_{cr}:

$$p_{cr} = \left(\frac{2}{\gamma+1}\right)^{\frac{\gamma}{\gamma-1}} \tag{5.11}$$

Where γ is specific heat ratio. Flow parameter C_m is calculated by:

$$\begin{gathered} C_m = \sqrt{\frac{2\gamma}{r(\gamma-1)}}\sqrt{\left(\frac{p_{dn}}{p_{up}}\right)^{\frac{2}{\gamma}} - \left(\frac{p_{dn}}{p_{up}}\right)^{\frac{\gamma+1}{\gamma}}} \quad if\ \frac{p_{dn}}{p_{up}} > p_{cr} \\ C_m = \sqrt{\frac{2\gamma}{r(\gamma+1)}}\left(\frac{2}{\gamma+1}\right)^{\frac{1}{\gamma-1}} \quad if\ \frac{p_{dn}}{p_{up}} \le p_{cr} \end{gathered} \tag{5.12}$$

For defined valve geometry, mass flow through the valve would depend on valve lift. Valve lift is normally defined as a function of crank shaft angle. If conventional camshaft is used for defining valve lift then normally valve lift is divided in five phases: opening ramp, main opening, dwell, main closing and closing ramp. Opening ramp is designed to gently lift the valve of the valve seat or it should be better said that it is the fastest valve lift designer dares to use at highest machine rotational speed. Main opening is in charge of lifting the valve from the end of ramp to maximum valve lift. Dwell is the period when valve is kept at maximum valve lift. Main closing and closing ramp have similar role like for the opening. Blair designs ramps and main lifts as 4th order polynomial equations. Later he used a smoothing technique to further smooth the valve lift profile. Valve lift profile defined this way offers low valve velocities, acceleration and jerk and it is the proper way of defining the valve lift. Nevertheless, for this study it was not important to have perfectly smooth profile, as valve velocities and acceleration were not considered at this point. That is why smoothing was not used, but effect it has on valve lift and consequently on mass flow through the valve is very small according to Blair. Symmetrical valve lift was used for opening and closing and it is defined by three stages: ramp, main lift and dwell. Ramp is defined by Ramp Duration (RD) representing crank shaft angles of ramp duration and Ramp Ratio (RR) representing the maximum valve lift ration for the ramp. Main opening/closing is defined only by Main Duration (MD) because start and end lift ratios are RR and 1. Dwell is defined only by duration. Total duration of valve lift is Valve Duration (VD). Valve lift schematic is represented in Figure 5.8.

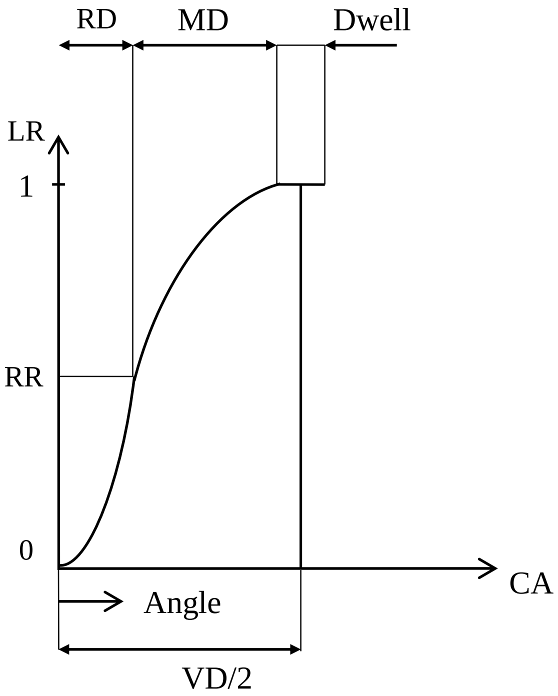

Figure 5.8. Lift profile definition

Blair [55] suggested the values for gasoline and diesel engines for RD, RR and MD. Typical ramp duration is 40 CA degrees while RR is typically 0.2 for spark ignition engines and 0.5 for slower compression ignition engines. Value for compression ignition engine was chosen because of faster opening. Even though ABC heat recovery makes sense only coupled to gasoline engine, as it was analyzed in Chapter 3, it is still expected that it would be relatively low speed engine so that higher RR can be used. For the main duration Blair from his experience and measured values from different engines recommends also 40 CA degree.

Ramp and main valve openings are defined by 4th order polynomial equation:

$$L_s = c_{r0} + c_{r1}\theta_s + c_{r2}\theta_s^2 + c_{r3}\theta_s^3 \tag{5.13}$$

where c_{r0}, c_{r1}, c_{r2} and c_{r3} are coefficients specific for each stage and engine type, L_s is specific lift and θ_s is specific angle. As for the ramp ratio it was chosen the value for diesel engine, the values for c coefficients were also taken from Blair for same engine type. Values of coefficients are represented in Table 5.1.

	c_{r0}	c_{r1}	c_{r2}	c_{r3}
Ramp	-0.00018552	0.045892	1.9795	-1.0256
Main lift	-0.0006083	1.9236	-0.84122	-0.082123

Table 5.1. Values of coefficients for valve lift

Specific lift L_s and specific angle θ_s are dimensionless ratios that range from 0 to 1. Valve lift for ramp is calculated by:

$$L = L_s \cdot RR \cdot L_{max} \tag{5.14}$$

Angle for the ramp is calculated by:

$$\theta = \theta_s \cdot RD \tag{5.15}$$

Regarding the maximum valve lift Blair gives the range:

$$L_{max} = 0.35 \div 0.4D_{is} \tag{5.16}$$

Raising further the valve would not be beneficial as the bottle neck would move to other area. Valve inner seat area is defined by:

$$A_{is} = D_{is}^2 - D_{st}^2 \tag{5.17}$$

Where D_{st} is valve stem diameter. From the Figure 5.4 recommended value is:

$$D_{st} = 0.2D_{is} \tag{5.18}$$

Maximum valve lift can be then calculated by equalizing inner seat area (5.17) with valve curtain area (5.9) for maximum valve lift.

It was determined that maximum valve lift can be set at:

$$L_{max} = 0.4D_{is} \tag{5.19}$$

For LP valves, if both open and close at the same time, they open for exhaust and stay open during the admission. This means that valve duration would be two piston strokes long (360 degrees). If LP valves open at the beginning of the exhaust, close at the end of exhaust, open again at the beginning of admission and close at the end of admission then valve duration would be one stoke long (180 degrees). In both cases, duration is long enough and there is no problem of using recommended value of 40 CA degrees for both ramp and main valve lift duration. Dwell is then easily calculated by:

$$Dwell = VD - 2RD - 2MD \tag{5.20}$$

For HP valves the situation is very different. Outlet valve must open and close in the second half of compression stroke. Valve duration is much less than one piston stroke (180 CA degrees).Expected value is probably closer to half piston stroke (90 CA degrees). Obviously ramp duration and main duration cannot be each 40 degrees long as it would take almost the whole valve duration just to open the valve. In this case it was decided to use same the value of one quarter of total valve duration for ramp and main duration: RD=MD=1/4 VD. As there is no time to lift the valve to full lift set by equation (5.19), new value has to be set for maximum lift. The maximum valve lift can be proportional to ratio of duration to open HP valve (half of the HP valve duration) and recommended opening duration. Recommended opening duration consists of 40 degree RD and 40 degree MD making a total of 80 degrees. Maximum valve lift for HP valve could then be estimated by:

$$L_{max,HP} = \frac{VD_{HP}}{80} L_{max,LP} \tag{5.21}$$

Valve timing is fully defined by defining the opening angle (OA) and the closing angle (CA) for all valves. Valve duration can be calculated as a difference in crank angle degrees between CA and OA. As there are 4 valves but both LP valves use the same timing that leaves 6 parameters to be optimized. The number of parameters could be decreased because some parameters have optimal values regardless of the values of other parameters. LP valves timing, HP outlet valve CA and HP inlet valve OA are to some extend independent of other parameters.

In theory, if valves would open to full lift instantaneously, LP valves should open when the piston reaches the BDC and starts moving upwards pushing the air form the last cycle out of the machine. This is the exhaust stroke that ends when piston reaches TDC. In the next stroke piston goes down and starts the admission that ends when piston reaches BDC. By the first strategy (2 strokes) valves open at the start of exhaust and stay open for two strokes. Because the valves are open when piston is at TDC there must be slots (reliefs) in the piston crown for the valves in order to avoid the contact between the piston and valves. These slots increase the minimum volume which negatively affects the volumetric efficiency. By the second strategy (1 stroke) valves open at the start of exhaust and close either fully or partially at the TDC and then open again at start of admission and close at the end of admission. If the valves close only partially there must be again reliefs in the piston crown but this time much smaller because valve lift is less than full lift.

Figure 5.9 shows the “2 stroke” LP valve timing strategies while Figure 5.10 shows the “1 stroke” strategies. For all the curves it was used the same HP valve timing: HP outlet valve OA 120 degrees, HP outlet valve CA 190 degrees, HP inlet valve OA 170 degrees, HP inlet valve CA 260 degrees. This timing was selected although some other HP valve timing would serve as well to explain the timing of LP valves. Initially, stroke was taken from the recommendation of bore to stroke ratio for ICE. Heywood [2] suggests stroke to bore ratio in the range of 0.9-1.1 for the passenger car application. The mean value of this range, the value of 1 was selected for stroke to bore ratio. Thereby, stroke was at first defined to be 120 mm. For the study of the influence of LP valve timing, the stroke was then changed in order to maintain the same mass flow of air as the mass flow of gas. This was done to separate the effect of ratio of gasses from the LP valve timing.

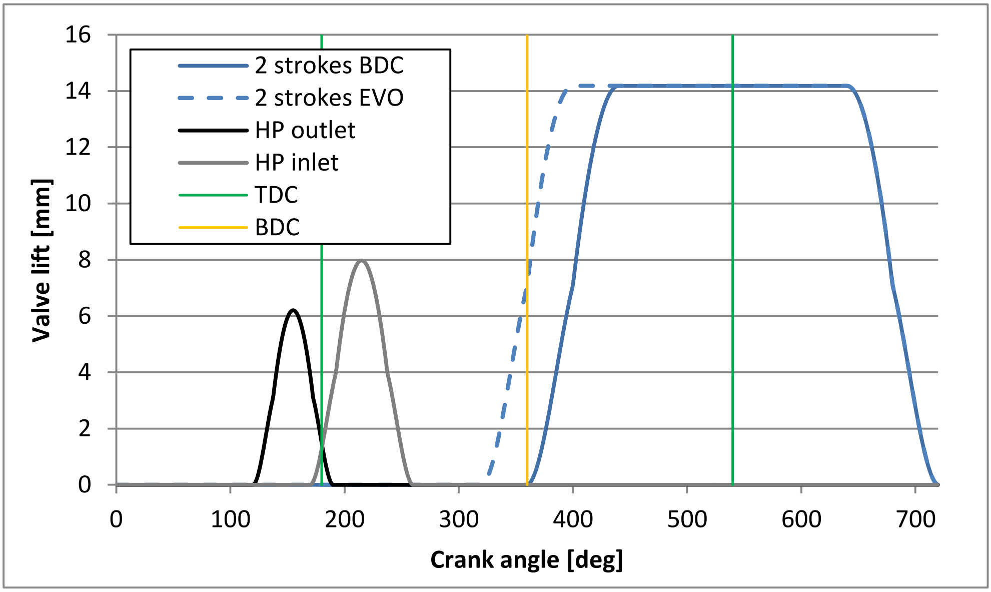

Figure 5.9. LP valve timing “2 stroke” strategies

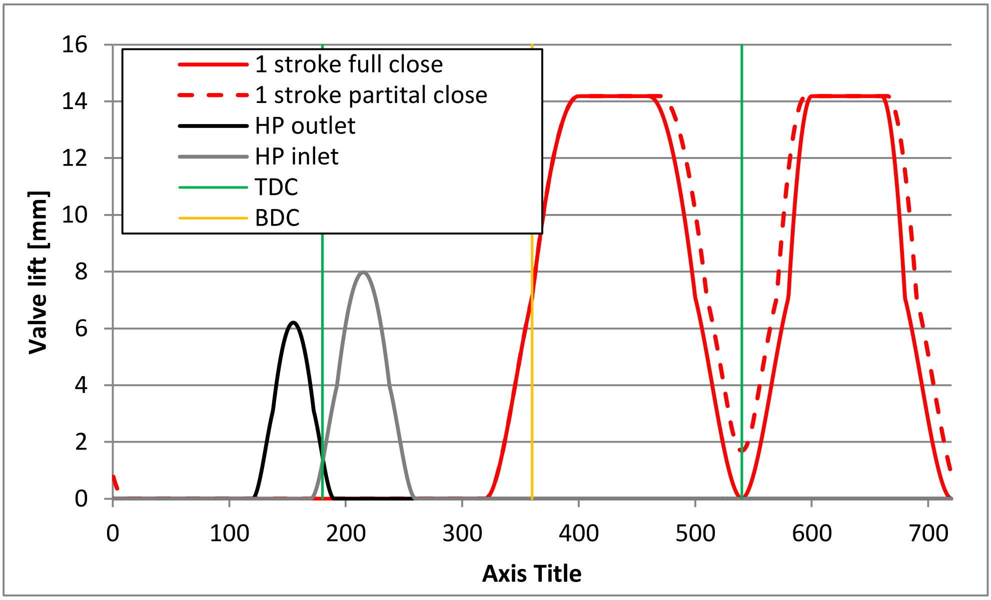

Figure 5.10. LP valve timing “1 stroke” strategies

For the first strategy in Figure 5.9 called “2 strokes BDC” both LP valves start opening at BDC (360 degrees), remain open during two strokes and close again at BDC (720 degrees). Because LP valves remain open at TDC, big reliefs must be placed in the piston crown for the maximum valve lift of 14.2 mm. This increases the dead volume which lowers the volumetric efficiency and in order to obtain the desired mass flow of 27.01 g/s of air piston stroke had to be increased to 130 mm.

For the second curve in Figure 5.9 called “2 strokes EVO” valves again stay fully open at TDC but this time they open before BDC. Thereby, this is referred to as Early Valve Open (EVO). Opening the valves before BDC (when pressure in the cylinder is higher than atmosphere pressure) helps expelling the air out and lowers the exhaust pumping losses. By lowering the initial exhaust pumping work, positive work also increases. Valves were opened 40 degrees before BDC. This value was obtained as optimal by simulation varying the opening angle of the LP valves. Earlier valve opening than this lowers the positive work of expansion. Later valve opening than this increases the negative work. Piston stroke for this strategy was also 130 mm.

The first strategy in Figure 5.10 called “1 stroke full close” represents the strategy when LP valves fully close and start opening again exactly at TDC. Depending on the piston and valve velocities there could still be a piston-valve contact so the piston and displacements had to be checked. It was determined that there would be no contact so there was no need for LP valve slots in the piston. Because there was no need for reliefs dead volume was smaller so the smaller stroke was able to provide desired mass flow. Stroke was 111 mm. As it was estimated for the second 2 stroke strategy that EVO is beneficial, the same opening angle (40 degrees before TDC) was used for both 1 stroke strategies but it was not explicitly stated in their name. Closing all valves at TDC creates a pressure rise at the end of exhaust because the air is being compressed as piston decreases the volume. The peak is higher if compression ratio is higher. Similar effect happens at the beginning of admission when all valves are still closed and air expands rapidly which lowers the pressure and results in higher negative work area.

The second strategy in the Figure 5.10 called “1 stroke partial close” deals with the pressure peaks at TDC. As the valves are not fully closed at TDC effective compression ratio is much lower than geometric. Piston does not have to work as much as for third curve to compress or expand air. Because valves are partially open at TDC, small reliefs had to be used. It was estimated that 1.7 mm valve lift at TDC offered good compromise of removing the negative pressure peaks at TDC and not increasing much dead volume. As pumping work is lower than for third curve, overall volumetric efficiency is better so the smaller piston stroke was used 110 mm. For this strategy Late Valve Closing (LVC) was also used which means closing the valves after BDC (720 degrees). Valves were closed 10 degrees after BDC in order to decrease a small drop of pressure at the BDC that makes the negative work higher.

Figure 5.9 and Figure 5.10 show the profiles of the valve lift where parts of the profile could be recognised: opening and closing ramp, main duration and dwell (only for LP valves). It can be seen that smoothing was not used between the ramp and main duration as it was mentioned earlier. They also show how valve lift had to be smaller for HP valves where less crank angle is available for valve duration.

Figure 5.11 shows the pressure-volume diagram for different LP valve timing strategies. It can be seen that 2 stroke strategies require much higher displaced volume, due to the dead volume increase. It also shows the pressure peak at TDC for “1 stroke full close” that creates high negative work. By maintaining the valves slightly open at TDC, like in the “1 stroke partial close” strategy, this pressure peak is largely reduced. This strategy offers both lower displaced volume (in comparison to 2 stroke strategies) and low negative work. Using LVC does not affect much the cycle. In Figure 5.11 it is barely visible the small pressure drop at BDC that makes the difference between the curves “1 stroke full close” when valves are closed at TDC and “1 stroke partial close” when valves are closed 10 degrees after BDC.

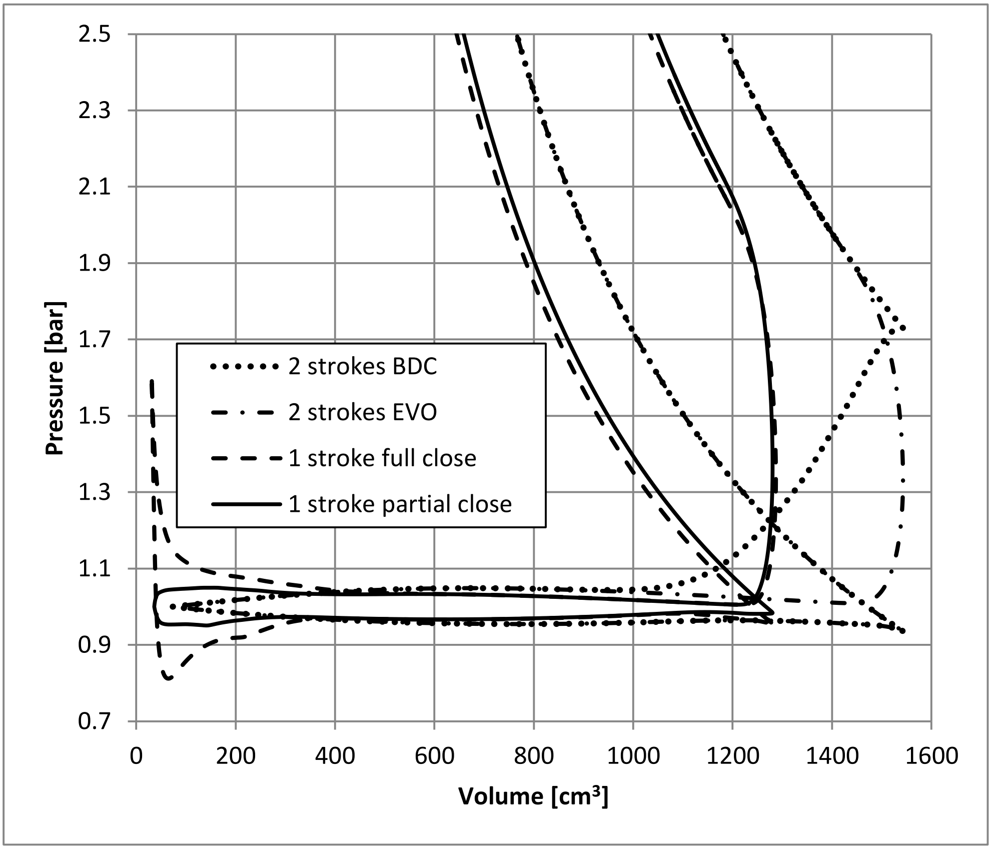

Figure 5.11. LP valve strategies in pV diagram

Table 5.2 shows recuperated power from exhaust gases for engine operating point G for all considered LP valve timing strategies. As “1 stroke partial close” offered best results, this strategy was adopted for further analysis.

Curve	2 strokes BDC	2 strokes EVO	1 stroke full close	1 stroke partial close
Recuperated power [W]	1263	1555	1693	1809

Table 5.2. Recuperated power for different LP valve timing strategies

For the HP valves there are two parameters that could be excluded from optimisation: HP outlet valve CA and HP inlet valve OA. HP outlet valve opens during compression and theoretically, if the valve closing would be instantaneous, it would close at TDC. Likewise, HP inlet valve would theoretically open at TDC and close during expansion. Nevertheless, as valve opening and closing is not instantaneous, it should be avoided to have all valves closed when the piston is at TDC as it would generate significant pressure peaks like it was already analysed for LP valves. For the LP valves, piston is at TDC between exhaust and admission stroke when the pressure is close to the ambient pressure. For the HP valves, piston is at TDC between compression and expansion stroke and the pressure is much higher than ambient pressure. Thereby potential pressure peaks that would appear as a consequence of having the valves closed at TDC would also be higher. Figure 5.12 shows the difference of pV diagrams when valves are closed at TDC and when valves are partially open (valve overlap). When the valves are partially open timing is such that HP outlet valve closes 10 degrees after TDC and HP inlet valve opens 10 degrees before TDC, thereby there is 20 degrees valve overlap. This timing is shown in Figure 5.9 or Figure 5.10. If there is no valve overlap the pressure in the cylinder goes too high. This is because, at small valve opening (during the valve ramp), the mass flow through the valves is very small. As the compression ratio is very high, at the last part of compression if the piston cannot push the air through the valve the pressures increases rapidly. Same thing happens at the first part of the expansion. If the valve is open very little and the piston cannot suck the air, the pressure in the cylinder decreases rapidly. Higher values of valve overlap were avoided in order to avoid the reflow from the HP inlet valve to HP outlet valve.

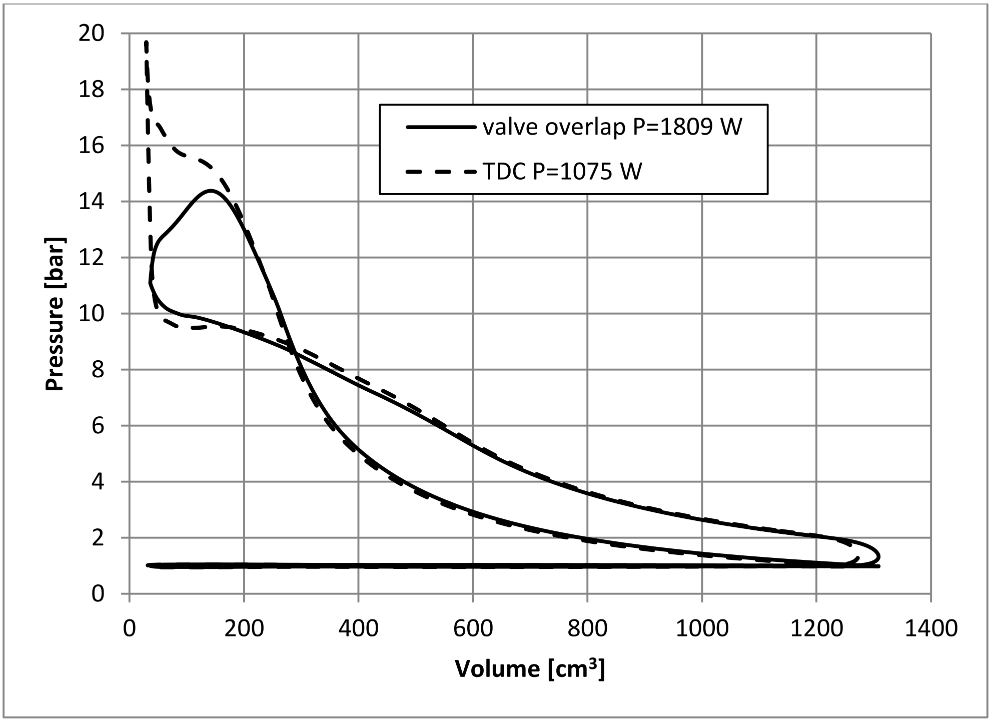

Figure 5.12. HP valves timing

This way, there are only 2 parameters left for valve timing optimisation: HP outlet valve OA and HP inlet valve CA. HP outlet valve OA was varied in the range 100-150 crank angle degrees with the 10 degrees step. HP inlet valve CA was varied in the range 230-290 crank angle degrees also with the 10 degrees step. For the study of maximum recuperated power it was decided to include also the third variable which was the piston stroke. Piston stroke was varied in the range 70-100 mm. This variation of piston stroke allowed sufficient variation of air mass flow. Air mass flow was varied in order to study the effect of AirGasRatio on recuperated power.

Figure 5.13 shows the recuperated power as a function of piston stroke, HP inlet valve CA and HP outlet valve OA. For the clarity, the plot shows only three values of HP outlet valve OA that provided the highest power. Results of the simulation showed that for any HP outlet valve OA the stroke of 80 mm always provided the highest recuperated power. The optimal HP outlet valve CA changes with HP inlet valve OA. For the HP outlet valve OA of 120 degrees the optimal HP inlet valve CA is 260 degrees but if the HP outlet valve OA decreases (110 degrees) than optimal HP inlet valve CA increases (270 degrees) and vice versa. Maximum recuperated power of 2031 W was obtained with HP outlet valve OA of 120 degrees, HP inlet valve CA of 260 degrees and stroke length of 80 mm.

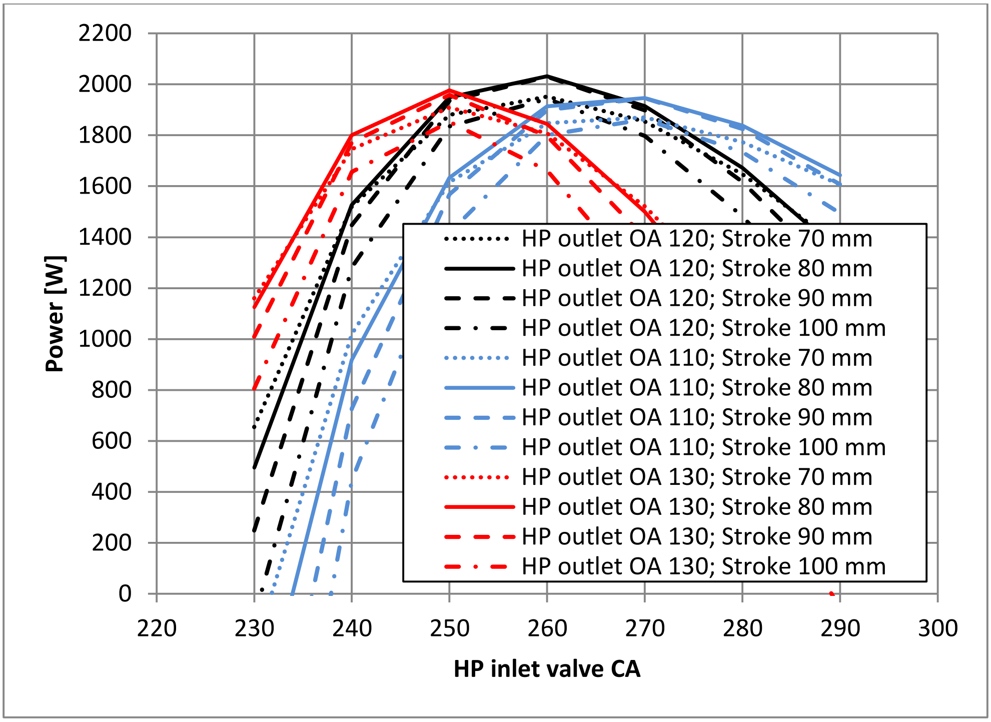

Figure 5.13. Recuperated power as function of stroke length, HP inlet valve CA and HP outlet valve OA

Maximum recuperated power was obtained for AirGasRatio of 0.71. This differs from what was concluded in Chapter 3 that the values lower than 1 would decrease the cycle efficiency. The difference comes from different cycle definitions and heat exchanger efficiency definitions. Simple model from Chapter 3 neither included LP and HP negative work loops nor increase of heat exchanger efficiency with the decrease of AirGasRatio.

For a fixed HP outlet valve OA and stroke, changing the HP inlet valve CA has a main effect on recuperated power and pressure in the heat exchanger with the secondary effect on air mass flow. This can be seen on Figure 5.14. HE pressure from the figure represents cycle mean value of the pressure in the heat exchanger. If the HP inlet valve closes later pressure in the heat exchanger will be lower and air mass flow higher. It can be concluded that there is an optimal value of pressure in the HE that results in highest recuperated power. Recuperated power was highest for HP inlet valve CA of 260 degrees and stroke of 80 mm when HE pressure was 9.49 bar. Thus, the conclusion from the Chapter 3 about the optimal pressure is still valid although the value of pressure is different because of already mentioned model differences.

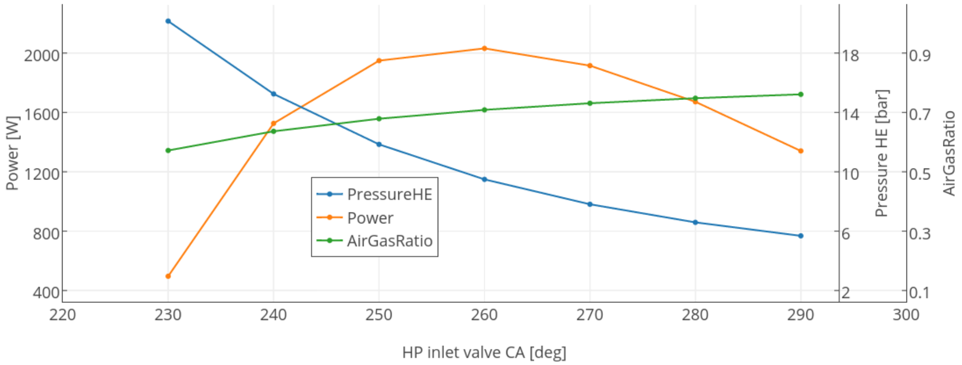

Figure 5.14. Effect of HP inlet valve CA on pressure in the HE, AirGasRatio and power; stroke 80 mm; HP inlet valve OA 120

Figure 5.15 shows the comparison of pressure-volume diagrams for the three cases of HP valve timing. These cases were the points of maximum power for each HP outlet valve OA value from Figure 5.13. The curves from Figure 5.15 were named in the following style *HP outlet valve OA-HP inlet valve CA-Stroke* followed by the recuperated power for that valve timing. Highest recuperated power was obtained in the case of HP inlet valve OA of 120 degrees as it was said before. Earlier HP inlet valve opening lowers the cycle pressure that improves the positive work in the lower pressure part of the cycle but decreases the positive work at the high pressure part. The opposite is valid for later HP inlet valve opening. Earlier HP outlet valve opening results in the decrease of both HE pressure and cylinder peak pressure. While the difference in power between 120 and 110 HP inlet valve OA is small 85 W, the difference in HE pressure is significant as the pressure decreases from 9.49 bar to 7.84 bar. If heat exchanger and other parts of high pressure installation would have a problem of sustaining high pressure then earlier HP inlet valve opening could be used to improve the component safety while sacrificing small amount of efficiency.

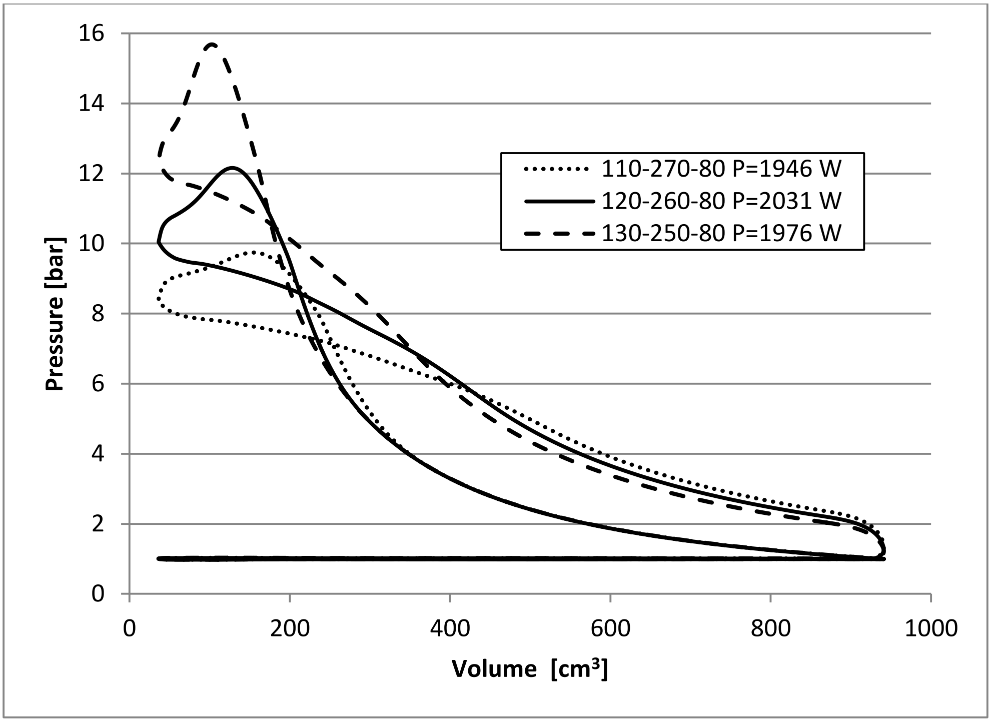

Figure 5.15. pV diagram comparison for different HP valve timing

The HP negative work area from the Figure 5.15 is significantly big. For the case when the recuperated power was maximal (2031 W), HP pumping losses consumed 1138 W while the HP positive work generated 3228 W. HP pumping loss is very high and it should be further analysed how to reduce it. The reason for this big loss is that the big quantity of air must be moved from the cylinder to the heat exchanger in a short time. This creates the high instantaneous mass flow rate that causes the high pressure drop in the HP outlet valve, heat exchanger and HP inlet valve. Pressure drop (pressure difference at the valve inlet and outlet) was highest in the HP outlet valve with the maximum pressure drop 2.2 bar. Pressure drop in the heat exchanger and HP inlet valve was much lower and did not exceed 0.7 bar. In order to reduce the HP negative work, HP outlet poppet valve (as a source of highest pressure drop) should be replaced with some other valve that could open faster, which should reduce the pressure drop and lower HP negative work.

The power of LP pumping losses was not significant, 59 W in the case of maximal recuperated power. LP pumping losses do not require further analysis.

5.2.2 Reed valve

Reed valve is a simple valve consisting of a thin plate called petal clamped at one side. The valve opens when there is a positive pressure difference on plate sides. This is schematically represented on the Figure 5.16 where arrows p2-p1 only represents the direction of positive pressure force. If the pressure p_2 is higher than the pressure p_1, the valve opens.

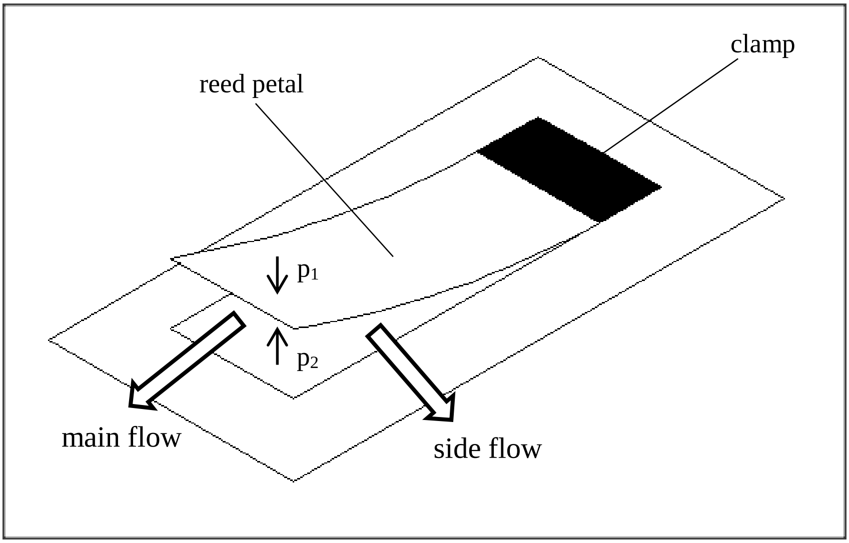

Figure 5.16. Reed valve schematic

The main advantage of this valve type is its simplicity, robustness, price and relatively fast aperture and closing. Fast opening and closing of high area passage is crucial for Brayton cycle. These valves have been studied a lot by engine engineers because of their use in two stroke engines. The other field of their application is in the reciprocating compressors where they are used to connect the cylinder with high pressure deposit or next compression stage. The former is very similar to Brayton cycle application.

Simplified reed valve model was made to be used in the Brayton WHR system model. The model considered the reed valve as a rigid flap rotating around one of its edges. Load on the flap was defined by defining the pressure distribution on each side of the valve. Moment of the inertia for the model was calculated knowing the dimensions and density of the material. Reed valve stiffness was modelled as a torsional spring. Torsion coefficient of the spring was a parameter for optimisation in order to fit better the model to the experimental values. The maximal rotation angle is limited by the maximum aperture of the valve’s free end.

Some authors [56], [57] consider the reed valve as a deflective cantilever beam which is a more realistic approach but it was considered that rotating flap model can offer a good precision and it is simpler. Figure 5.17 shows the illustration of the reed valve model. Reed valve with petal length l is closed in the horizontal position. When pressure in the cylinder is higher than the pressure in the heat exchanger the flap rotates and aperture of the free end of the valve is L. Maximum valve aperture is L_{max}. Blair [58] considered that the maximum reed valve aperture is defined as a maximum ration of valve aperture and petal length. Blair found $(L/l)_{max}$ to be around 0.3 and this value was used in the present thesis.

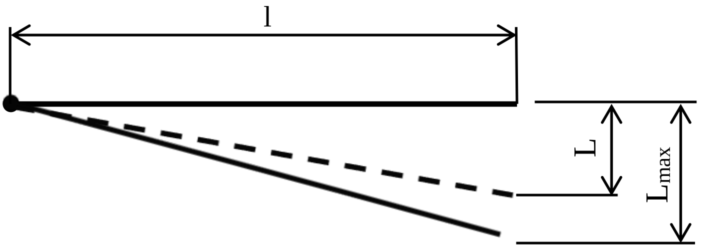

Figure 5.17. Model of the reed valve as a rotating flap

The key to modelling the aperture of reed valve is predicting well the pressure distribution on petal sides.

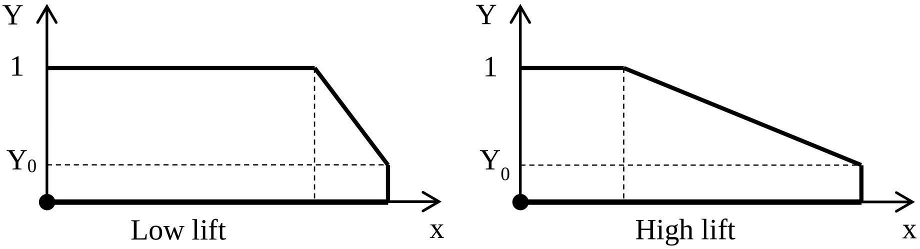

Figure 5.18. Reduction factor as a function of petal length for two different valve lifts

When the valve is closed overall pressure differential is uniform along the petal and it is equal to the difference between upstream and downstream pressure:

$$\Delta p = p_{up} - p_{down} \tag{5.22}$$

When the valve starts to open some part of the pressure distribution remains uniform while the other part look more like a triangle distribution. At very low lift, pressure differential along the petal length follows the overall differential except at the very end. At high lift, the pressure distribution tends to have a more triangular shape. Figure 5.18 shows the reduction factor Y(x). This factor is a dimensionless factor that corrects the pressure distribution along the petal length axis x.

$$\Delta p(x) = \Delta p \cdot Y(x) \tag{5.23}$$

Fleck [57] estimated that one part of the distribution remains uniform regardless of valve lift. This part was marked as Y_0 in Figure 5.18. Fleck fixed the Y_0

value at 0.3 and did not give the function for Y(x). In the present thesis the value of $Y_0=0.3$ was used.

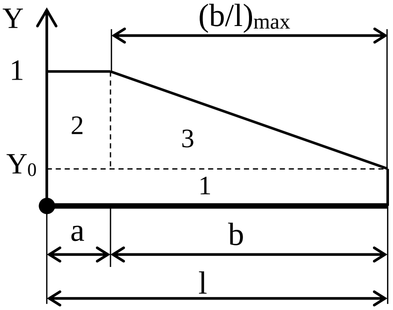

Figure 5.19. Reed valve pressure distribution

Figure 5.19 shows the three load areas marked 1-3. These areas are defined by pressure distribution along the petal. Each of the loads creates a torque that contributes to total torque that makes the petal rotate. When the valve is closed the pressure distribution is uniform and b is equal to zero. When valve starts opening b starts augmenting from zero to the maximum value defined by ration $(b/l)_{max}$. For simplicity it was chosen the value of $(b/l)_{max}=1$. In other words, when the valve is fully open b is equal to l.

Reed valve model was validated using the data from Blair's experiments [58]. Blair measured pressures on both sides of the reed valve and petal tip aperture. He also modelled the valve as a cantilever beam and compared his simulation results with measured values. To validate the present thesis's model same pressures measured by Blair were imposed in the model. Same dimensions, material and mass for reed valve were also used in the model as in the Blair's experiment.

Figure 5.20 shows the results of reed valve model validation. It can be seen that the valve lift of the rotary flap model used in the present thesis fits very well with the experimental values. For comparison it also shows the valve lifts obtained by the Blair's model of cantilever beam with inertia and the author's model of cantilever beam without inertia. Rotary flap model does not predict precisely the timing of closing the valve but it does generally predict better the valve lift than Blair's model of cantilever beam. The cantilever beam model without inertia does not predict well the valve lift.

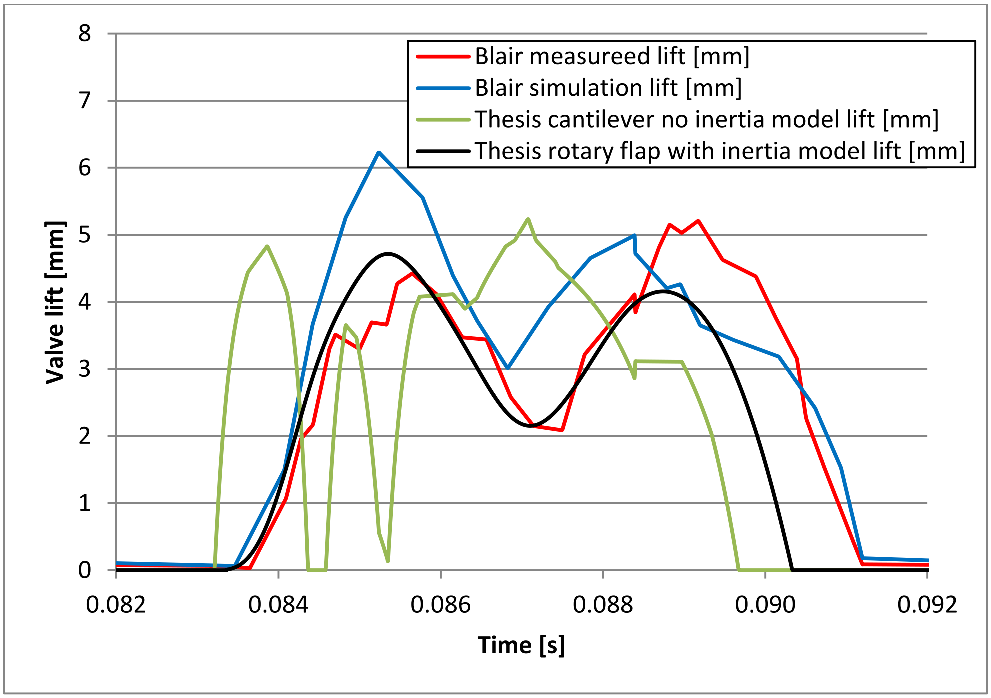

Figure 5.20. Reed valve lift simulations and measurements

Valve flow area is composed of 3 surfaces: one main flow area and two side flow areas. This is represented on the Figure 5.16. In some cases, for example if the channel is too tight on the cylinder sides or if there are two valves next to each other, side flow could be partially or totally blocked. Figure 5.21 shows that two reed valves were used. As they are placed close to each other it was considered that flow on the sides of the valves that are close to each other would be insignificant. Total reference area of both reed valves was then calculated by:

$$A_r = L_{val1}W_{val1} + \frac{1}{2}L_{val1}l_{val1} + L_{val2}W_{val2} + \frac{1}{2}L_{val2}l_{val2} \qquad (5.24)$$

Where W_{val1} and W_{val2} are the widths of the respective reed valves, L_{val1} and L_{val2} are lifts and l_{val1} and l_{val2} are petal lengths. Mass flow rate through the valve is calculated by the same equation (5.10) like for the poppet valve. Discharge coefficient was considered to be constant C_d=0.7. This value was chosen as minimal value measured by Blair et al [59]. Flow parameter C_m was calculated the same was as for the poppet valve by using the equation (5.12).

Reed valve model was used to substitute the poppet HP outlet valve. Two reed petals were placed in the place of substituted poppet valve. The distance between the reed valve and other valves was the same as it was for all poppet valves, when recommendations were used.

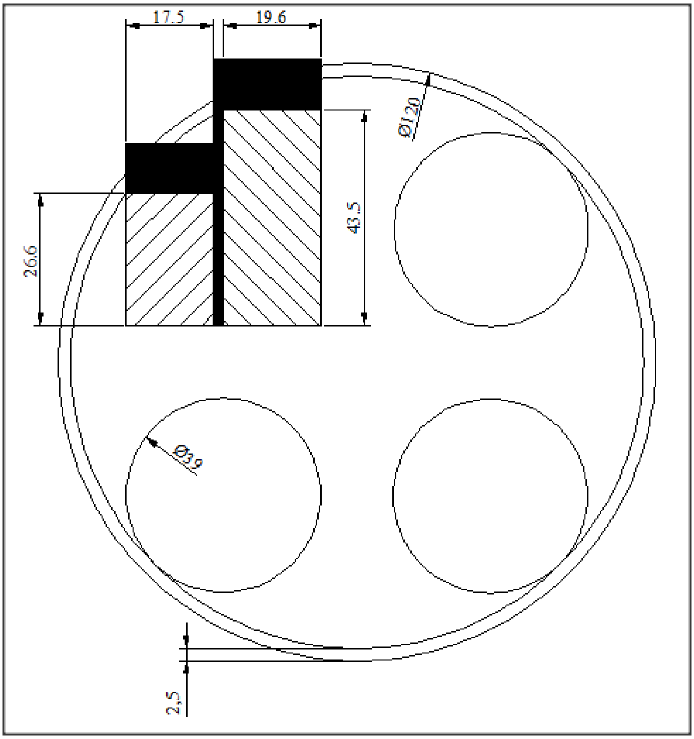

Figure 5.21. Placement of reed valve in the cylinder head

Figure 5.21 shows the dimensions and placement of the reed valves in the cylinder head. It was decided to use two valves. Dimensions were chosen arbitrary but with the idea to use as much area as possible. The flow on one side of each valve was not taken into account because it was considered that there would be significant masking on the sides of the valves that are next to each other.

Timing of the LP valves and HP inlet valve OA were kept the same as for poppet valve. As reed valve opening and closing is automatic that leaves only 1 parameter for valve timing optimisation – HP inlet CA. This parameter was varied in the range 230-270 degrees with the 10 degrees step. Piston stroke was used as a second variable to include the effect of ratio of air and gas mass flows (AirGas-Ratio). Stroke was varied in the range of 50-120 mm with the 10 mm step. Results are presented in Figure 5.22. The maximum recuperated power was 2296 W for HP inlet valve CA 250 degrees and AirGasRatio 0.77 that corresponds to the piston stroke of 90 mm. The recuperated power was higher than the one that was obtained with poppet valve (2031 W).

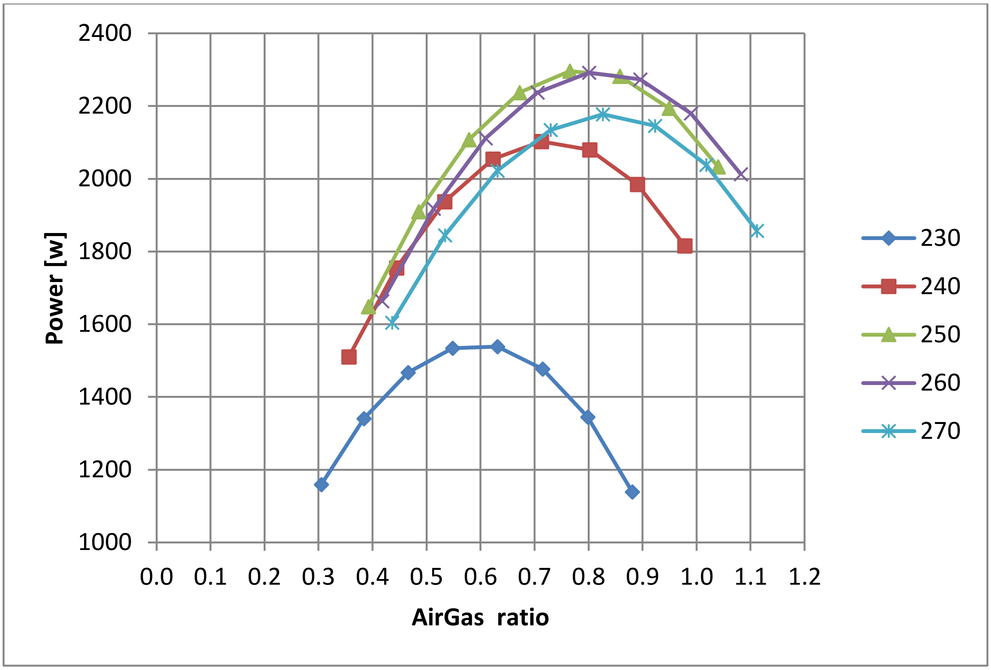

Figure 5.22. Recuperated power as a function of the HP inlet valve CA

Figure 5.23 shows the comparison of pV diagrams for reed and poppet valve. The values of HP inlet valve timing and piston stroke that provided best recuperated power were different for each valve type. Curve named “reed” represents the pV diagram of the reed valve model for the values of HP inlet valve CA of 250 degrees and stroke of 90 mm that provided the maximum recuperated power. Likewise, the curve “poppet” refers to pV diagram of the poppet valve for HP inlet valve CA 260 degrees and stroke of 80 mm that provided the maximum recuperated power. Because of earlier HP inlet valve closing the pressure of the reed valve is higher and because of the longer stroke the volume is also higher. This makes it difficult to compare directly two valve types in the pV diagram. The curve named “reed comparison” was added in order to compare reed and poppet valve in similar conditions. For this curve the same HP inlet valve timing and stroke was used as for poppet valve. Clearly, the HP negative work of the reed valve is less than poppet valve.

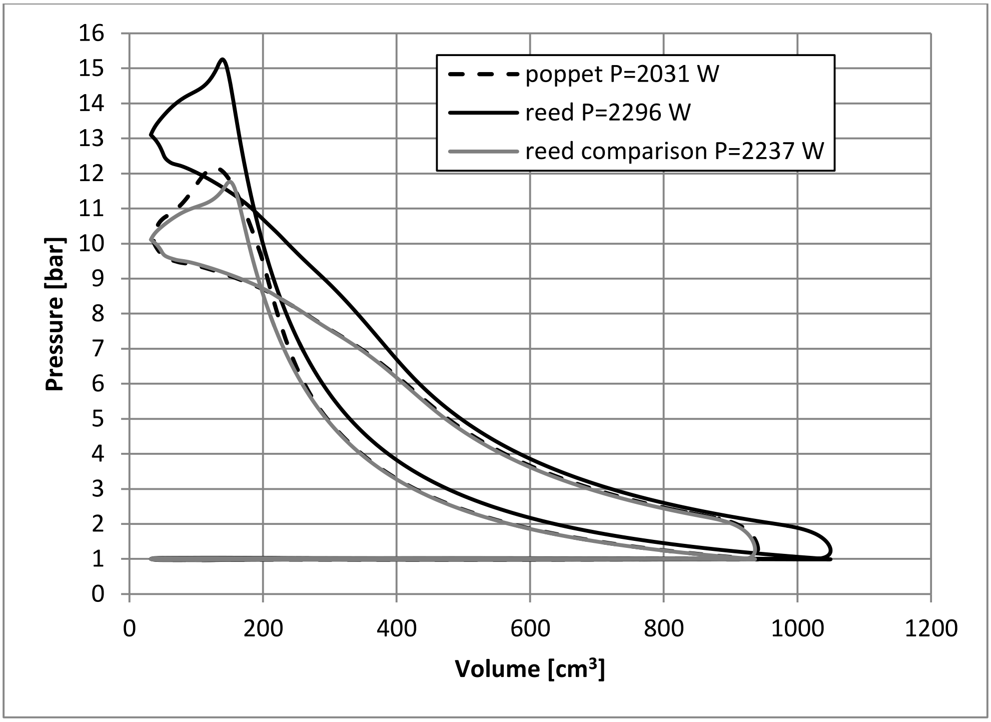

Figure 5.23. Reed valve pV diagram

Using the reed valve as outlet valve represents an improvement over the poppet valve in both simplicity and recuperated power. For the inlet valve, the reed valve cannot be used or any other valve that opens with the difference of pressures on each valve side. This is because heat exchanger and connecting pipes must be pressurized and automatic valve would depressurize them during the admission and exhaust stroke. Opening and closing the cam operated HP poppet valve is too slow. Some camless systems could open the valve faster and it should be explored the possible gain of using this type of actuator.

5.2.3 Camless poppet valve

There are various types of camless systems for actuation of poppet valves. Usually, these systems are divided by actuation mechanism to: electrohydraulic, electropneumatic and electromagnetic. It was not in the interest of the present thesis to study in detail those systems. But, it was interesting to look for the shortest valve lift time that those systems could offer. Lou et al. [60] experimentally investigated the electrohydraulic system capable of lifting the valve to 10 mm for 3 ms. Closing the valve from the same lift was possible for the same time. Company Freevalve claims that their electropneumatic actuator [61] can lift the valve form 1 mm to 8 mm in 2.5 ms. Closing the valve form 8 mm to 1 mm takes 2.6 ms. Valve lift velocity can be defined as the ratio of the valve lift and time needed for this lift:

$$v_{val} = \frac{L[mm]}{\tau[ms]} \tag{5.25}$$

Considering this equation, electrohydraulic actuator has the valve velocity of 10/3=3.33 mm/ms while the electropneumatic has the valve velocity of 7/2.5=2.8 mm/ms. Both claim that the valve impact with the seat is not damaging the seat. Freevalve electropneumatic actuator has done many kilometres of real life tests installed in an engine of Saab 9-5 for both intake and exhaust valves. Pneumatic valve technology could actually be compatible with the ABC because compressor of the ABC produces the high pressure air that pneumatic actuator requires [61].

It was supposed in a first approximation that camless actuator is capable of lifting the valve to the maximum valve lit defined by equation (5.19). Valve lift was modelled as linear. If the valve duration was not sufficient to fully open and close the valve, then valve lift was decreased but it was maintained the same valve velocity. If valve duration was longer than the time necessary to fully open and close the valve, then dwell was used and the valve was kept fully open.

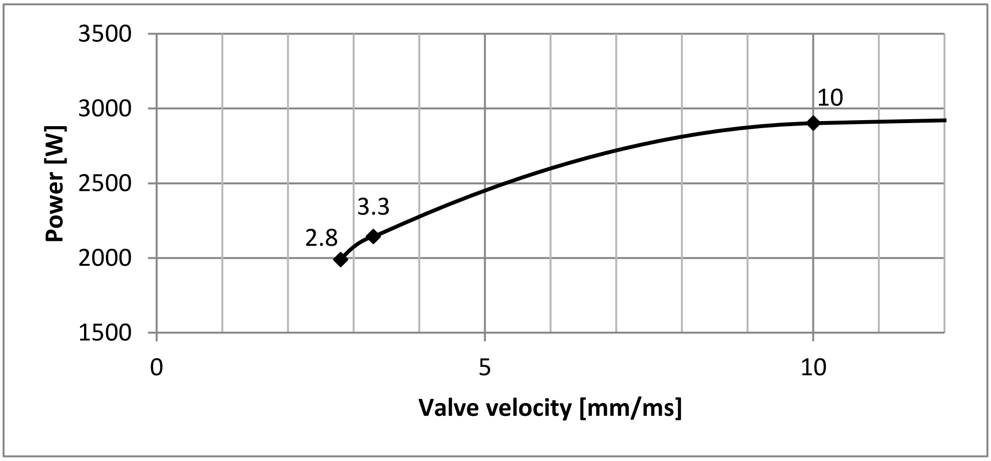

Figure 5.24. Power as a function of valve velocity

Camless valve actuator was used for both HP valves. HP outlet valve OA and HP inlet valve CA were varied for each value of valve velocity, in order to look for the maximum recuperated power for each valve velocity. Plots like Figure 5.13 were obtained for each valve velocity. The maximum recuperated power for each valve velocity is represented in Figure 5.24. Velocity of 10 mm/ms represents the possible faster actuators that could be developed in the future. Maximum recuperated power for electropneumatic valve was 1989 W which is a little bit less than what was estimated with cam actuated valve (2031 W). Recuperated power for electrohydraulic actuator was 2143 W which is higher than cam valve but lower than reed valve recuperated power (2296 W). Increasing the valve velocity, at lower velocity values, increases significantly the recuperated power. Increasing the valve velocity from 3.3 to 10 mm/ms improved the recuperated power for 758 W. Further increasing the valve velocity does not increase the recuperated power significantly which can be seen on Figure 5.24 as the curve of recuperated power becomes more flat after 10 mm/ms valve velocity.

Considering the current state of the art, camless actuators seem not to be fast enough for this application. Pressure–volume diagrams of poppet, reed and electrohydraulic valves are presented in Figure 5.25. Valve types were compared in same conditions: HP inlet valve CA 260 degrees, stroke 80 mm, HP outlet valve OA 120 degrees (for poppet and electrohydraulic valve). These parameters were used in order to compare different valves but these were not the one that provided the maximum recuperated power for 3.3 mm/ms valve velocity.

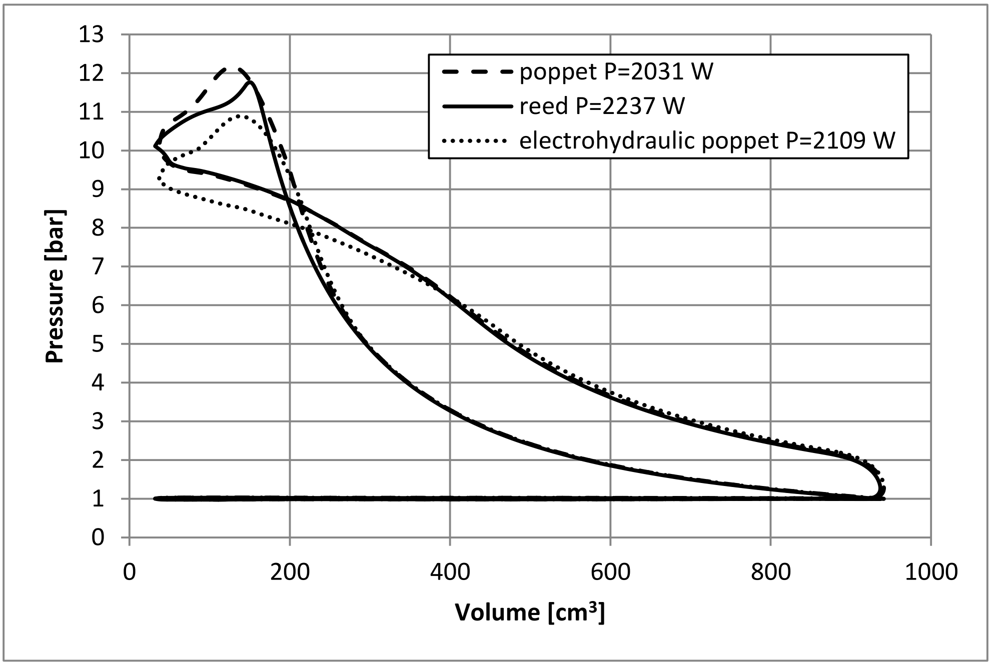

Figure 5.25. pV diagram comparison

One interesting feature of using the camless actuator is the possibility to adjust the pressure in the heat exchanger by changing the valve timing. This would be beneficial for other working points. As it was demonstrated optimal cycle pressure changes with the change of the engine working point. Nevertheless, complexity and price of variable valve actuation technology would hardly justify the benefits.

5.3 Heat exchanger tube length

Pressure waves travel along the tubes that connect the heat exchanger with the cylinder. If the tube is longer the wave needs more time to reach the end of the tube. The length of the tube can therefore decide which part of the pressure wave (low pressure or high pressure peak) reaches the valve when it opens or closes. The length of the inlet and outlet tube of the heat exchanger could have an important effect on the pressure wave synchronisation, which affects the high pressure loop.

Figure 5.1 helps to clarify the naming convention for the tubes. It could be said that valves belong to the machine and tubes to the heat exchanger. The outlet of the machine represents the inlet of the heat exchanger and vice versa. The machine outlet valve connects with the heat exchanger inlet tube. Same way, the heat exchanger outlet tube connects with the machine inlet valve.

Analysis of the pressure wave synchronization required the use of the 1D heat exchanger model described in the section 4.4. Inlet and outlet tubes were modelled as 1D straight tubes with the mesh size of 10 mm. The 0D heat exchanger model was replaced with two 1D tubes and the heat exchanger, the rest of the model was not changed. Reed valves were used as HP outlet valve and HP inlet valve was a camshaft actuated poppet valve. Timing of LP valves and HP inlet valve opening was already defined in section 5.2.1. HP outlet valve was automatic so it required no timing. HP inlet valve closing angle was used as a parameter for optimisation. Values for HP inlet valve CA of 250, 260 and 270 degrees were selected. Analysis from the section 5.2.2 showed that for the 0D model recuperated power was highest in this HP inlet valve CA range.

Other parameter for optimisation was the piston stroke. The values of 80, 90 and 100 mm were used.

Last two parameters for optimisation were the lengths of the inlet and outlet tube. Two possible goals could be aimed by synchronization of pressure pulses. The first goal could be to select the tube lengths in such a way that the pressure pulse, that is created when HP outlet valve opens, reaches the HP inlet valve in the moment when that valve is opened. That way a pressure pulse would enter the cylinder and raise the pressure thereby decreasing the HP negative work and increasing the HP positive work. Additionally, pressure pulse that is created when HP outlet valve opens, travels to HP inlet valve and rebounds as a reflected negative pressure pulse. Then, it travels back to HP outlet valve when it rebounds again. Pressure wave travels in between two valves and it depends on the tube lengths how many times it will reach HP outlet valve and what part of the wave (high or low pressure) would reach the HP outlet valve when it is opened. The second goal could be to try to obtain a low pressure part of the wave at the HP outlet valve when it opens in order to reduce the HP negative work.

Average temperatures in the inlet, outlet tube and heat exchanger should be estimated first in order to estimate the speed of sound and the lengths of the tubes. By simulation it was determined that mean temperature was 660 K in the inlet tube, 780 K in the heat exchanger and 940 K in the outlet tube. Resulting speeds of sound were 515 m/s, 560 m/s and 615 m/s respectively. It should be noted that the equivalent heat exchanger length determined in section 4.4 was 660 mm (taking into account the heat exchanger core, diffusers and bends). HP outlet valve is an automatic reed valve so the exact timing of aperture could not be known exactly but it is approximately around 130 degrees of crank angle while the HP inlet valve opening is at 170 degrees. That makes around 40 CA degrees between the openings of two consecutive valves. As machine rotating speed is determined by ICE rotational speed (2623 rpm) it can be easily calculated that 40 CA degrees takes 2.54 ms. As the approximate time and speed of sound are known, considering that both inlet and outlet tube lengths are equal, it can be easily calculated that tube lengths should be around 400 mm in order to obtain the desired pressure wave synchronisation for the first goal or multiple values as, 200 mm, 100 mm or 50mm if we consider several rebounds of the pressure waves.

As the machine rotary speed is known, it is easy to calculate that the period between the two cycles is 45.74 ms. It can be further calculated that, in between the two cycles, the peak of the pressure wave would reach the HP outlet valve 8 times for 400 mm tube lengths. For the second goal it would be interesting to determine the range of tube lengths in such a way that the peak of the pressure wave would reach the HP outlet valve at least one time less (7 times) and one time more (9 times). That way it would be assured that two extreme cases were studied: first when low pressure peak reaches the HP outlet valve when it opens and second when it is the high pressure peak. It can be easily calculated that 300 mm tube lengths would provide at least one more pressure peak while 500 mm tube lengths would provide at least one less pressure peak. Thereby, for the study of heat exchanger tube lengths it would be enough to define the range of lengths from 300 to 500 mm in order to satisfy both goals if both tubes have the same length. Nevertheless, it would be interesting to study also the cases when the tube lengths are not the same. For that reason range of the lengths was amplified.

Inlet tube length was varied in the range: 200-1000 mm with the 200 mm step. For each inlet tube length, outlet tube length was varied in the range 200-1000 mm with the 50 mm step. Shorter tube length was not considered because it was believed that it would be hard to place the heat exchanger closer to the machine. Longer tubes were not considered because it was believed that it would not be beneficial for recuperated power and compactness of the system. It was decided to use the smaller step for one tube length in order to see better the effect of tube length.

Recuperated power was highest for HP inlet valve CA of 260 degrees and piston stroke of 90 mm. These values were in the middle of their respective range meaning that the range was well selected. Figure 5.26 shows the plots of recuperated power for HP inlet valve CA of 260 degrees and various piston strokes and tube lengths. For the clarity, only three curves of inlet tube length that provided the highest recuperated power were presented for each stroke length plot. Recuperated power was highest for 90 mm piston stroke, inlet tube length of 600 mm and outlet tube length of 250 mm. Highest recuperated power was 2579 W for AirGasRatio 1.01. It can be seen that plots are very similar for all piston strokes. Recuperated power was always high for short outlet tube regardless of inlet tube length. Increasing the outlet tube length up to around 450 mm the power is dropping for all inlet tube lengths. Further increasing the outlet tube length creates positive and negative power peaks. For short inlet tube (200 mm) these peaks are more frequent. For 400 mm inlet tube length there is a significant power rise when the outlet tube length is high (1000 mm) and a smaller power peak for outlet tube length of around 600-650 mm. If heat exchanger could not be placed close to the machine then it would be beneficial to use longer tube lengths that still provide high recuperated power, like in the case of 400 mm inlet tube length and 1000 mm outlet tube length. For short outlet tube, recuperated power generally increases with the increase of inlet tube length, however further increasing inlet tube length above 600 mm decreases the power and for 800 mm the power was even less than for 200 mm which is why it is not represented on the plot.

Figure 5.27 shows the plots of recuperated power for piston stroke 90 mm and different HP inlet valve timing and tube lengths. For each HP inlet valve CA timing recuperated power was highest for 90 mm piston stroke. Thereby, these plots provide the comparison between different HP inlet valve timing separated from piston stroke effect. It can still be concluded that recuperated power is high for short outlet tube for all inlet tube lengths. The highest recuperated power was obtained for HP inlet valve CA of 260 degrees, inlet tube length of 600 mm and outlet tube length 250 mm as it was already said.

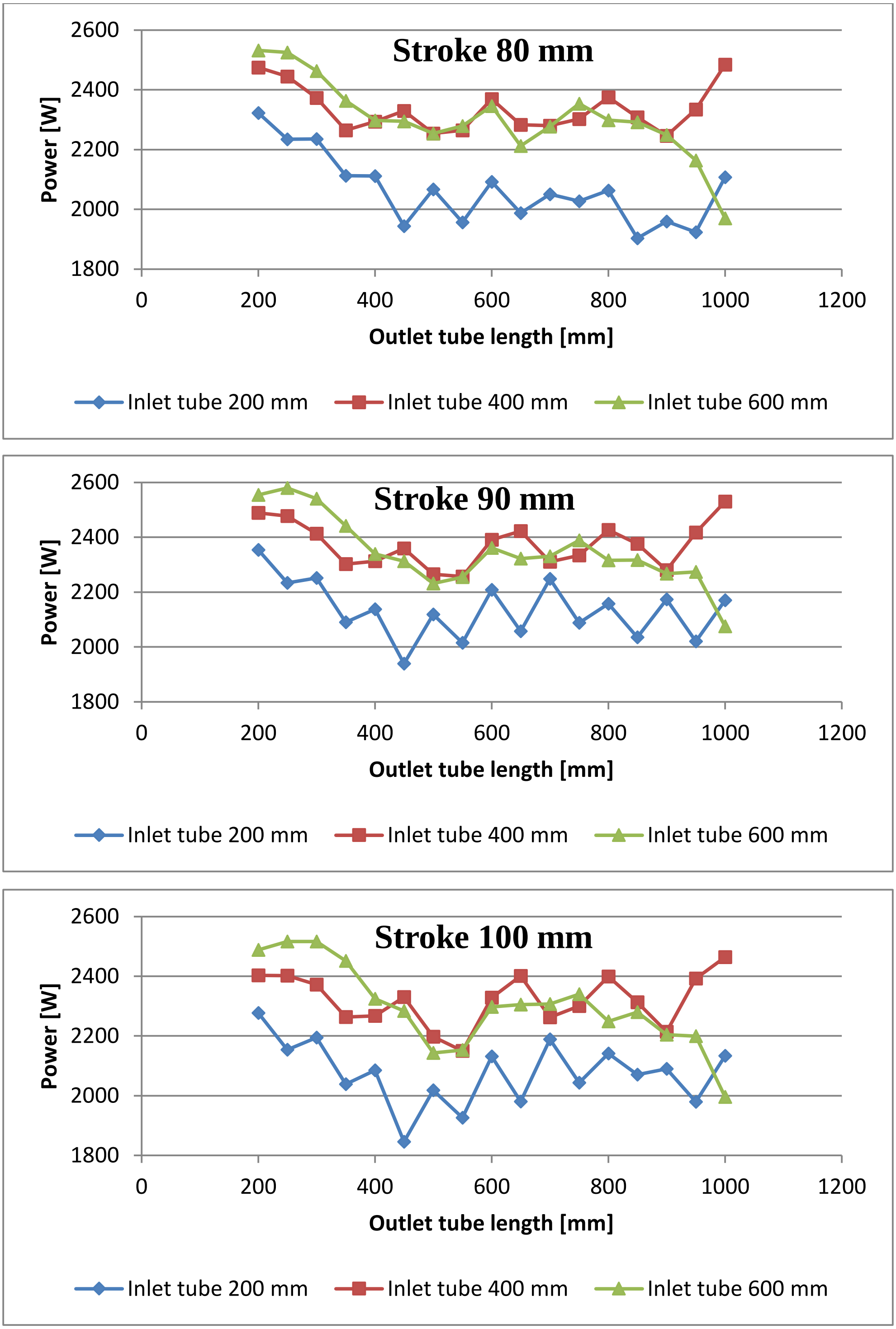

Figure 5.26. Recuperated power; HP inlet valve CA 260 degrees

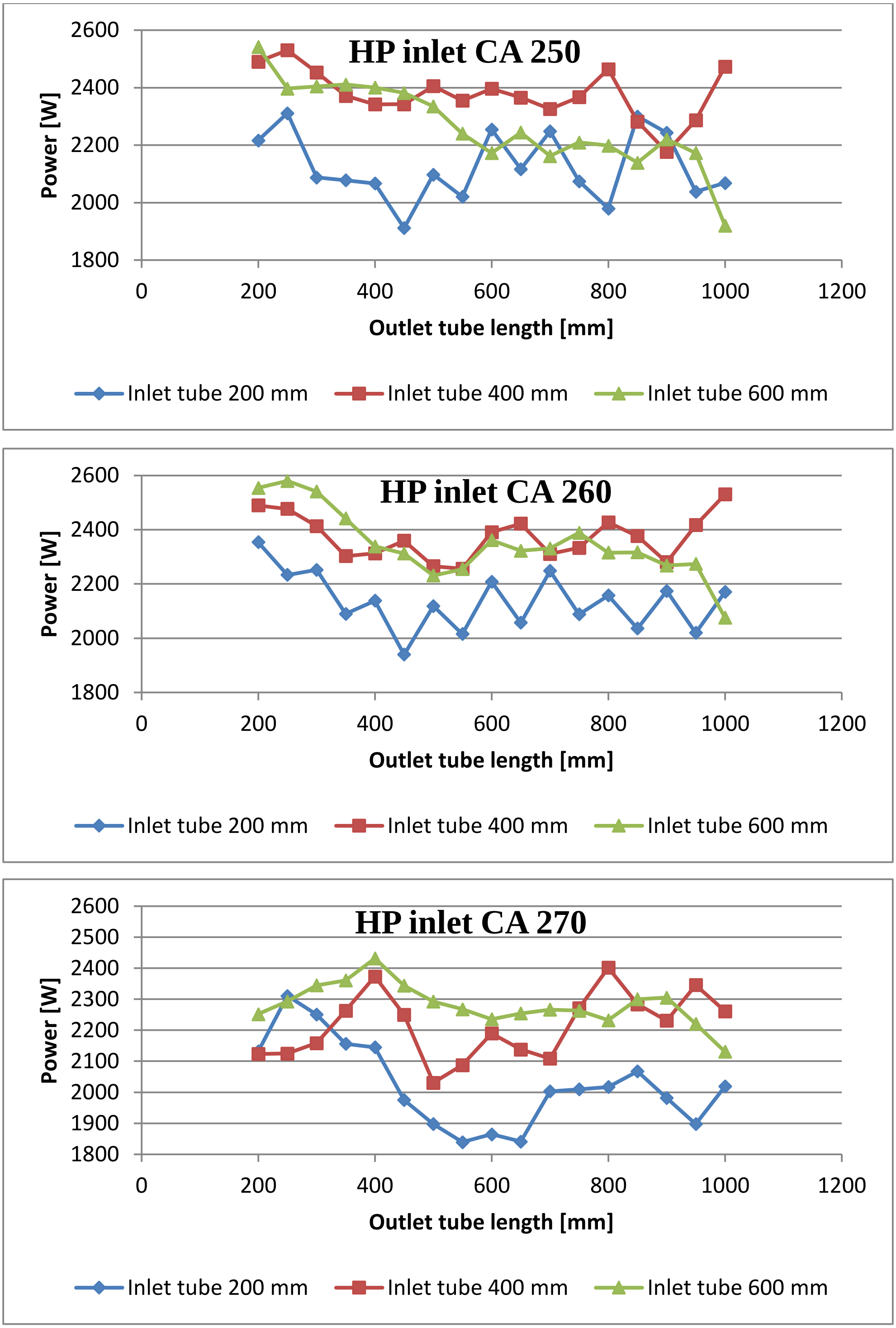

Figure 5.27. Recuperated power; stroke 90 mm

As it was shown, changing the tube length has an influence on the recuperated power. On the pressure-volume diagram it can be seen the origin of this difference in recuperated power. Figure 5.28 shows two diagrams both for HP inlet valve CA of 260 degrees and 90 mm piston stroke. Inlet tube length 600 mm and outlet tube length 250 mm provided the highest recuperated power from all tested tube lengths. Inlet tube length 600 mm and outlet tube length 500 mm provided 348 W less (2231 W) than for 250 mm shorter outlet tube. Figure 5.28 shows that the main difference between two plots is during the compression stroke when outlet valve opens. In the case of lower power, maximum cycle pressure is 1 bar higher than in the case of highest power. This produces higher HP negative work loop and lowers the recuperated power.

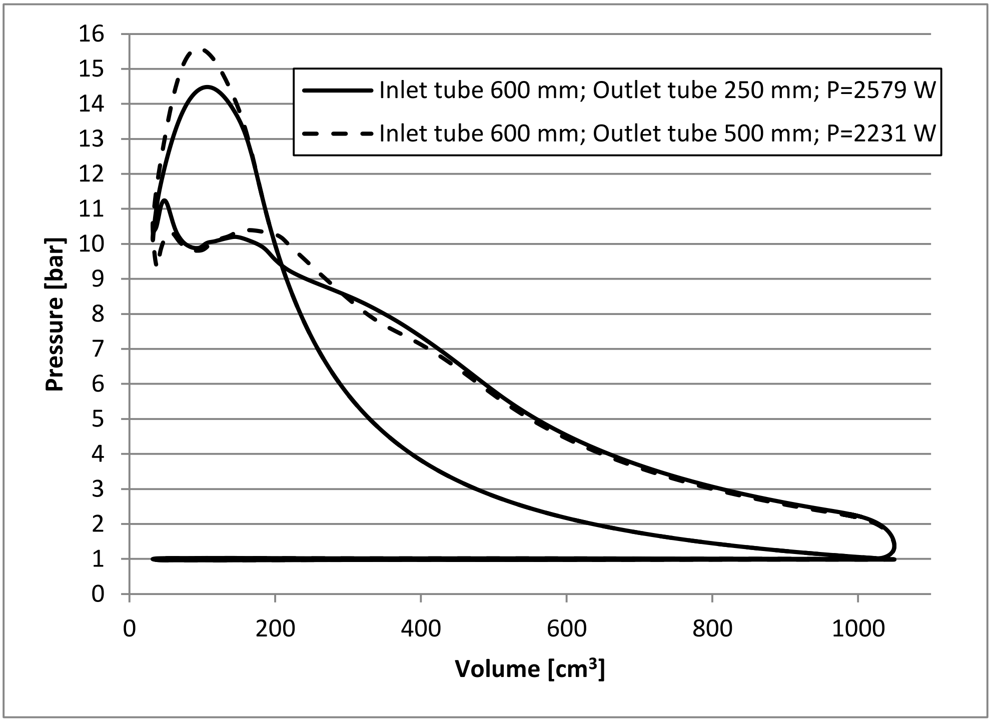

Figure 5.28. pV diagram of two different tube lengths

Pressure-volume diagram is good for comparison of two cycles but it does not reveal why the pressure is higher for longer outlet tube. This can be observed in the plot of pressure in the cylinder and the pressures at the heat exchanger side of the HP inlet and HP outlet valve. Figure 5.29 shows the pressures for outlet tube length of 250 mm and Figure 5.30 for 500 mm. Inlet tube lengths were 600 mm in both cases. It can be seen that for 500 mm outlet tube length the “cylinder” curve crosses the “HP outlet valve” curve when “HP outlet valve” curve is at its peak (at around 3.941 seconds). Pressure wave peak at the HP outlet valve stops the reed valve from opening and raises the pressure in the cylinder thereby augmenting the HP negative work.

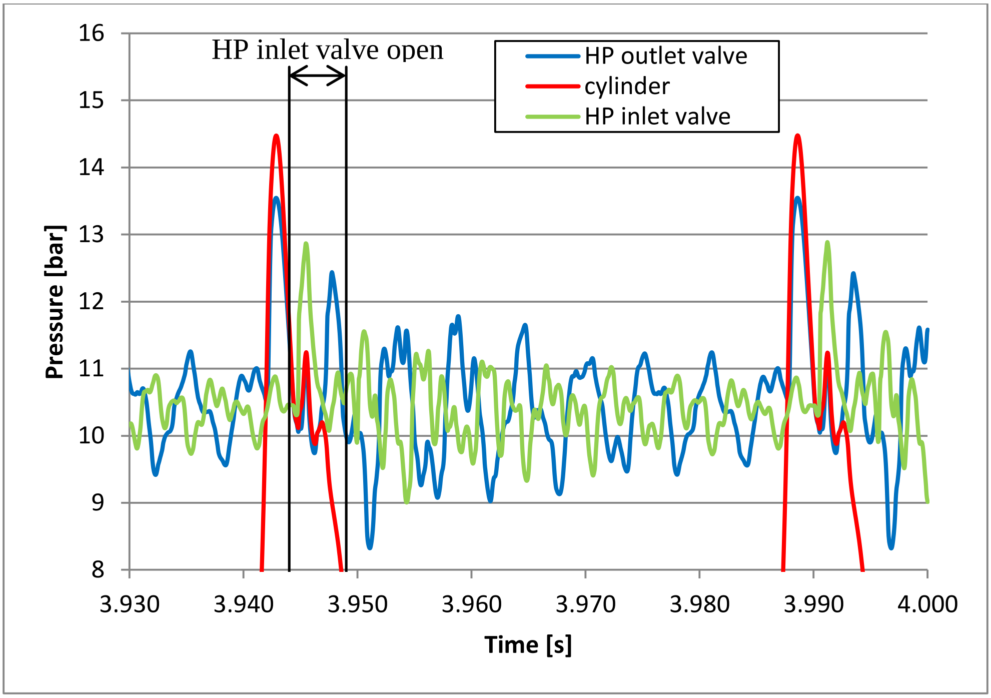

Figure 5.29. Pressures in the cylinder and at the valves; outlet tube 250 mm

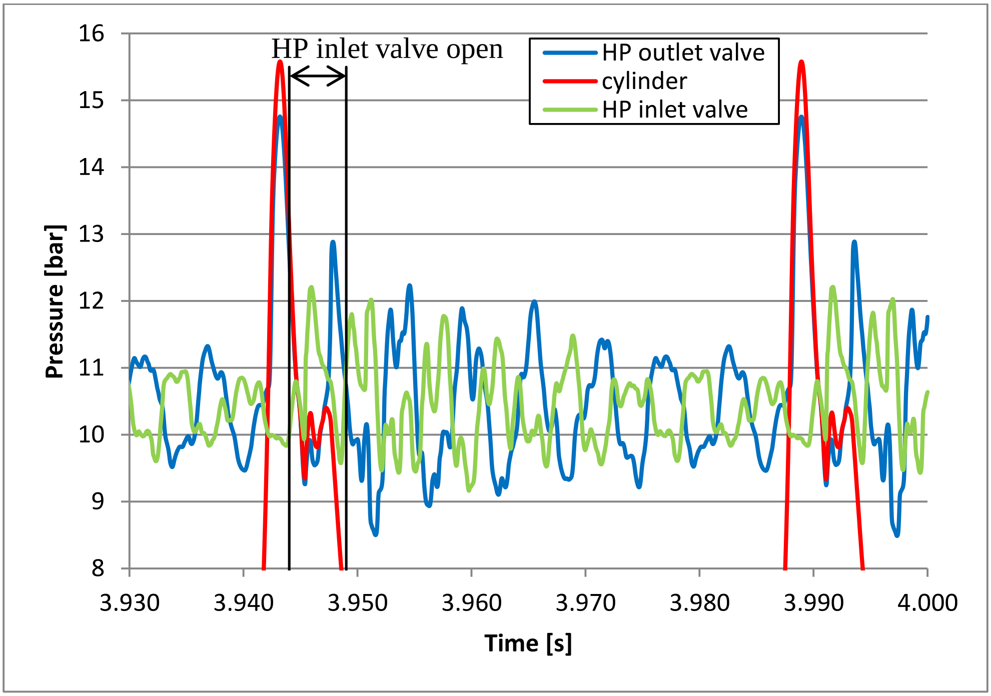

Figure 5.30. Pressures in the cylinder and at the valves; outlet tube 500 mm

For the 250 mm outlet tube length, the “cylinder” curve crosses the “HP outlet valve” curve when the former is in the lower pressure peak which positively affects the pumping losses. Pressure wave is in better synchronization with the HP outlet valve opening in this case. For both outlet tube lengths, when the HP inlet valve is opened there are two cylinder pressure peaks that improve the cycle power and cause additional mass flow through the HP outlet valve. If the peak is at the HP negative work loop it will lower this negative work zone. If the peak is at the positive work zone it enlarges the positive work. For the 500 mm outlet tube length, the second pressure peak is later than for 250 outlet tube length which at first gives slightly better positive work but later pressure drops faster which lowers the positive work. Pressure peaks during expansion had less effect on recuperated power than the pressure peak generated during compression when the outlet valve is opened. This is obvious by comparing the areas of positive and negative work from the Figure 5.28 for two tube lengths.

Synchronization of pressure waves in the high pressure part of the cycle did not bring significant improvement in recuperated power (in comparison with 0D model) but it did point out that significant loss could occur if pressure waves are not well synchronized.

5.4 Heat transfer model

Heat transfer from the hot air trapped in the cylinder to colder cylinder walls can be the cause of significant efficiency loss. This heat loss lowers the temperature of the air which comes from the heat exchanger, and consequently the pressure during the expansion, which leads to less work. During the last part of expansion, temperature of the wall gets to be higher than temperature of the air and there is a positive effect of heat transfer but it is to be expected that this part is small. During the compression, pressure and temperature in the cylinder rise. While the temperature of air is less than the cylinder wall temperature, the heat is being transferred from the wall to the air. This warms the air and raises the pressure, which leads to higher work needed for compression. Same as for expansion, during the last part of compression it is possible that the wall temperature gets lower than air temperature and positive effect of heat transfer occurs but it is reasonable to believe that would the small part. In order to take these important effects into account, a heat transfer model was applied.

For ICE there are few models of heat transfer that are very known and widely used like the models of Annand [62] and Woschni [63]. In the present Thesis the model of Annand was used. For four stroke engines he defined the Nusselt number as:

$$N_u = 0.49 R_e^{0.7} \tag{5.26}$$

where R_e is the Reynolds number calculated by:

$$R_e = \frac{S_p D_p}{\nu} \tag{5.27}$$

where S_p [m/s] is mean piston velocity, Dp [m] is piston diameter and ν [cSt] is kinematic viscosity.

Heat transfer coefficient ht is calculated using the definition of Nusselt number:

$$ht\left[\frac{W}{m^2K}\right] = \frac{k \cdot Nu}{D_p} \tag{5.28}$$

where k is the thermal conductivity of air.

The heat exchanged is then calculated by:

$$Q = ht \cdot A_{HT}(T_{air} - T_{wall}) \tag{5.29}$$

Area for the heat transfer A_{HT} is the sum of piston surface, head surface that is considered to be equal to piston surface and the area of cylinder whose height would depend of crank angle.

In the model, heat is transferred between the air and a single mass (node). This mass represented the sum of piston, cylinder and head equivalent mass. As all tests were for stationary points, weight of this mass (thermal inertia) was not important. It was assumed that there was no heat transfer between this mass and the ambient.

Heat transfer model was applied to the 0D cycle model where reed valve is used as a HP outlet valve and poppet valve as HP inlet valve. Variables were piston stroke and HP inlet valve closing angle (CA). Piston stroke was varied in the range 50-120 mm and HP inlet valve CA in the range 230-270 degrees. Figure 5.31 shows the results of recuperated power with the heat transfer model included. The maximum recuperated power of 1576 W was obtained with HP inlet valve CA of 260 degrees and piston stroke of 80 mm that provided the AirGasRatio of 0.67. Maximum recuperated power was 720 W (31%) less than it was for the model without heat transfer (2296 W). AirGasRatio that provided the maximum recuperated power was lower than for the model without the heat transfer. Consequently, the piston stroke that provided the maximum power was 10 mm shorter.

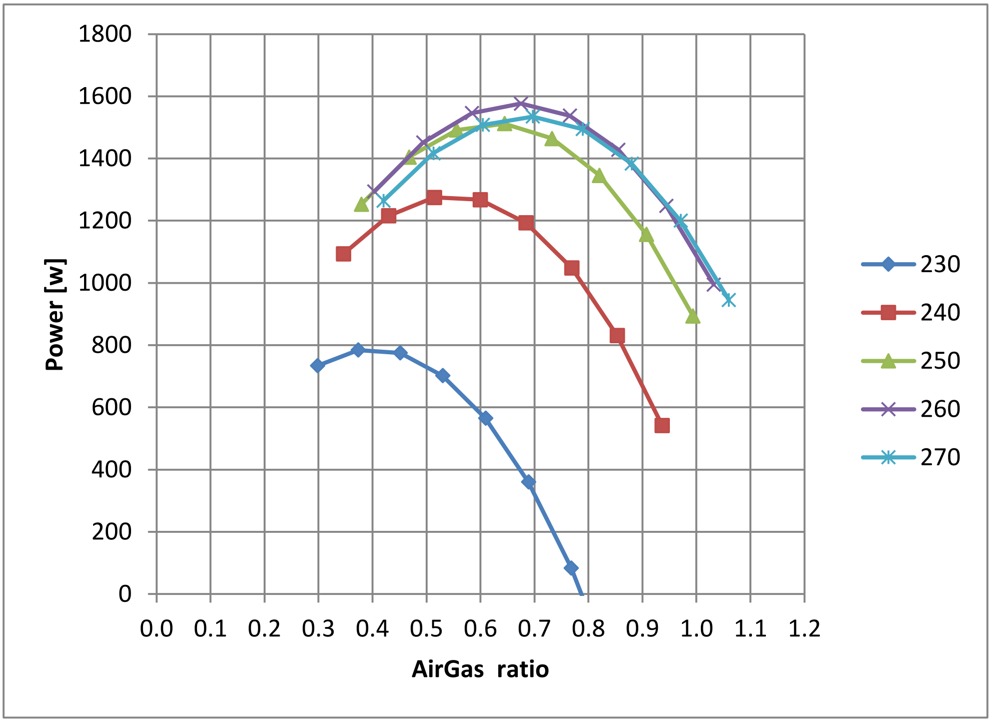

Figure 5.31. Recuperated power with the heat transfer model

Pressure-volume diagram of the cycle is represented in Figure 5.32 along with the same plot for the cycle without the heat transfer. Same parameters were used for both plots, the ones that provided the maximum recuperated power for the model with heat transfer (HP inlet valve CA 260 degrees, stroke 80 mm). For the model without the heat transfer these HP inlet valve CA and stroke were not the ones that gave the highest recuperated power (2296 W). The areas of pressure-volume diagrams cannot be easily compared if HP inlet valve CA and stroke are not the same for both plots. For that reason it was decided to use the same values for both plots and the ones that gave the maximum power for the model with heat transfer were used. The main difference between the two cycles is that, with the heat transfer, the positive work area is narrower. Compression curve is higher because heat transfer from the warm cylinder wall rises the temperature and the pressure of the air. Expansion curve is lower because heat is transferred from the air to the cylinder wall which decreases the air temperature and pressure. This decreases significantly the cycle power. Cycle mean temperature of the mass was 258 °C which was acceptable considering that for ICE, a similar machine, this is the typical temperature of the piston crown surface [2].

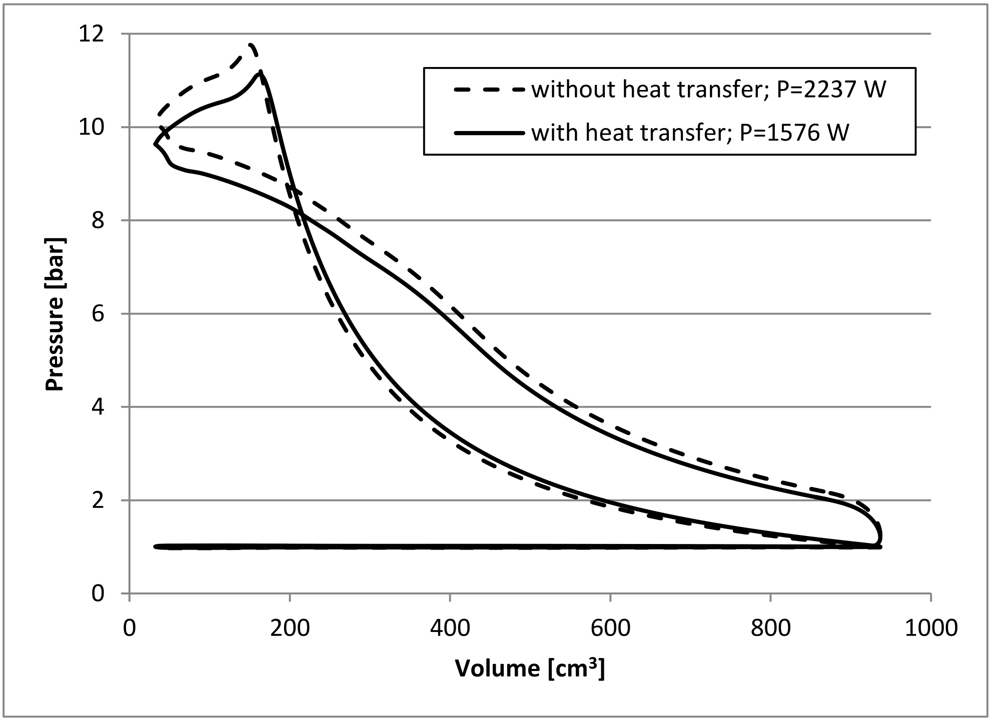

Figure 5.32. pV diagram of the cycle with and without the heat transfer

5.5 Mechanical losses

The model for the mechanical losses is based on the article by Sandoval and Heywood [64]. In this article authors estimate the mechanical losses for different components of gasoline engines. These losses are represented in form of mean effective pressure. Losses are divided in three groups:

crankshaft – main bearings, front and rear main bearings oil seals reciprocating – connecting rod bearings, piston skirt and piston rings

valvetrain – camshafts, cam followers, valve actuation mechanism

Crankshaft friction represents the friction losses related to the crankshaft. It is defined by:

$$
\begin{aligned}
cfmep[kPa] &= 1.22 \cdot 10^{5} \left(\frac{D_{bc}}{B^{2}S}\right) \\
&+3.03 \cdot 10^{4} \sqrt{\frac{\mu}{\mu_0}} \left(\frac{N D_{bc}^{3} l_{bc} n_{bc}}{B^{2}S}\right) \\
&+1.35 \cdot 10^{-10} D_{bc}^{2} N^{2} n_{bc}
\end{aligned}
\tag{5.30}
$$

where D_{bc}[mm] is the crankshaft main bearing diameter, B[mm] is the cylinder bore , S[mm] is the piston stroke, μ[cSt] is the oil dynamic viscosity, l_{bc}[mm] is the crankshaft bearing length, n_{bc} is the number of bearings and N[rpm] is the engine speed. Viscosity μ_0 is a reference viscosity of 10.6 cSt, that is the value for 10W30 oil at 90 °C. In the equation (5.30) the first term represents friction of the bearing seal, second term is main bearing hydrodynamic friction and third term is turbulent dissipation which represents the work required to pump the oil through the main bearing flow restriction.

Reciprocating friction includes the friction losses around the piston group. Sandoval and Heywood suggest two equations for reciprocating friction losses. The one without the gas pressure loading was chosen because in this application there is no peak of high pressure like the one caused by combustion in the ICE.

$$
\begin{aligned}
rfmep[kPa] &= 2.94 \cdot 10^{2} \sqrt{\frac{\mu}{\mu_0}} \left(\frac{S_p}{B}\right) \\
&+4.06 \cdot 10^{4} \left(1 + \frac{500}{N}\right) \left(\frac{1}{B^{2}}\right) \\
&+3.03 \cdot 10^{-4} \sqrt{\frac{\mu}{\mu_0}} \left(\frac{N D_{br}^{3} l_{br} n_{br}}{B^{2}S}\right)
\end{aligned}
\tag{5.31}
$$

where S_p[m/s] is the mean piston velocity, D_{br}[mm] is the connecting rod bearing diameter, l_{br}[mm] is the connecting rod bearing length and n_{br} is the number of connecting rod bearings. The first term from the equation (5.31) represents the piston friction, assuming hydrodynamic lubrication. The second term is the piston rings friction under mixed lubrication. The third term is the hydrodynamic friction in the connecting rod journal bearing.

Valvetrain friction covers the frictional losses in the valvetrain. It is defined by:

$$vfmep[kPa] = 244\sqrt{\frac{\mu}{\mu_0}}\frac{Nn_{bv}}{B^2S} + C_{rf}\frac{Nn_{val}}{S} + C_{oh}\sqrt{\frac{\mu}{\mu_0}}\frac{L_{max}^{1.5}N^{0.5}n_v}{BS} + C_{om}\left(1+\frac{500}{N}\right)\frac{L_{max}n_{val}}{S} \tag{5.32}$$

where n_{bv} is the number of camshaft bearings, n_{val} is the number of valves, C_{rf} is the constant for friction of roller follower, C_{oh} is the constant for oscillating hydrodynamic friction, C_{om} is the constant for oscillating mixed friction and L_{max}[mm] is the maximum valve lift. The first term represents the hydrodynamic friction losses in camshaft bearings. Second term represents the friction losses between roller follower and cam. Third term represents the oscillating hydrodynamic losses in the parts where there is hydrodynamic lubrication like valve lifter or valve guide. Fourth term represents the losses of the parts in motion where there is mixed lubrication like between valve and valve seat.

Dimension	Recommended range [54]	Chosen value
B		120 mm
D_{bc}	(0.6-0.7)B	70 mm
l_{bc}	(0.45-0.6)D_{bc}	30 mm
n_{bc}		2
D_{br}	(0.55-0.65)B	65 mm
l_{br}	(0.45-0.6)D_{br}	29 mm
n_{br}		1
n_{bv}		2
n_{val}		3
C_{rf}	0.0151	0.0151
C_{oh}	0.5	0.5
C_{om}	21.4	21.4

Table 5.3. Chosen dimensions for calculation of mechanical losses

As a first approximation, dimensions of crankshaft main bearings, crank rod bearings and valve bearings can be taken from recommendations for gasoline engines [54]. From the range of recommended values it was always chosen the minimal one because in the heat recovery machine there is no peak pressure caused by combustion so the stress on the crankshaft is much smaller. Also, for the same reason, the piston and connecting rod can be lighter thereby reducing the inertial forces that are also a big source of stress on bearings. Recommendations and chosen values are presented in Table 5.3. Number of valves that was chosen was 3 because the model considered that HP outlet valve was reed valve as it provided better results than poppet valve. Thereby, the three valves were two LP valves and one HP inlet valve.

The power of the mechanical losses is calculated by:

$$P_{ml}[W] = fmep[kPa] \cdot V_{disp}[dm^3] \frac{N}{120} \tag{5.33}$$

For warmed up machine, the term $\sqrt{\frac{\mu}{\mu_0}}$ from equations (5.30) to (5.32) can practically be ignored because oil viscosity μ would be similar to reference viscosity μ_0. Mechanical losses further depend on machine speed and piston stroke. Machine rotary speed was fixed because it was supposed that machine speed is the same as ICE speed and its speed was fixed for operative point G to 2623 rpm. Thereby, for all other parameters defined, mechanical losses would depend on piston stroke. Figure 5.33 shows this dependency.

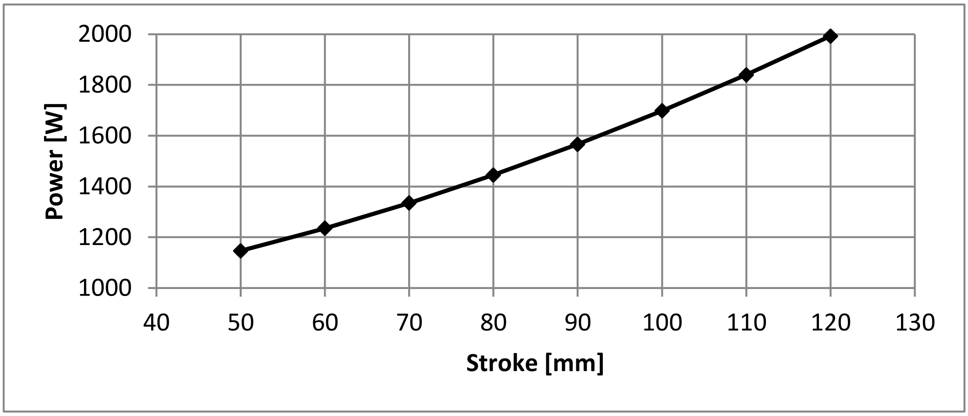

Figure 5.33. Power of mechanical losses as a function of piston stroke

Figure 5.34 shows the calculated friction mean effective pressure (fmep) for each member from the equations for a piston stroke 80 mm. Total calculated fmep was 68.67 kPa. Calculated power of mechanical losses was 1445 W. These high mechanical losses would waste almost all the power obtained by the cycle (1576 W obtained by the model with heat transfer). Thereby, it should be looked for a way to reduce them.

It can be seen that piston hydrodynamic friction, friction in main bearings and mixed friction in the valvetrain represent the most significant losses. These are the main losses that should be addressed in order to reduce the total mechanical losses.

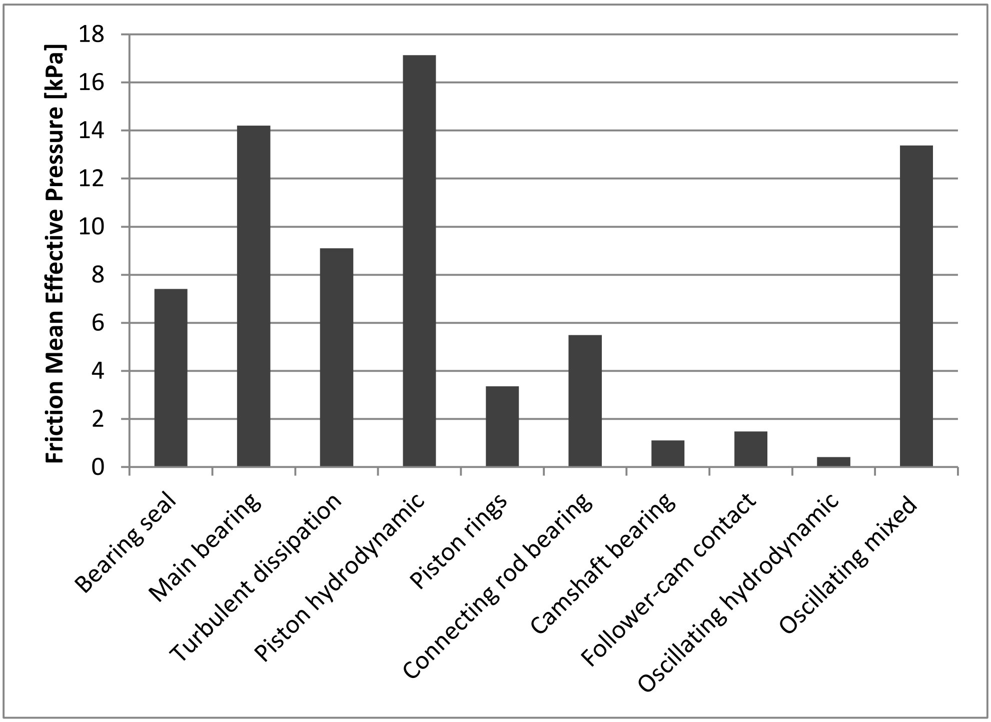

Figure 5.34. Friction mean effective pressure of each member; Stroke 80 mm

5.6 Indirect losses

Indirect losses are not directly affecting the WHR cycle efficiency. Those losses take into account how application of Brayton cycle WHR system affects the efficiency of the internal combustion engine in the vehicle. As the objective of the WHR is to improve ICE efficiency and lower the fuel consumption of the vehicle those losses must be taken into account. Indirect losses can be divided in two sources: pumping losses because of the additional exhaust backpressure and fuel consumption increase because of the additional vehicle weight.

5.6.1 Exhaust backpressure pumping losses

Placing the heat exchanger in the exhaust line increases the exhaust backpressure. This increases the ICE pumping losses because the pistons have to push the exhaust gasses harder to pass them through an additional resistance of heat exchanger. Pressure drop in the heat exchanger increases the negative work of the pumping losses.

Equation from [50] was used to estimate the power loss in this process:

$$P_{pl} = \frac{\dot{m}}{\rho}\Delta p \tag{5.34}$$

Where density ρ is the mean value of heat exchanger inlet and outlet density. Exhaust gas was again considered to have the characteristics of air as an ideal gas. Inlet and outlet densities were calculated as a function of inlet and outlet temperature as it was done in Chapter 3. Outlet temperature was calculated from the heat exchanger energy balance from the equation (3.8). For the point G defined in Chapter 3 mass flow of exhaust gas was 27.01 g/s and gas inlet temperature 733 °C. For the calculation of power lost because of exhaust backpressure, mass flows of air and gas were equal, gas inlet temperature was known and air inlet and outlet temperatures were calculated by the model. For the model that used reed valve as HP outlet valve and without the heat transfer air inlet temperature was 371 °C while the air outlet temperature was 649 °C. Outlet gas enthalpy and gas temperature were then easily calculated. Outlet gas temperature was 460 °C. Pressure drop Δp=1.45 kPa was calculated from the model described in Chapter 4.

Heat exchanger in the exhaust line creates additional back pressure that for the point G would lower the engine power for P_{pl}=89 W. This pumping loss represents 3.87 % of reference recuperated power (0D model with reed valve and without heat transfer). It should be subtracted from the recuperated power of WHR system.

5.6.2 Additional weight

Implementing the WHR system contributes to additional vehicle weight. With the added weight engine would have to produce more power for the vehicle to travel at the same velocity as it was without the additional weight. This additional engine power would effectively deny the part of the energy produced by the WHR system. In the paragraph 3.2 the way to calculate the engine power was suggested in order for the vehicle to travel at certain velocity. For the gasoline engine Ford Mondeo was used as an example of the vehicle. It was estimated that for the vehicle that weights 1569 kg and cruises at 120 km/h (velocity of the point G from NEDC) engine should produce 22556 W. The coefficient of rolling resistance was given in Table 3.2. WHR system weight should be added to the vehicle weight, new engine power should be calculated and the difference between the old and new power represents the power loss because of the additional weight.

Waste heat recovery system is composed of two main parts: heat exchanger and piston machine. Apart from these two main parts other possible components could be: tubes that connect the heat exchanger and piston machine, control system, clutch to detach the machine from the engine when the machine cannot produce power, pulleys and belt or other system to connect the machine with the engine etc. Nevertheless, probably the biggest part of the system weight goes on two main components. Heat exchanger prototype exists so it was possible to measure its weight. The heat exchanger that was used in this study weighted 10 kg. It should be noted that this is a prototype of the heat exchanger and it is reasonable to believe that a production version would be lighter. As no prototype of the piston machine was made, its weight had to be estimated. The weight of several aluminium internal combustion engines with different displacement and cylinder number was used to estimate the weight per volume ratio of these engines. The engines that were used as a sample were: 1 cylinder 600 cm^3 motorcycle engine, 10 cylinder 5000 cm^3 car engine and 4 cylinder 2000 cm^3 car engine. They weight per displaced volume ratio was in the range 45-48 kg/dm3. As displaced volume of the WHR machine is 0.936 dm^3 for the 80 mm stroke, machine weight was estimated at 43 kg.

Total WHR system weight was estimated at 55 kg. Engine power with added weight was then calculated to be 22756 W. Engine has to make 200 W more to compensate the additional weight. This power represents 8.71 % of recuperated power for the reference model (0D model with reed valve and without heat transfer) and should be subtracted from the WHR recuperated power.

6 Conclusions and future work

Contents

6.1 Conclusions 139
6.2 Future work 142

6.1 Conclusions

Car manufacturers are put to a big challenge as they are legally obliged to improve the Internal Combustion Engine efficiency or use other propulsion technologies in order to lower vehicle CO_2 emission. One way to improve ICE efficiency is to use Waste Heat Recovery because an important part of power is lost through the energy of hot exhaust gasses. This study started by analysing several WHR technologies and it was concluded that there is a significant lack of publications on Brayton cycle WHR systems. Few publications that were available revealed that Brayton cycle maybe is not the most efficient but it could be a simple and compact solution that could solve the space availability restrictions on actual vehicles. It was decided that Brayton cycle WHR system should be further studied.

In the Chapter 3, the cycle was theoretically analysed. The most important parameters that affect the cycle efficiency were determined to be: engine operative point, ratio of air and exhaust gas mass flows, pressure at the end of compression (p_2), compressor efficiency and expander efficiency.

At first the ideal cycle was analysed. Ideal cycle assumed that compressor and expander efficiencies were 100%. The engine operative point that provided the highest recuperated power (from the points that were considered) was the point when vehicle speed would be 120 km/h which is the considered point with the highest engine speed and load in real conditions of steady operation of the engine. At that point, ideal WHR Brayton cycle would provide 2.8 kW for the studied diesel engine and 6.2 kW for the studied gasoline engine. The main reason for this big difference in recuperated power between two engine types was the difference in exhaust gas temperature. For the diesel engine the temperature was 324 °C while for the gasoline engine it was 733 °C. The other important parameter was the ratio of air and exhaust gas mass flow. For the ideal cycle it was estimated that this ratio should be equal to or higher than 1 to maximise the recuperated power. For the values higher than 1 recuperated power remained the same as for the value of 1. For the values lower than 1 the power drops linearly with the drop of AirGasRatio. Regarding the pressure at the end of compression it was estimated that there is an optimal value that gives the maximum power. For the diesel engine the optimal pressure was 3.5 bar while for the gasoline engine it was 10 bar. Outside of optimal pressure the power drops in exponential manner.

A non-ideal cycle introduced losses in the compression and expansion processes. Compressor and expander efficiencies had to be estimated in order to evaluate the non-ideal cycle efficiency. The reference engine operating point was the same as for the previous ideal cycle (120 km/h vehicle speed). Barber-Nichols diagram was used to look for the machines that could be used for the cycle and to estimate the compressor and expander efficiencies. It was determined that alternating piston machine fitted best with the machine speed and geometrical limitations. Furthermore, same piston machine could be used as both compressor and expander to make the system more compact and simple. Maximum compressor and expander efficiencies were estimated to be 80% and this value was used to calculate recuperated power of non-ideal cycle. Maximum recuperated power was 397 W for diesel engine and 2461 W for gasoline engine. The big difference in recuperated power between ideal and non-ideal cycle highlights the importance of compressor and expander efficiencies. Minimal system efficiency drop could be obtained by multiplying the compressor and expander efficiencies. Irreversibilities of compression and expansion had bigger influence on diesel engine because the efficiency of the ideal cycle was lower for diesel engine. The recuperated power dropped by 86 % for diesel engine while for the gasoline engine the power drooped by 60 %. The optimal compression pressure also changed, for the diesel engine it was 1.6 bar while for the gasoline engine it was 4 bar. As maximum recuperated power for diesel engine was low it was decided to continue the investigation only for the gasoline engine. The estimated value of maximum recuperated power for gasoline engine was considered to be worth further cycle analysis. For this the more realistic model was needed that included many more losses.

In the Chapter 4, the main characteristics of the heat exchanger were validated. Heat exchanger efficiency was estimated to be 77% for the engine operative point that corresponds to vehicle speed of 120 km/h. This estimation was based on the experimental measurements of the heat exchanger prototype that was specifically designed for this application. Models of the pressure drop for both gas and air side were made based on the pressure drops measured on the heat exchanger test bench.

In the Chapter 5 the model of the heat recovery system was completed and performance of the system was estimated. At first, simple model was used to analyse the use of different valves. Recuperated power of the gasoline engine for the machine that uses poppet valves was estimated at 2031 W. It was concluded that negative high pressure (HP) loop could be lower and HP outlet valve was replaced with the reed valve because it was thought that it could decrease the pressure drop in the valve. Recuperated power increased to 2296 W. The use of poppet valve actuated by a camless technology that permits faster valve opening was investigated but it was determined that current state of the art actuators do not provide fast enough opening. Thereby, it was decided to continue the study using the reed valve as HP outlet valve.

A model with 1D tubes in the high pressure (HP) part of the model (heat exchanger and tubes that connect the heat exchanger with the machine) was developed. Synchronization of pressure waves in the high pressure part of the cycle did bring improvement in recuperated power (in comparison with referent 0D reed valve model) from 2296 W to 2579 W. This improvement of power for 12.3 % is not negligible but it is also not very significant. It was also concluded that instead of 2579 W, the recuperated power can drop by 13.49 % to 2231 W in the case of tube lengths when the pressure waves are not well synchronized.

To make the cycle more realistic various losses were added to the model. Heat transfer between the air and machine parts (cylinder, piston and head) was added to take into account the cycle heat losses. Model of heat transfer for internal combustion engines was applied. Heat transfer caused the decrease of cycle positive work. During the compression the heat was added to the air because machine parts were hotter than the air and during the expansion heat was taken from the air because it was hotter than surrounding machine parts. Heat transfers in the opposite direction of what would be beneficial for the cycle. By applying heat transfer model to the reference 0D model that used the reed valve as HP outlet valve, recuperated powered decreased by 31.3 % from 2296 W to 1576 W. Heat transfer introduced big losses to the cycle but not as much as the next losses that were considered: mechanical losses. The model of mechanical losses estimated that 1445 W of crankshaft power would be spent on friction. This represents 62.9 % of the power recuperated by the reference 0D reed valve model without the heat transfer. This amount of mechanical losses would effectively make the cycle non-viable as it uses almost all the recuperated power that was left after applying the heat transfer model. The model of mechanical losses used empirical equations that were obtained from the measurements of mechanical losses in internal combustion engines. As in the Brayton cycle machine there is no combustion, pressures are much lower than in ICE. Thereby stress on the machine parts is much lower. Machine parts that would be less loaded are primarily piston, piston rings, connecting rod, connecting rod bearings, crankshaft and crankshaft bearings. Big part of mechanical losses comes exactly from those parts. Piston hydrodynamic friction losses and friction losses in the main bearings make for almost 42% of all mechanical losses. If piston and main bearings are dimensioned lighter it is reasonable to believe that mechanical losses could be less than what was estimated by the model that was fitted with ICE experimental values.

Indirect losses included the losses that do not occur directly in the cycle but represent the losses for the vehicle caused by the addition of WHR system. First indirect loss was the additional power that engine has to produce to overcome the additional exhaust back pressure caused by the heat exchanger in the exhaust line. It was estimated that this loss would be 89 W representing around 3.87 % of the powered recuperated by reference model. The second indirect loss was the additional engine power needed to overcome the additional vehicle weight. This loss was estimated to be 200 W or 8.71 % of the power recuperated by the reference model.

	Contribution	Power [W]	% of power for reference model
Positive	Basic cycle with reed valve as HP outlet valve	+2296	+100
Negative	Heat transfer losses	-720	-31.35
	Mechanical losses	-1445	-62.93
	Additional back pressure	-89	-3.87
	Additional weight	-200	-8.71
Sum		**-158**	**-6.86**

Table 6.1. Cycle power summary

In the Table 6.1 it is represented the summary of cycle positive and negative contributions. It is evident that losses overcome the cycle positive work. In order for the cycle to be viable mechanical and heat losses have to be reduced. Basic cycle could also be improved.

At first, Brayton cycle seemed like a promising solution for WHR because of the simplicity and compactness compared to Organic Rankine Cycle for example. After the more detailed analysis it was concluded that in order for the cycle to function, even with bad efficiency, system would have to employ some special techniques like: very low friction materials, insulating materials that would cover chamber surface to reduce the heat transfer, valves that could open very fast, high efficiency heat exchanger etc. These techniques have high cost which reduces the viability of the Brayton cycle.

6.2 Future work

Regarding the results from Table 6.1 it seems hard to imagine that cycle could be made viable. Nevertheless, some parts of the cycle deserve further study. Heat exchanger efficiency is of them. During the experimental tests the target mass flow (27.01 g/s) and temperature at the gas inlet (733 °C) were not reached. Furthermore temperature at the air inlet was lower (200 °C) than it was estimated by simulation (357 °C for reed valve model). Experimental measurement should be done in these conditions to better estimate the heat exchanger efficiency. Furthermore, test was done with constant air mass flow while the air flow in the alternating piston machine is very pulsating. Pulsating flow could be important for the heat transfer. Many researchers investigated the effect of pulsation on heat transfer. The ones that experimentally investigated heat transfer enhancement with air are more relevant for this thesis. Different studies [65], [66], [67], [68] showed that, depending on conditions, pulsating flow could increase or decrease the heat transfer coefficient compared to constant flow. Maximum heat transfer coefficient increase in those studies was as high as 50%, while the maximum decrease was around 40 %. This big discrepancy in the results suggests that the heat exchanger should be tested with the pulsating flow that would resemble the desired machine operative point as much as possible. Heat exchanger efficiency directly affects the recuperated power so it is important to have the right estimation.

Other part that could be improved is the model of mechanical losses. Cylinder pressure from the current model could be used to calculate the stress on the crankshaft and connecting rod bearing journals. This could allow more precise estimation of journal diameters. Journal diameters would in that case be smaller than what was estimated by the current model. This would lower the corresponding part of mechanical losses as they are directly related to journal diameter. Current model of mechanical losses estimated that the biggest part of losses comes from piston hydrodynamic friction. This model is very simple. It takes into account piston diameter, mean piston velocity and one coefficient that was used to fit the model with the measurements from various internal combustion engines. However, these engines were mostly with four or more cylinders and the model does not take into account the number of cylinders which could cause the overestimation of losses as WHR machine has only one cylinder. Other important difference between the current model that is based on data from ICE and WHR machine is that the temperatures in the machine are lower than in ICE. This could maybe allow the use of some special low friction materials that could not be applied in ICE because of high temperatures.

Finally, some other kind of the machine could be considered. Barber-Nichols diagram that was used in this study to select the machine type only covers few machine types. Maybe some existing machine design or newly developed prototype could serve well for this purpose. Perhaps some rotating machine with less moving parts could provide lower mechanical losses that would improve the cycle efficiency.

7 Bibliography

[1] "Wikipedia." [Online]. Available: www.wikipedia.org.

[2] J. B. Heywood, *Internal Combustion Engine Fundamentals*, vol. 21. 1988.

[3] D. Clerk, "The Gas and Oil Engine," *Science (80-.).*, vol. 4, 1896.

[4] D. Clerk, *The Gas, Petrol and Oil Engine*. 1910.

[5] E. Barrieu, "EHRS Impact on Engine Warm up and Fuel Economy," in *DEER Conference*, 2011.

[6] "ACEA agreement," 2015. [Online]. Available: http://europa.eu/rapid/press-release_IP-98-734_en.htm?locale=en.

[7] E. Comission, "Monitoring the CO2 emissions from new passenger cars in the EU: data for the year 2008."

[8] "EU CO2 target." [Online]. Available: http://ec.europa.eu/clima/policies/transport/vehicles/cars/index_en.htm.

[9] P. Freeland, J. Taylor, D. Oudenijeweme, P. Stansfield, and M. Warth, "Advanced technologies for downsized direct injection gasoline engines," in *Thiesel*, 2012, vol. 1.

[10] P. Mock, "The International Council of Clean Transportation," 2013. [Online]. Available: http://www.theicct.org/blogs/staff/art-cooking-popcorn-and-2013-eu-statistical-pocketbook.

[11] R. Toom, "Waste Heat Regeneration systems for internal combustion engines," in *Engine Expo*, 2007.

[12] J. W. Fairbanks, "Automotive Thermoelectric Generators and HVAC," in *2012 Anual Merit Review DOE Vehicle Technologies Program and Hydrogen and Fuel Cells Program*, 2012.

[13] I. Arsie, A. Cricchio, V. Marano, C. Pianese, M. De Cesare, and W. Nesci, "Modeling Analysis of Waste Heat Recovery via Thermo Electric Generators for Fuel Economy Improvement and CO 2 Reduction in Small Diesel Engines," *SAE*, 2014.

[14] D. M. Rowe, J. Smith, G. Thomas, and G. Min, "Weight penalty incurred in thermoelectric recovery of automobile exhaust heat," *J. Electron. Mater.*, vol. 40, no. 5, pp. 784–788, 2011.

[15] N. B. E. and F. A. L. J. C. Bass, "Performance of the 1 kW Thermoelectric Generator for Diesel Engines," in *AIP*, 1994.

[16] D. Crane, G. Jackson, and D. Holloway, "Towards Optimization of

Automotive Waste Heat Recovery Using Thermoelectrics," *SAE*, vol. 2001-01–10, 2001.

[17] J. Mccoy, "Thermoelectric Technology: Materials, Processes, Devices & Systems," in *ASM Meeting*, 2012.

[18] P. Patel and E. Doyle, "Compounding the truck diesel engine with an organic Rankine-cycle system," in *Automotive Engineering Congress and Exposition*, 1976.

[19] T. Endo, T. Endo, S. Kawajiri, S. Kawajiri, Y. Kojima, Y. Kojima, K. Takahashi, K. Takahashi, T. Baba, T. Baba, S. Ibaraki, S. Ibaraki, T. Takahashi, T. Takahashi, M. Shinohara, and M. Shinohara, "Study on Maximizing Exergy in Automotive Engines," *SAE*, no. April, pp. 2007–2007, 2007.

[20] M. Kadota and K. Yamamoto, "Advanced Transient Simulation on Hybrid Vehicle Using Rankine Cycle System," *SAE Int. J. Engines*, vol. 1. pp. 240–247, 2008.

[21] H. R. Freymann, W. Strobl, and A. Obieglo, "The turbosteamer: A system introducing the principle of cogeneration in automotive applications," *MTZ Worldw.*, vol. 69, no. 5, pp. 20–27, 2008.

[22] J. Ringler, M. Seifert, V. Guyotot, and W. Hübner, "Rankine Cycle for Waste Heat Recovery of IC Engines," *SAE Int. J. Engines*, vol. 2. pp. 67–76, 2009.

[23] R. Freymann, J. Ringler, M. Seifert, and T. Horst, "The Second Generation Turbosteamer," *MTZ Worldw.*, vol. 73, no. 2, pp. 18–23, 2012.

[24] T. A. Horst, W. Tegethoff, P. Eilts, and J. Koehler, "Prediction of dynamic Rankine Cycle waste heat recovery performance and fuel saving potential in passenger car applications considering interactions with vehicles' energy management," *Energy Convers. Manag.*, vol. 78, pp. 438–451, Feb. 2014.

[25] C. Sprouse and C. Depcik, "Review of organic Rankine cycles for internal combustion engine exhaust waste heat recovery," *Applied Thermal Engineering*, vol. 51, no. 1–2. pp. 711–722, 2013.

[26] D. Seher, T. Lengenfelder, J. Gerhardt, N. Eisenmenger, M. Hackner, and I. Krinn, "Waste Heat Recovery for Commercial Vehicles with a Rankine Process," in *21 st Aachen Colloquium Automobile and Engine Technology 2012*, 2012.

[27] W. R. Martini, "Stirling engine design manual." 1978.

[28] M. Bianchi and A. De Pascale, "Bottoming cycles for electric energy generation: Parametric investigation of available and innovative solutions for the exploitation of low and medium temperature heat sources," *Appl.*

Energy, vol. 88, no. 5, pp. 1500–1509, May 2011.

[29] R. J. Meijer, “The Philips Stirling thermal engine,” Technical University of Delft, 1960.

[30] L. G. Thieme, “Low-power baseline test results for the GPU3 Stirling engine,” 1979.

[31] Y. Timoumi, I. Tlili, and S. Ben Nasrallah, “Design and performance optimization of GPU-3 Stirling engines,” *Energy*, vol. 33, no. 7, pp. 1100–1114, Jul. 2008.

[32] C. J. Paul and A. Engeda, “A Stirling engine for use with lower quality fuels,” *Energy*, vol. 84, pp. 152–160, May 2015.

[33] D. G. Thombare and S. K. Verma, “Technological development in the Stirling cycle engines,” *Renew. Sustain. Energy Rev.*, vol. 12, no. 1, pp. 1–38, Jan. 2008.

[34] B. Kongtragool and S. Wongwises, “A review of solar-powered Stirling engines and low temperature differential Stirling engines,” *Renew. Sustain. Energy Rev.*, vol. 7, no. 2, pp. 131–154, Apr. 2003.

[35] A. J. Organ, *The Air Engine: Stirling Cycle Power for a Sustainable Future*. Elsevier Science, 2007.

[36] M. Bailey, “Comparative Evaluation of Three Alternative Power Cycles for Waste Heat Recovery from the Exhaust of Adiabatic Diesel Engines,” 1985.

[37] W. M. Farrell, “Air cycle thermodynamic conversion system,” 1987.

[38] F. Wicks, G. Berven, and D. Marchionne, “A Combined Cycle With Gas Turbine Topping and Thermodynamically Ideal Gas Turbine Bottoming,” 1992.

[39] O. Bolland, M. Førde, and B. Hånde, “Air Bottoming Cycle: Use of Gas Turbine Waste Heat for Power Generation,” *J. Eng. Gas Turbines Power*, vol. 118, no. 2, pp. 359–368, Apr. 1996.

[40] J. Kaikko, L. Hunyadi, A. Reunanen, and J. Larjola, “Comparison between air bottoming cycle and organic Rankine cycle as bottoming cycles,” in *Proceedings of Second International Heat Powered Cycles Conference, HPC*, 2001, vol. 1, p. 195.

[41] B. Song, W. Zhuge, R. Zhao, X. Zheng, Y. Zhang, Y. Yin, and Y. Zhao, “An investigation on the performance of a Brayton cycle waste heat recovery system for turbocharged diesel engines,” *J. Mech. Sci. Technol.*, vol. 27, no. 6, pp. 1721–1729, 2013.

[42] Z. Xu, J. Liu, J. Fu, and C. Ren, “Analysis and Comparison of Typical Exhaust Gas Energy Recovery Bottoming Cycles,” in *SAE 2013 World*

Congress & Exhibition, 2013.

[43] S. Mitani, “Heat energy recovery apparatus,” US 7,448,213 B2, 2008.

[44] F. Thevenod, “Heat engine with external hot source,” 2011.

[45] F. O. Thevenod, “Heat engine with external heat source and associated power generation unit and vehicle,” 2013.

[46] ECE, “Uniform provisions concerning the approval of vehicles with regard to the emission of pollutants according to engine fuel requirements.” 2011.

[47] V. Dolz, R. Novella, A. García, and J. Sánchez, “HD Diesel engine equipped with a bottoming Rankine cycle as a waste heat recovery system. Part 1: Study and analysis of the waste heat energy,” *Appl. Therm. Eng.*, vol. 36, pp. 269–278, Apr. 2012.

[48] “NIST database.” [Online]. Available: http://webbook.nist.gov/chemistry/fluid/.

[49] K. E. Nichols, “How to Select Turbomachinery For Your Application.” Barber-Nichols Inc.

[50] S. Kakaç, H. Liu, and A. Pramuanjaroenkij, *Heat Exchangers: Selection, Rating, and Thermal Design, Second Edition*. Taylor & Francis, 2002.

[51] I. E. Idel′chik and M. O. Steinberg, *Handbook of Hydraulic Resistance*. Begell House, 1996.

[52] R. Van Basshuysen and F. Schäfer, *Internal Combustion Engine Handbook: Basics, Components, Systems, and Perspectives*. 2004.

[53] J. Erjavec, *Automotive Technology: A Systems Approach, Volume 2*. Cengage Learning, 2005.

[54] F. Payri and J. M. Desantes, *Motores de combustión interna alternativos*. 2013.

[55] G. P. Blair, *Design and Simulation of Four-stroke Engines*. Society of Automotive Engineers, 1999.

[56] E. T. Hinds and G. P. Blair, “Unsteady Gas Flow Through Reed Valve Induction Systems,” 1978.

[57] R. Fleck, A. Cartwright, and D. Thornhill, “Mathematical Modelling of Reed Valve Behaviour in High Speed Two-Stroke Engines.” SAE International , 1997.

[58] G. P. Blair, *Design and Simulation of Two-stroke Engines*. Society of Automotive Engineers, 1996.

[59] G. P. Blair, H. B. Lau, A. Cartwright, B. D. Raghunathan, and D. O.

Mackey, “Coefficients of Discharge at the Aperatures of Engines,” *SAE*, no. 412, 1995.

[60] Z. D. Lou, Q. Deng, S. Wen, Y. Zhang, M. Yu, M. Sun, and G. Zhu, “Progress in Camless Variable Valve Actuation with Two-Spring Pendulum and Electrohydraulic Latching,” *SAE Int. J. Engines*, vol. 6, no. 1, pp. 2013-01–0590, Apr. 2013.

[61] “Cargine G5,” 2012. [Online]. Available: http://www.freevalve.com/wp-content/uploads/2013/01/Cargine-Free-Valve-Actuator-G5-Specification-2012-09-291.pdf.

[62] W. J. D. Annand and D. Pinfold, “Heat Transfer in the Cylinder of a Motored Reciprocating Engine,” 1980.

[63] G. Woschni, “A Universally Applicable Equation for the Instantaneous Heat Transfer Coefficient in the Internal Combustion Engine,” 1967.

[64] D. Sandoval and J. B. Heywood, “An Improved Friction Model for Spark-Ignition Engines,” *SAE Tech. Pap.*, no. 2003-01–0725, 2003.

[65] M. A. Habib, A. M. Attya, A. I. Eid, and A. Z. Aly, “Convective heat transfer characteristics of laminar pulsating pipe air flow,” *Heat Mass Transf.*, vol. 38, no. 3, pp. 221–232, Feb. 2002.

[66] M. A. Habib, A. M. Attya, S. A. M. Said, A. I. Eid, and A. Z. Aly, “Heat transfer characteristics and Nusselt number correlation of turbulent pulsating pipe air flows,” *Heat Mass Transf.*, vol. 40, no. 3–4, pp. 307–318, Feb. 2004.

[67] E. A. M. Elshafei, M. Safwat Mohamed, H. Mansour, and M. Sakr, “Experimental study of heat transfer in pulsating turbulent flow in a pipe,” *Int. J. Heat Fluid Flow*, vol. 29, no. 4, pp. 1029–1038, Aug. 2008.

[68] A. E. Zohir, M. A. Habib, A. M. Attya, and A. I. Eid, “An experimental investigation of heat transfer to pulsating pipe air flow with different amplitudes,” *Heat Mass Transf.*, vol. 42, no. 7, pp. 625–635, May 2006.